A Combined Experimental-Computational Method to Generate Reliable Subject Specific Models of the Knee's Ligamentous Constraint

by

Chadd W. Clary

Submitted to the graduate degree program in Mechanical Engineering and the Graduate Faculty of the University of Kansas School of Engineering in partial fulfillment of the requirements for the degree of Doctor of Philosophy

_____
Dr. Lorin Maletsky, Chairperson

_____
Dr. Arvin Agah, Committee Member

_____
Dr. Michael Detamore, Committee Member

_____
Dr. Kenneth Fischer, Committee Member

_____
Dr. Terence McIff, Committee Member

_____
Dr. Albert Romkes, Committee Member

Defended July 7th, 2009

The Dissertation Committee for Chadd W. Clary certifies
that this is the approved version of the following dissertation:

A Combined Experimental-Computational Method to Generate Reliable Subject Specific Models of the Knee's Ligamentous Constraint

_____
Dr. Lorin Maletsky, Chairperson

_____
Dr. Arvin Agah, Committee Member

_____
Dr. Michael Detamore, Committee Member

_____
Dr. Kenneth Fischer, Committee Member

_____
Dr. Terence McIff, Committee Member

_____
Dr. Albert Romkes, Committee Member

Defended July 7th, 200

Abstract

With the advancement of computational models of the knee, the opportunity exists to utilize patient-specific computational models of the knee intra-operatively to assist surgeons. A critical component for evaluation of whole knee mechanics is configuration of the soft tissue ligament structures surrounding the knee. The overarching purpose of the current research was to develop a unique methodology, utilizing both experimental and computational techniques, for efficient development of patient-specific ligament constraint model. To this end, an experimental method to manually assess knee laxity was developed, and used to evaluate changes in knee laxity after total knee replacement in eight cadaveric specimens. A computational model of ligament constraint was developed to complement the knee laxity data collected during the experimental protocol. A sensitivity study performed on the model identified the most critical ligament parameters affecting knee laxity. Subsequently, these ligament parameters were optimized using the simulated annealing algorithm to minimize the difference between the model predicted knee laxity and the experimentally observed knee laxity for four cadaveric specimens. The optimized ligament parameters were used to predict knee kinematics during an experimental assessment in a quasi-static knee loading rig. Knee kinematic predictions using the optimized ligament parameters were compared to predictions using previously published ligament parameters, and subsequently reduced the RMS difference between the predictions and the experimental kinematics by more than 50% for knee rotations.

Table of Contents

List of Abbreviations

A-P	Anterior-Posterior
ALC	Anterior Lateral Capsule
BMI	Body Mass Index
CAS	Computer Aided Sugery
CR	Cruciate-Retaining
DOF	Degree of Freedom
F-E	Flexion-Extension
FFL	Fabello-Fibular Ligament
GA	Genetic Algorithm
I-E	Internal-External
KKS	Kansas Knee Simulator
LCL	Lateral Collateral Ligament
M-L	Medial-Lateral
MCL	Medial Collateral Ligament
MRI	Magnetic Resonance Imaging
OA	Osteoarthritis
PC	Posterior Capsule
PCE	Posterior Capsular Extension
PCL	Posterior Cruciate Ligament
PFL	Popliteal-Fibular Ligament
PS	Posterior Stabilized
QKR	Quasi-Static Knee Rig
ROM	Range of Motion
RMS	Root Mean Square
SA	Simulated Annealing
S-I	Superior-Inferior
TKR	Total Knee Replacement
Vr-Vl	Varus-Valgus

List of Figures

List of Tables

Acknowledgements

To my wife Karen for allowing me to continually hit the snooze button on our life and stay in graduate school for over six years. She showed me that there is a lot more to life than work. She is wonderful.

To my family, particularly my mother, father, and sister. My parents told me when I was a young child I would be an engineer. They sacrificed a lot to make sure I had that opportunity and I will always owe them a debt of gratitude.

To my advisor Dr. Lorin Maletsky for his guidance and support. I'll admit there were times when I wished he would just say the answers to those questions he always posed (the answers which he already knew) instead of trying to coerce the answer from me. He is a teacher in everything he does and he does it very well.

To the other graduate students in the lab (Nathan, Nick, Amit, Amber, and Kevin), don't forget to check the bottoms of your shoes before leaving the lab. It's a dirty job, but we're helping improve people's quality of life. This kind of work isn't possible without the support of a talented team.

To the Self Graduate Fellowship, graduate school is way easier when you aren't broke; it provides intellectual freedom. I will use the skills they cultivated in me for years to come.

To DePuy, Inc. for providing access to world class surgeons and a unique insight into the realm of implant design.

Chapter 1: Overview

Orthopedic surgeons are faced with a variety of challenging decisions in the operating room while performing total knee replacement surgery that will directly affect the patient's outcome. These questions primarily revolve around the appropriate alignment of the implanted components relative to the patient's existing bony and soft tissue anatomy. Surgeons currently rely on past training and experience to formulate these decisions. However, with the advancement of computational models of the knee and incorporation of kinematic tracking systems into the operating room, the opportunity exists to utilize patient-specific computational models of the knee intra-operatively to assist surgeons with these difficult surgical decisions. These models could provide vital information on implant kinematics, internal stress distribution in the implants and bones, and wear characteristics of the polyethylene components.

There exist a number of difficult challenges associated with efficient generation of patient-specific computational models. Current imaging technology (magnetic resonance and computed tomography), coupled with statistical shape models of the bones in the knee, provide an efficient method to generate patient-specific bones with accurate material properties. Furthermore, computer-aided design (CAD) models of the implants can be easily incorporated into computational models to evaluate the change in the articular geometry. The missing component for evaluation of whole knee mechanics is configuration of the soft tissue structures surrounding the knee (ligament, tendons, and muscles). While the rough geometries

of these structures are visible with some imaging modalities, it is currently impossible to estimate their mechanical properties using these imaging techniques.

A number of studies have been devoted to determining ligament mechanical properties *in vitro*. While mean stiffness values have been measured for most ligaments around the knee, there is a large amount of variability between subjects. A study by Blankevoort and colleagues illustrated that employing the mean value for ligament stiffness and reference strain in a knee computational model resulted in poor prediction of patient-specific knee mechanics [1]. Instead, a combined experimental and computational methodology, which could be applied to patients, is needed to define the ligament constraint for a particular subject.

The overarching purpose of the current research was to develop a methodology for efficient development of patient-specific ligament constraint models from experimental assessment of knee ligament laxity. Many previous efforts to develop generic knee models have been limited by the amount and type of experimental data available for model validation in the literature. The current research is unique in that from the onset, the experimental methodology was developed in conjunction with the computational model, providing a seamless coordination between the model and experimental results.

Three research objectives were established to accomplish the above purpose:

1) Develop a reliable experimental method to quantify knee laxity that could potentially be employed on TKR patients before or during surgery

2) Develop an efficient computational model of knee ligament constraint capable of reproducing patient-specific knee laxity
3) Utilize the experimental subject-specific laxity to customize the computational model of ligament constraint to reproduce subject-specific knee laxity

The following five chapters report the steps taken to address each of these objectives. Chapter two contains a review of the current literature, including reviews of: knee anatomy, experimental assessments of ligament properties, mathematical ligament models, and optimization methods for multi-variable problems.

Chapter three describes in detail the experimental method developed to assess knee laxity. Included in chapter three is an assessment of the method's reliability and potential for experimental error. The experimental method was used on eight cadaveric knees to assess the change in knee laxity after total knee replacement.

Chapter four describes the computational model of ligament constraint, including the mathematical formulation for knee ligaments and model boundary conditions. Two separate models were constructed based on two knees tested experimentally. The models' ligaments were configured using the experimental data and material properties were assigned using literature values. A Monte-Carlo analysis was performed where the ligament attachment locations and material properties were varied within a normal distribution and the resultant predicted knee laxity was quantified. From the Monte-Carlo simulation, the ligament parameters that had the largest influence on knee laxity were identified. The 5%-95% confidence

intervals of knee laxity predicted by the computational models were compared to the experimentally determined knee laxity to confirm the computational ligaments provided the appropriate level of constraint.

In chapter five, a simulated annealing optimization algorithm was applied to the ligament model to customize the model's constraint. An objective function was formulated based on the difference between experimental and computational knee laxity. The optimization algorithm was used to minimize this objective function for four different knees tested experimentally. In addition, variations of the objective function were evaluated to assess the most efficient and accurate functions for ligament constraint optimization.

The final chapter contains an overall assessment of the methods used in the current study and how they could be adapted for use in the operating room. The final chapter also contains a number of suggestions for future improvements to the current research and additional studies that should be carried out.

Chapter 2: Literature Review

This review of the literature is primarily focused on the functional knee anatomy that influences the passive laxity of the knee joint and how these structures behave after total knee replacement. Additional review has been provided concerning the various mathematical representations of these ligaments, previously published computational models of the knee, and large-scale optimization techniques.

In order to build an effective computational model of the knee, it is important to first understand the contribution of the various structures of the knee anatomy to knee kinematics. Motions of the knee can either be classified as passive or active. Passive motions, like knee laxity, are primarily influenced by the articular surfaces of the tibia and femur and the soft tissue structures around the knee. Passive motions are not weight bearing nor do they require muscle activation. On the other hand, active motions, like walking and climbing stairs, are primarily driven by the muscles that span the knee joint and external forces that act across the knee, but are certainly influenced by the same structures that determine the passive knee motion. For example, co-contraction of the quadriceps and hamstrings muscles when landing from a jump stabilize the A-P motion of the knee joint, in conjunction with the passive constraint provided by the ACL. However, when the musculature across the knee is relaxed (like when a patient is under anesthesia) it does not actively contribute to knee stability.

2.1 Articular Surfaces

The articular surfaces of the knee are located on three separate bones: the distal end of the femur, the proximal end of tibia, and on the posterior face of the patella. The distal end of the femur terminates in two separate spheroid structures called the medial and lateral condyles. These two condyles contact two relatively flat surfaces on the proximal end of the tibia, known as the medial and lateral tibial plateaus. The medial plateau is rounder and more conforming than the lateral plateau. A majority of the compression transmitted through the knee passes through the medial plateau. Conversely, the lateral plateau is longer in the A-P direction and less conforming so that when the tibia rotates internally or externally relative to the femur, the lateral condyle is free to translate along the lateral tibial plateau while the medial condyle is more stationary [2]. The trochlear groove is on the anterior aspect of the distal femur and runs superior and lateral between the condyles from the distal end of the femur. The posterior face of the patella slides along this groove as the knee is flexed and extended.

Each of the articular surfaces is covered in a thin layer of highly organized connective tissue comprised of collagen and elastin fibers known as articular cartilage. The articular cartilage provides a near frictionless surface between the mating bones. Over time, the articular cartilage in the knee can wear away exposing the rougher bone below resulting in pain and loss of function (also known as osteoarthritis (OA)). In advanced cases of OA, the articulating surfaces of three bones in the knee are removed and replaced during total knee arthroplasty. Modern

knee replacement components attempt to replicate the motion and function of the natural knee by mimicking the complex curvature of the femoral articular geometry. The relative size and shape of the natural articular surfaces [2, 3], as well as the shape of total knee replacement components [4, 5], have a dramatic influence on knee kinematics and knee laxity. In general, the articular surfaces between the tibia and femur, on their own, do not provide enough restraint to stabilize the joint during weight bearing activities. Instead, the stability of the knee is determined by a complex balance of constraint provided by the articular surfaces and the complementary soft tissue.

2.2 Ligaments and Soft Tissue

The passive constraint of the knee joint is provided by an extensive network of ligaments and soft tissues spanning the knee joint. A majority of this constraint is provided by four primary ligaments: the medial collateral ligament (MCL), the lateral collateral ligament (LCL), the posterior cruciate ligament (PCL), and the anterior cruciate ligament (ACL). Unlike the other ligaments, the ACL is removed during total knee replacement and is therefore not discussed in depth in this section. Over the past several decades numerous studies have been devoted to measuring the specific morphological and biomechanical properties of each of these ligaments.

2.2.1 Medial Collateral Ligament

The medial collateral ligament (MCL) is a broad span of collagen fibers, with multiple origin and insertion points, that spans the medial aspect of the knee (Fig.

2.1). For most functional investigations the MCL is divided into the three distinct components: the superficial-MCL (s-MCL), the deep-MCL (d-MCL) and the postero-medial capsule (PMC). The s-MCL originates from the inferior face of the medial epicondyle [6]. The origin site is typically oval in shape with the 20-mm major diameter in the S-I direction [6]. The fibers of the s-MCL insert into the medial side of the tibia approximately 60-80 mm distal to the joint line, forming an oval insertion site with an A-P radius of 2-4 mm and S-I radius of 10-13 mm [6].

The d-MCL spans the knee joint just deep to the s-MCL. The d-MCL originates on the femur distal and posterior to the s-MCL from an oval-shaped attachment with an A-P length of approximately 7 mm [6]. The fibers of the d-MCL form a bundle 5-7 mm wide and move distally and slightly anterior across the knee joint until they insert 2-3 mm distal to the articular cartilage of the tibia. The fibers of the MCL posterior to the s-MCL and d-MCL, which fan from an origin site on the adducter tubercle and insert all along the postero-medial aspect of the tibia, are classified together as the postero-medial capsule (PMC).

The primary function of the MCL is to resist valgus torques applied to the tibia, although it is also a secondary restraint to anterior force and internal and external torques [7]. Different fibers of the MCL are tensed and relaxed throughout the flexion range. Both the s-MCL and d-MCL remain taught with flexion, but the anterior fibers of the s-MCL are tightest in flexion while the posterior fibers are tightest in extension (Fig. 2.2). The PMC is stressed in full extension, and then quickly becomes slack as the knee is flexed. Internal rotation of the tibia increases

the tension in the fibers of the s-MCL and the PMC (but only in extension), while external rotation increases tension in the s-MCL and the d-MCL [8]. The s-MCL and d-MCL both become tense when a valgus load is applied to the knee.

Several different stiffness values for the MCL have been reported in the literature, primarily for the ligament as a whole. Most recently, Robison et al. [9] separated the three components of the MCL and reported the stiffness of each component independently. The study found that the s-MCL, d-MCL, and PMC had stiffnesses of 80±8, 42±14, and 56±20 N/mm, respectively.

2.2.2 Lateral Collateral and Popliteo-Fibular Ligaments

The soft tissue on the lateral aspect of the knee is comprised of the lateral collateral (LCL) and the popliteo-fibular ligaments (PFL) that both originate from the femur and insert onto the head of the fibula (Fig. 2.1). The LCL originates 19-20 mm anterior from the most posterior point on the lateral condyle and 20-21 mm proximal from the most distal point on the lateral condyle, which is also 3-4 mm posterior to the apex of the lateral epicondyle [10]. The origin attachment site is oval shaped with A-P and S-I diameters of 10 mm and 12 mm [10]. The fibers of the LCL form a 3-4 mm wide bundle that runs distally, and slightly posterior and lateral to attach on the most distal portion of the plateau of the fibula. The distal insertion of the LCL is pear shaped with A-P and S-I diameters of 8 and 13 mm [10]. The PFL originates on the femur just distal and anterior to the LCL ligament and runs postero-distally to the proximal posterior lip of the fibular head [11].

The LCL and PFL work together to resist varus and external rotations of the tibia. The LCL is tense at full extension, but slackens significantly with knee flexion. Meanwhile, the PFL tends to remain tense all the way through the flexion cycle. Since the LCL is tightest near full extension, the LCL primarily resists external and varus rotations when the knee is extended. With flexion, the role of resisting external rotation is assumed by the PFL [10]. Using the same setup and testing apparatus as Robinson et al. [9] used for the MCL, Sugita and Amis measured the stiffness of the LCL and PFL to be 58.1±22.8 and 43.6±14.8 N/mm, respectively [11].

2.2.3 Posterior Cruciate Ligament and Posterior Capsule

The posterior cruciate ligament (PCL) spans the posterior aspect of the knee joint between the medial and lateral condyles. The PCL has two functional bundles. The antero-lateral PCL (a-PCL) originates from the anterior portion of the roof on the medial side of the inter-condylar notch and attaches on the mid-line of the posterior aspect of the tibia. The postero-medial PCL (p-PCL) originates from a broad attachment along the medial wall of the intercondylar notch just superior to the articular cartilage and attaches just posterior to the a-PCL attachment [12]. The overall purpose of the PCL is to provide a restraint to posterior translation of the tibia relative to the femur. The two bundles work in tandem to provide this restraint. During flexion, the a-PCL tightens between approximately 30° and 90° knee flexion. Beyond 90°, the p-PCL tightens while the a-PCL begins to slacken. Neither bundle of the PCL is tight in full extension. The average stiffness of the separate a-PCL and p-PCL were 125 and 60 N/mm, respectively [13].

Since the PCL is slack in full extension, additional structures across the posterior aspect of the knee are responsible for restraining tibial posterior translation in extension. This complex network of fibers are grouped together and called the posterior capsule. The posterior capsule is comprised of the oblique popliteal ligament (OPL), the fabello-fibular ligament (FFL), the medial posterior capsule (m-PC), and the popliteus capsular extension (PCE) (Fig. 2.1). This highly integrated sheath of collagenous fibers is intimately connected with the musculature crossing the posterior aspect of the knee [14]. In general, the structures in the posterior capsule tighten in full extension, as the posterior aspect of the medial and lateral condyle move posterior into the fibers stretching them out. These structures limit the amount of extension in the knee and are primarily responsible for knee stability at full extension.

2.2.4 Knee Ligaments in Total Knee Replacement

In the healthy knee, the mechanical axis of the leg in full extension forms a straight line from the center of the ball of the hip through the center of the knee, terminating at the center of the ankle. This ideal mechanical axis facilitates efficient load transmission from the torso to the foot without creating excessive buckling moments at the knee. As OA in the knee progresses, the articular surfaces of the knee break down causing a decrease in the joint space and change in the mechanical axis of the leg. If the OA is isolated to the medial side of the knee, the medial joint space will decrease causing a varus deformity of the knee. Conversely, although less common, isolated lateral OA leads to a valgus deformity of the knee.

Previous research has suggested that through the breakdown of the joint space, OA leads to increased levels of varus-valgus laxity [15-18] and decreased knee function. It is still unclear how ligaments change in response to OA, although it is thought that ligaments tend to become more compliant [15] and sometimes contract to tighten the joint. When a surgeon performs a knee replacement, they attempt to recreate the appropriate mechanical axis of the knee through the alignment of tibial and femoral components relative to their bones. In knees with extreme varus or valgus deformities, the soft tissue around the knee may have changed so dramatically that it is very difficult to fully correct the deformity without creating excessive force in the knee's soft tissue.

The current generation of knee replacements offers two different styles of components: cruciate retaining (CR) and posterior stabilized (PS). In a CR knee replacement, the articular surfaces of the natural knee and ACL attachment sites are removed with special care taken to preserve the attachments of the PCL. In this design, the PCL, working in conjunction with the posterior capsule and collateral ligaments, provide the necessary restraint to anterior femoral translation relative to the tibia. Some surgeons prefer the PS design that replaces the PCL with a post on the tibia and a mating cam on the femur to restrict anterior femoral translation. Despite the style of implant used, surgeons must pay special attention to the implant alignment and tension in the soft tissue structures to ensure the knee is "balanced" and the ligaments provide the appropriate level of restraint throughout flexion without developing excessive ligament forces [19].

There are several techniques employed by surgeons to create balance in the knee joint after TKR [20]. Generally, balance is assessed by observing the gap between the distal bone cut on the femur and the tibial cut with the knee in full extension. Likewise, the gap between the posterior femoral cut and the tibial cut are compared at 90° knee flexion. Ideally, both the extension and flexion gaps are perfectly rectangular and of equal dimension. If the gaps do not initially match, the surgeon has several options depending on the nature of the imbalance. Surgeons can re-cut the femur or tibia, or make selective resections to the MCL, LCL, PCL, or posterior capsule. The techniques for which ligaments are cut and in what sequence varies greatly between surgeons. More recently, instrumented blocks [21] and tibial trays [20] have been recommended to measure joint compressive force through the flexion cycle to aid in the ligament balancing procedure. Regardless of the technique used, attaining the appropriate ligament balance is critically important for the long term survivorship of the implant [22].

2.3 Mathematical Ligament Models

The foundation for the proposed work lies in previously developed mathematical representations of ligament constraint. These models vary in sophistication from single line-of-action force-producing elements to full three-dimensional continuum finite-element representations of whole ligaments. Each mathematical representation is based upon the complex force vs. displacement behavior observed during uni-axial ligament mechanical testing. A comprehensive summary of published ligament models can be found in Table 2.1.

It has been previously demonstrated that ligaments exhibit a complex material behavior, characterized by transverse isotropy and viscohyperelasticity [23-25]. These material models have primarily been employed to predict strain distribution in the ACL, but are currently too computationally expensive to implement for the entire knee. Researchers interested in representing the constraint of knee ligaments without the desire to predict localized ligament strain distributions often assume a simpler non-linear elastic ligament material behavior. One of the most common anatomically-based dynamic three-dimensional models currently employed to represent the soft tissue constraint in the knee was developed by Abdel-Rahman et al. [26]. This ligament model employed twelve non-linear spring elements to represent the soft tissue structures around the knee: anterior ACL, posterior ACL, a-PCL, p-PCL, a-MCL, oblique MCL, deep MCL, LCL, medial posterior capsule, lateral posterior capsule, oblique popliteal ligament, and arcuate popliteal ligament. Each spring element exhibited a three-part force versus elongation behavior that was defined by the ligament free length, the length at the end of the toe region, and the linear ligament stiffness. The ligament produced no force when the ligament length (linear distance from origin to insertion nodes) was shorter than the ligament free length. To represent the toe region, the spring element exhibited a parabolic force response as the ligament elongated from its free length to the transition length. Finally, beyond the transition length, the ligament exhibited a linear response to increased elongation. This ligament model was coupled with a contact model between simplified rigid representations of the femoral and tibial geometries to

generate a second-order set of ordinary differential equations. These equations were then solved using a custom differential/algebraic systems solver to predict the resultant knee kinematics.

This particular representation also provided one of the first comprehensive three-dimensional characterizations of the soft tissue structures around the knee, including origin/insertion sites, ligament stiffnesses, and ligament free lengths for each element derived from literature values. Due to its simple mathematical representation and comprehensive nature, this particular model has been employed in multiple predictive knee models [27, 28], including the commercially available knee replacement design tool KneeSIM™ (Biomechanics Research Group, Inc). A newer version of the same model incorporating deformable cartilage and the patello-femoral mechanism was recently published [29].

While Adbel-Rahman's model has been widely employed as an acceptable knee soft tissue representation, more anatomic representations have been proposed in a series of mechanical and computational studies by Mommersteeg et al. [30-34]. The key observation that motivated this research was that individual ligaments are composed of several different functional bundles that have variable force-elongation behavior patterns depending on the relative orientation of the origin and insertion sites [30, 34, 35]. In these studies, it was determined that single spring elements were not able to completely characterize the complex ligament response. Instead, an alternative multiple fiber representation was proposed where each ligament was represented by a series of four to seven non-linear spring elements with variable pre-

strains and stiffnesses. Using a numerical least-squared optimization method the pre-strain and stiffness of each element were approximated to reproduce the overall force-elongation behavior of bone-ligament-bone complexes.

This approach was then extended to the whole knee by measuring knee kinematics during controlled Vr-Vl and A-P laxity assessments on a cadaveric knee, obtaining and testing bone-ligament-bone tensile specimens for the four major ligaments (ACL, PCL, LCL, MCL), optimizing the pre-strain and stiffness properties for each tensile specimen, then incorporating those ligament representations into a whole knee mathematical model [32, 33]. Ultimately, this process was applied to a single cadaveric knee and the resultant laxity predictions compared very favorably to the measured experimental knee laxity. Unfortunately, this process to predict subject specific ligament properties was extremely time consuming and required complete dissection of the knee joint. Such a comprehensive approach was not feasible for use intra-operatively during total knee replacement surgery.

Both mathematical ligament models discussed thus far utilized combinations of non-linear spring elements as a simplified representation of ligament function. Such a representation neglects the effects of ligament fibers wrapping around bones (as in the MCL spanning the medial border of the tibia) and ligaments wrapping around other ligaments (as in the ACL-PCL interaction). More recently, several three-dimensional finite-element continuum models of ligaments have been proposed [36], including homogeneous, isotropic, incompressible, hyperelastic material models for the ACL [23, 25, 37], and subject specific models of the MCL [38]. Certainly, the

formulation and validation of these models have demonstrated the predictive power of ligament continuum finite element approximations and the ability to overcome the simplifying assumptions of neglecting ligament-bone wrapping and ligament-ligament wrapping. These models are capable of accurately predicting the complex ligament stress and strain responses in addition to predicting knee kinematics. However, despite the increased sophistication of these models, it has still not been demonstrated they can more accurately predict whole knee kinematics than the simplified non-linear spring methods discussed previously, despite the dramatically increased computational cost.

The primary challenge in each of these models is refining a generic soft-tissue construction to represent a subject-specific model. In most cases, this is done by either identifying the ligament origin/insertions sites from a set of MR-images [25] or manually digitizing the origin/insertion sites in some local reference frame [32], and then manually extending a ligament representation between origin and insertion sites. This type of ligament representation is feasible intra-operatively as the surgeon could easily use a digitizing probe to identify the major ligament bundles in the local coordinate system of the CAS framework. However, a technique has recently been proposed by Chen et al. [39] where experimental passive kinematics of an analog knee after total knee replacement were used in conjunction with a simple whole knee mathematical model to predict the origin and insertions of the analog MCL and LCL representations. This technique was able to predict the S-I, M-L and A-P femoral origins of the LCL and MCL to within 2 mm. Such an accurate prediction of

ligament locations gives hope that with the appropriate whole knee model and enough input kinematics, similar predictions could be made for the remaining soft tissue structures in the knee.

2.4 Ligament Optimization

Few attempts exist in the literature to optimize ligament configurations constructed to provide accurate whole-knee kinematic constraint. Blankevoort and colleagues were the first to implement a ligament optimization routine into their computational model of the natural knee, discussed in the previous section [1]. A gradient-based non-linear optimization algorithm was used to predict the stiffness and reference strain parameters of the four major knee ligaments required to minimize the difference between predicted and observed knee kinematics under isolated internal-external torques. The optimization routine found reasonable solutions to the optimization problem; however, the researchers found that including additional kinematics (i.e. A-P translation during I-E rotation) into the objective function led to different sets of optimized ligament parameters.

For the Blankevoort model, with only a handful of design variables, gradient based methods may have been sufficient to find the optimum solution; however, when using simple springs to represent a continuum ligament structure, assumptions are made about where to position the attachment sites of the discretized ligament springs inside the actual ligament attachment footprint. It has been previously shown that the location of these springs relative to the knee flexion axis significantly affect their elongation patterns through the flexion range. Therefore, it is necessary to

include the ligament attachment sites as variables in the optimization routine. Doing so increases the number of unknown variables included in the optimization and adds complexity to the solution space of the model's predicted knee laxity.

While few researchers have attempted to optimize ligament constraint around the knee, the optimization problem is analogous to another well-studied optimization problem in biomechanics: muscle force prediction in dynamic models of human movement. The two optimization problems are similar in that soft tissue parameters are optimized in both problems to recreate an observed joint motion. Both optimization problems also have large numbers of design variables and a complex solution space. Initial attempts to optimize muscle forces in a dynamic model of human movement also used gradient-based optimization algorithms [40, 41]; however, subsequent studies demonstrated that gradient-based methods led to over-prediction of muscle forces because local optima in the solution space "trapped" the optimization algorithm. Several random-search algorithms were proposed to overcome the limitations associated with these gradient-based algorithms, including simulated annealing (SA) [42, 43], genetic algorithms (GA) [43], and particle swarm algorithms [44].

The simulated annealing algorithm is derived from the thermodynamics of quenching metals [45, 46]. Simulated annealing overcomes the limitations of gradient-based optimizations methods by incorporating a stochiastic heuristic that allows the optimization to escape local minima. In general, SA performs a random search of the solution space by serially perturbing each input variable and evaluating

the objective function. If the perturbation improves the objective function, the current state of the optimization is set to the new input variable. If the objective function is not improved, a stochastic criterion is invoked to determine if the perturbation is accepted. The probability of accepting an "uphill" move is governed by the model "temperature" and temperature reduction rate. Early in the optimization with a high temperature, "uphill" moves have a higher probability of acceptance; later in the optimization after the temperature has decreased, "downhill" moves are more likely. In this way, the SA algorithm randomly samples the solution space early in the optimization, and then focuses the search in the most promising region later in the algorithm. While the simulated annealing algorithm is not guaranteed to find the true global minimum, previous research has demonstrated that the simulated annealing algorithm provides better solutions than traditional gradient based methods [42, 43].

Genetic algorithms seek a global optimum solution following the model of evolution [47]. An initial "population" of solutions (or search space) to the optimization problem is generated with various combinations of the model parameters. Subsequently, a new population of models is generated by combining the parameters associated with members of the parent generation (also called crossover and mutations). Those parents with the highest fitness score will be the most likely to pass on their genes (model parameters) to the subsequent generation. Exactly how the parents are selected and how their genes are combined can be influenced by heuristics (rules) incorporated into the genetic algorithm. With each passing generation, the current generation becomes more like the target. Genetic algorithms avoid

convergence to local optima by randomly "mutating" the parameters of a few members of each generation, there by forcing them out of local optima.

Particle swarm algorithms distribute "particles" throughout the search space and randomly assign initial velocities along each of the design variables [44]. At each time step, the velocity vector of each particle is adjusted towards the best solution encountered by that particular particle and the best solution experienced by any particle. As the algorithm progresses, the magnitudes of the velocity vectors for each particle are decreased, intensifying the search in the area of the best solutions, and causing a "swarming" of the particles around the optimum solution.

Each of these algorithms have been proven effective at finding globally-optimized solutions for problems with moderate to large numbers of variables and complex solution spaces. Each algorithm can also be "parallelized," such that sequential function evaluations can be distributed over a number of processors to improve the convergence time. Simulated annealing has proven particularly effective in biomechanics applications because the algorithm parameters can be easily tuned for each application to provide balance between algorithm convergence time and solution accuracy [42]. For example, the temperature reduction rate could be increased to decrease the probability of the uphill moves more quickly. While doing so decreases the likelihood of finding the true "global optimum," it also decreases the number of function evaluations required for convergence to a solution. In applications where a true globally optimized solution is not required, this control is very convenient.

2.5 Tables and Figures

Table 2-1: Published knee computational models and ligament formulations

Author	Journal	Year	University	Ligaments	Ligament Representation	Articular Surfaces	Insertion Sites	Ligament Parameters	Loading Type
Clary		2009	KU	PCL, MCL, LCL, PCAP	13 non-linear spring elements	Rigid TKR	MRI/Proped Points	SA optimization	Manual Assessment
Abdel-Rahman	Med Eng Physics	1998	U of Toledo	ACL, PCL, MCL, LCL, Pcap	12 non-linear spring elements	Rigid Idealized Natural	Literature Values	Literature Values	COM Impact (Decaying Sine)
Chen	Med Img Comp	2006	Queens U, Canada	MCL, LCL, PCL (springs)	Springs	Rigid TKR (probed)	Optimized	Known	Passive Flexion
Halloran	J Biomech	2005	U of Denver	Quad and Some Ligaments	Membrane elements	Deformable TKR	Visable Human CT	Literature (Staubli '99, Quap '98)	Simulator (Purdue)
Hurschler	J Biomech Eng	2003	U of Winconsin-Madison	Single Ligaments	Microstructural based (strain-energy)	None	Ligerature	Probabalistic	Hypothetical
Mommersteg	J Biomech	95, 96, 96, 97	U of Nigmegen, Netherlands	ACL, PCL, MCL, LCL	Four non-linear spring element bundles (ACL, PCL, MCL, LCL), bone contact for MCL and LCL	Natural Stereophotogrammetric, deformable cartilage	RSA of attachments	Uniaxial tested bundles	Vr-Vl, A-P Laxity
Shelburne	J Biomech	97	U of Texas Austin	ACL, PCL, MCL, LCL, Pcap, Extensor, Muscles	11 Non-linear Elastic (Blankevoor and Huskies, 1991)	Idealized	Literature (Garg and Walker '90)	Literature (Blankevoort, '91)	A-P, Quad
	Med Sci in Sports and Exercise	2005	Steadman Hawksins						
Donahue	J Biomech Eng	2002	UC Davis (Michigan Technological University)	ACL (2), MCL(5)	Non-linear springs	Deformable Natural (CT scan)	Laser scan of bone	Literature (Pandy '97, Li '99)	Compression
Li	J Biomech Eng	1999	Harvard	ACL (4), PCL(4), MCL(5), LCL(3), meniscus (6)	Non-linear springs	Deformable Natural (MRI)	From MRI	Literature (Butler '86, Blankevoort '96, Andriacchi '83), optimized to Robot eval	A-P, I-E
	Clinical Biomech	2003							
	Annals of Biomedical Eng	2002		Added Muscles					
Pena	Clinical Biomech	2005, 2005, 2006	U of Zaragoza, Spain	ACL, PCL, MCL, LCL, Meniscus	isotropic, hyperelastic solids (incompressible Neo-Hookean behavior)	Deformable Natural (MRI)	MRI	Literature (Weiss '01)	Static Compression
Mesfar, Moglo, Shiraz-Adl	Comp Meth Biomech Biomed Eng	2006	Ecole Polytechnique, Canada	ACL(6), PCL(6), MCL(3), LCL(3), MPFL(4), LPFL(3), PT(9), Quad, Meniscus	Non-linear springs	Deformable Natural	Literature (Butler '86, Staubli '99, Atkinson '00, Moglo '03ab)	Literature (Butler '86, Staubli '99, Atkinson '00, Moglo '03ab)	Quad loads
Perillo-Marcone	J Biomech Eng	2007	Southampton	MCL(1), LCL(3), PCL(2)	Non-linear springs	Deformable TKR	Literature (Abdel-Rahman)	Literature (Blankevoort '91)	Stance phase gait
Song	J Biomech	2004	U of Pittsburgh	ACL	incompressible, hyperelastic, homogenous, isotropic solid	Bones (MRI)	Digitized	Fit to robot experiment	passive flexion, anterior force
Hirokawa	J of Biomech	2000	Kyoshu U	ACL	Fiber matrix composite solid, homogenous, hyperelastic, incompressible	None	Isolated ligament (Hirokawa '92)	Literature	Passive Flexion kinematics
Limbert	J of Biomech	2004	Southampton	ACL	fiber reinfoced composite, neo-Hookean, incompressible, isotropic, hyperelastic,	None	Literature (Martelli '00)	Optimized to Pioletti '97	Passive Flexion kinematics
Ellis, Gardiner, Weiss	J Ortho Res	2003, 2006	U of Utah	MCL	Transversely isotropic, hyperelastic, incompressible solid	Rigid Bones (CT scan)	CT scan (copper wire)	Uni-axial testing (Gardiner '03)	V-V, A-P experimental kinematics

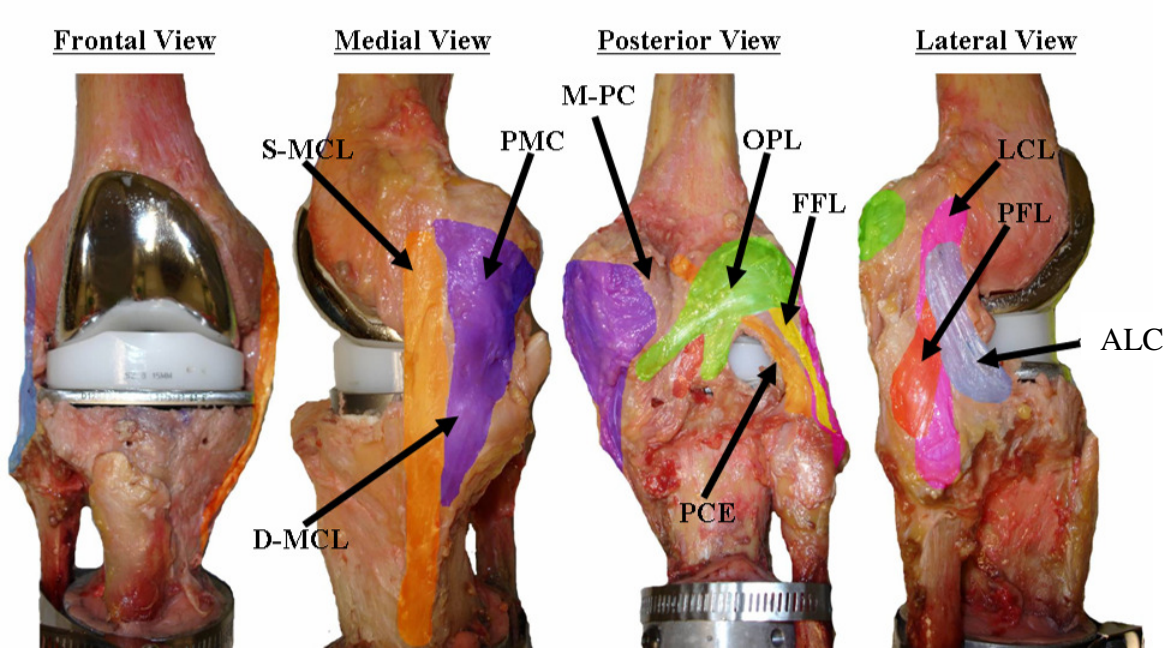

Figure 2-1: Ligament structures around the knee after removal of the skin and the extensor mechanism. The highlighted structures include the medial collateral ligament (orange), posterior medial capsule (purple), posterior lateral capsule (green), lateral collateral ligament (pink), and popliteal-fibular ligament (red). Structures identified by arrow include superficial MCL (s-MCL), deep MCL (d-MCL), postero-medial capsule (PMC), medial posterior capsule (m-PC), oblique popliteal ligament (OPL), posterior capsular extension (PCE), fabello-fibular ligament (FFL), LCL, popliteal fibular ligament (PFL), and the anterior-lateral capsule (ALC).

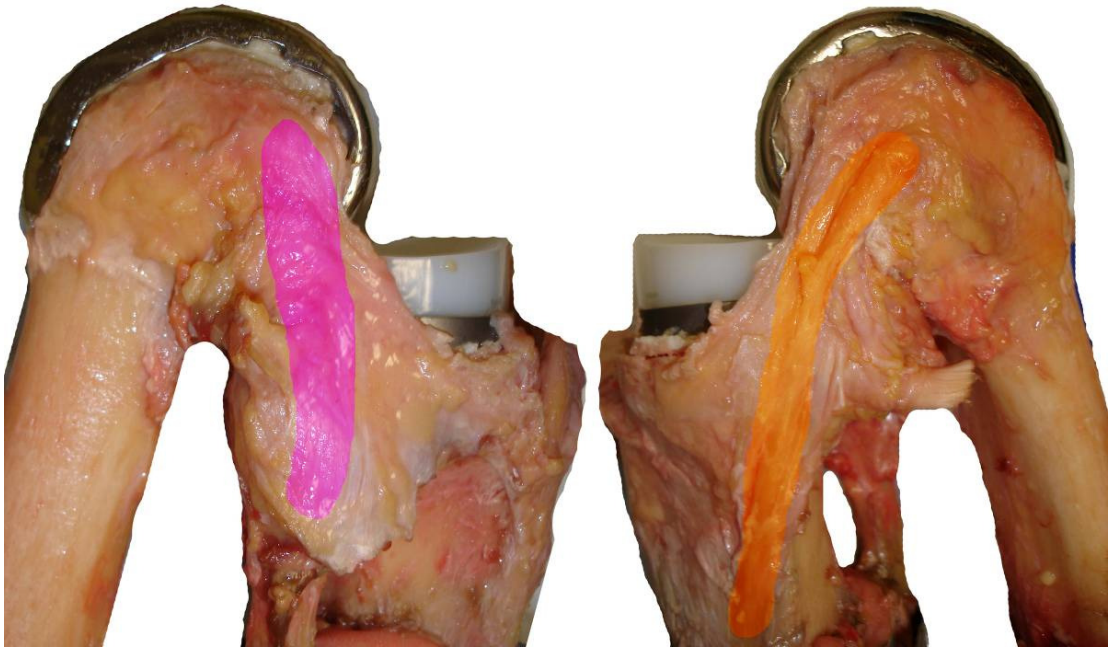

Figure 2-2: The location of the medial collateral ligament (orange) and lateral collateral ligament (purple) in deep knee flexion.

Chapter 3: Change in Knee Laxity Envelope with Total Knee Replacement

3.1 Introduction

The ligamentous structures and articular geometry of the intact natural knee provide stability during a wide range of functional activities throughout the flexion range. After total knee replacement, some patients lose the sense of stability [48, 49]. Several mechanisms are thought to contribute to knee instability after total knee replacement, ranging from implant geometry, to implant alignment, to balance of the soft tissue surrounding the knee.

Ligament balancing during total knee replacement (TKR) is performed at the discretion of the surgeon performing the operation, who may adhere to any of a variety of different balancing philosophies. Most balancing philosophies strive towards attaining rectangular gaps between the distal or posterior resections surfaces of the femur and the proximal resection surface of the tibia with the knee at full extension and at 90° flexion. However, this type of balancing procedure disregards the balance of the knee through the rest of the flexion range. Research has indicated that poor ligament balance can contribute to implant failure through increased wear rates [50], abnormal kinematics [51], or knee instability [48, 49, 52]. Despite the deleterious effects of ligament imbalance, there is little agreement on what constitutes a "well balanced knee," particularly in knee mid-flexion.

Many believe that ligament balance after TKR should return the knee to the ligament balance of the healthy intact knee joint, despite the dramatic changes to the

articulating surfaces and ligament constraints of the knee with TKR [53]. Unfortunately, when most patients arrive for knee replacement, their natural ligament balance has been adversely affected by knee OA, so it is difficult to know the healthy balance of a particular knee before the changes induced by onset of the disease.

Previous researchers have studied laxity of the knee joint in a variety of ways: intra-operatively using a CAS system and balancer [54, 55], on patients using an arthrometer [56-58] or manual manipulation [59-61], and in cadavers using custom loading devices [53, 62, 63]. Only a handful of these studies have compared the intact natural knee with the same knee after TKR, often with conflicting results. Using a CAS system intra-operatively, Casino et al. [59] documented a decrease in Varus-Valgus (Vr-Vl) laxity at full extension and no change at 30° flexion after TKR under manual Vr-Vl loading. In a cadaveric study, Van Damme et al. [53] found no difference in Vr-Vl rotation after TKR at full extension, but found a decrease in Vr-Vl ROM at 30°. Bull et al. [63] found no change in Vr-Vl ROM throughout the flexion range in cadaveric knees after TKR. These confounding results merit additional research to understand how knee laxity changes after TKR.

The purpose of the current study was to compare the Vr-Vl and Internal-External (I-E) laxity of healthy, intact knees before and after TKR through the entire flexion range and across a continuum of torque levels. My hypothesis was that knee laxity would be very similar before and after TKR at full extension and 90° flexion, where ligament balancing was performed, but may be different in mid-flexion.

3.2 Methods

3.2.1 Knee Preparation

Eight fresh frozen whole cadaveric legs (All Male, Age = 63 ± 12 years (mean ± standard deviation), BMI = 26 ± 4, 3 Right / 5 Left) were acquired for this experiment. The knees were screened radiographically for previous knee injury or scars from knee surgery and were excluded if found. Each leg was thawed at room temperature for 24 hours prior to testing. All soft tissue was removed from the leg beyond approximately 125 mm from the epicondylar axis with care taken to preserve knee ligamentous and capsular attachments. In addition, the tendons of the quadriceps musculature were isolated from the surrounding muscle tissue and preserved. The femur and tibia were sectioned 225 mm proximal and 175 mm distal to the epicondylar axis. Post dissection, MR images were acquired for each knee using a Siemans 1.5 Tesla MRI (CISS sequence). Following the MRI, tubular aluminum fixtures were cemented to the femur and tibia concentric with and parallel to the bone's intermedulary canal.

3.2.2 Manual Assessments

Each knee was subjected to a manual evaluation of the natural knee's envelope of motion. For the evaluation, the knee was arranged with the proximal end of the femur rigidly mounted to a base plate (Fig. 3.1). A 6-DOF load cell (JR3 Inc., Woodland, CA) was rigidly mounted to the distal end of the tibial fixture, 230-mm distal to the epicondylar axis with the long axis of the load cell roughly parallel to the S-I axis of the tibia. An analog lower limb, consisting of an aluminum tube for the

tibia affixed to an anatomically-shaped mannequin foot, was attached distal to the load cell. In this configuration, manual loads were applied to the knee via the analog foot while the forces and torques measured by the load cell were displayed on a monitor in view of the observer. Knee motion was captured during the assessments by tracking rigid arrays of infrared-light emitting diodes mounted to the tibial and femoral fixtures using an Optotrak 3020 camera system (NDI, Waterloo, Canada). The accuracy of relative rotations and translations measured using this system were 0.05° and 0.03 mm, respectively [64]. Load cell feedback and kinematic data were sampled at 100 Hz and synced using an electronic trigger and custom LabView Virtual Instrument subroutine (National Instruments Inc., Austin, Texas).

In this configuration, separate Vr-Vl and I-E manual envelope assessments were performed. During the Vr-Vl assessment, the knee was manually positioned in full extension, where a varus torque of approximately 10 N-m was applied and released over a period of one second, followed by a corresponding valgus torque. Subsequently, the knee was flexed approximately 5° and the load application repeated. This routine was repeated through the flexion range from full extension to full flexion, and back. The observer was careful to apply isolated varus and valgus torques by monitoring the load-cell output and correcting the applied torques as necessary. A corresponding evaluation was performed with I-E torques of approximately 8 N-m.

Following characterization of the natural knee's laxity envelope, a cruciate retaining (N=1) or posterior stabilized (N=7) total knee replacement (PFC Sigma,

Depuy Orthopaedics Inc., Warsaw, IN, USA) was implanted by a group of experienced surgeons. The surgery was performed through a medial sub-vastus approach using standard instrumentation and implants were cemented into place using bone cement. Implant alignment and soft tissue balancing were performed at the discretion of the surgeon until a "well-balanced knee" was attained. After TKR, the Vr-Vl and I-E envelope assessments were repeated.

The orientation of the load cell and the location of the TKR components and the existing bones were recorded relative to their respective tibial and femoral reference frames using a digitizing probe. Key geometric features of the load cell and implant geometry, along with point clouds of the implanted surfaces, were recorded.

3.2.3 Registration of Coordinate Systems and Knee Kinematics

Femoral and tibial anatomic coordinate systems were created and aligned with the native anatomy according to the system described by Grood and Suntay (Fig. 3.2) [65]. Using these coordinate systems as reference, the loads measured at the load cell were resolved into loads and torques applied about the knee. At each time step, the relative position between the femoral coordinate system and the coordinate systems of the tibia and load cell were calculated. Direction cosines were used to calculate the I-E component of measured load-cell torques applied along the S-I axis of the tibia. To calculate the Vr-Vl torque applied to the knee, a floating A-P axis was calculated mutually perpendicular to the femoral M-L axis and the tibial S-I axis and passing through the femoral origin at each time step. Contributions to the Vr-Vl torque from the measured load cell moments and forces were calculated independently. The

component of the measured load cell moments about the floating A-P axis was combined with the M-L force applied at the load cell multiplied by the moment arm along the S-I axis from the load cell origin to the floating A-P axis. Together, these combined moments constituted the total Vr-Vl torque applied to the knee. The 6-DOF kinematics between the tibia and femur were calculated using the same floating A-P axis as part of a three-cylindrical open chain system.

CAD geometry supplied by the manufacturer of the tibial and femoral components were manually placed into their respective local reference frames relative to the rigid bodies, in line with their probed locations during the experiment. The implant surfaces were meshed using 1-mm triangular elements. The nodes in these meshes were tracked during the envelope assessments, and the lowest node in the tibial S-I direction on the medial and lateral condyles were identified at each time step. Estimates of condylar lift-off were performed by subtracting the minimal S-I height of the condyle from the maximal S-I height observed at each flexion angle.

3.2.4 Calculating Knee Stiffness

Due to the nature of the manually applied loads, there were inherent variations in the torque versus rotation behavior between load application cycles. These variations were attributed to differences in the rate, direction, and magnitude of the torques applied by the researcher. Any manual knee assessment performed by a physician would be subject to these same variations.

The soft tissue structures around a healthy knee are variably recruited at different flexion angles, indicating that the soft tissue constraint around the knee is

continuous through the flexion range (i.e. there is not a discrete jump in the constraint between two adjacent flexion angles because a particular ligament was instantaneously recruited) [62]. Based on these anatomical and functional observations, a custom fitting routine was developed to determine the overall torque versus rotation response of the knee through the flexion range. For each Vr-Vl or I-E envelope assessment, the load application portions (from zero to peak torque at a particular flexion angle) of the evaluation were isolated. For each load application cycle, knee rotations at particular load levels (0 N-m through 8 N-m for internal and external rotations and 0 N-m through 10 N-m for varus and valgus rotations) were extracted and fifth-order polynomials were fit to the extracted rotations at each torque level through the flexion range (Fig 3.3a). Each of these polynomials were evaluated at 0°, 30°, 60°, and 90° knee flexion to determine the overall torque versus rotation response of the knee (Fig. 3.3b).

3.2.5 Sensitivity to Experimental Error

It has been previously demonstrated that three-cylindrical open chain kinematic descriptions of knee motion are sensitive to positioning of the anatomic reference frames [66]. In particular, very small mal-alignment of the M-L axis of the femur can create "cross-talk" between the axes such that knee flexion appears as Vr-Vl rotation. While only a small percentage of the flexion rotation is manifested as Vr-Vl rotation, when analyzing motions through the entire flexion range, this artifact can become significant. To understand how small variations in the alignment of the femoral and tibial coordinate systems influence the evaluated torque verse rotation

behavior of the knee, a Monte-Carlo analysis was performed. A series of finite rotations and translations about or along all six kinematic degrees of freedom were applied to both the femur and tibia coordinate systems for one particular knee subject. The magnitudes of these perturbations were randomly selected from a normal distribution with standard deviations of 1° for rotations and 0.5-mm for translations, based on the repeatability of registering the implant CAD geometry with probed features on the implant. Using the new coordinate systems, the above analyses were performed. This process was repeated 500 times to establish the range of variation created by inaccuracies in the experimental process. To quantify the amount of resultant variation in the I-E and Vr-Vl laxity measurements, the 5% and 95% confidence intervals were calculated.

To isolate Vr-Vl rotation in the Vr-Vl envelope measurement from any kinematic artifacts of knee flexion, the "passive" Vr-Vl rotation as a function of flexion, determined by calculating the average Vr-Vl rotation of the knee at each flexion angle while zero torque was applied to the knee, was subtracted from the envelope Vr-Vl laxity calculation at each flexion angle. This same adjustment was performed on all Vr-Vl envelope assessments analyzed for this study.

3.2.6 Inter-observer Variability

While all of the envelope assessments reported in this study were performed by the same researcher (CC), it was important to characterize the inter-observer repeatability of the assessment for future research. After a demonstration of the technique, five different researchers were asked to perform the Vr-Vl and I-E

envelopes on the same natural specimen. The standard deviations of the observed Vr-Vl and I-E rotations were calculated across all five observers at the smallest peak loads applied by any of the observers for both Vr-Vl and I-E assessments.

3.2.7 Statistical Analysis

To determine significant changes in the behavior of the knees through the flexion range and before and after TKR, 2-way repeated measures ANOVA tests were performed on the internal, external, varus, and valgus peak rotations for each group of knees. For each 2-way repeated measures ANOVA, the two factors were flexion angle (0°, 30°, 60°, and 90°) and knee condition (Natural versus TKA). Tukey HSD post hoc tests were performed to determine more specifically where significant differences existed.

3.3 Results

3.3.1 Natural versus Post-TKR Envelopes

On average, the natural knee was tightest in full extension for both Vr-Vl and I-E rotations. The overall Vr-Vl range of motion (ROM) increased from 2.6° at full extension to 6.7° at 30° flexion, after which the Vr-Vl ROM remained relatively consistent with increasing knee flexion (Fig. 3.7, Table 3.2). At full extension and 30° flexion, the natural knee was balanced with the overall ROM divided evenly between varus and valgus rotations. At 60° and 90° flexion, there was more varus laxity than valgus, indicating the lateral soft tissue structures were, on average, more lax than the medial in deeper flexion.

The average I-E ROM significantly increased from 14.0° at full extension to 29.1° at 30° flexion (Fig. 3.8, Table 3.3) ($p<0.00$). The overall I-E ROM remained consistent beyond 30° flexion. Unlike Vr-Vl rotation, the overall I-E ROM was evenly distributed between internal and external rotations.

After TKR, the only significant change in knee laxity was an increase in varus rotation ($p<0.03$). Tukey Post Hoc tests indicated the significant increases occured at 30° and 60° flexion (Fig. 3.7, Table 3.2). Increased varus laxity at 30° and 60° was observed in all eight specimens tested. There were no significant changes in the Vr-Vl laxity at full extension or at 90° flexion, or in I-E laxity at any flexion angle. In terms of condylar lift off, increased varus rotation at 30° and 60° corresponded to 5.4 mm and 5.2 mm of lateral condyle lift off, compared to 1.8 mm at full extension and 3.7 mm at 90° flexion (Fig. 3.9, Table 3.4). On the medial side, the valgus torque caused 1.2 mm of medial condyle lift off at full extension, and between 2 and 3 mm of lift off through the rest of the flexion cycle.

3.3.2 Experimental Variability

The calculated knee laxity was sensitive to the orientation of the coordinate systems. For Vr-Vl envelopes, the average 5% - 95% confidence interval for rotations calculated at 10 N-m was ±2.42° (Fig. 3.4a). For I-E envelopes, the same average confidence interval, calculated at 5 N-m, was ±2.46° (Fig. 3.5). Although of similar magnitude, the variations were more severe for Vr-Vl rotation than for I-E rotation because of the decreased overall ROM of Vr-Vl rotations. Most of the observed variation in Vr-Vl rotations could be attributed to an offset of the Vr-Vl rotation with

flexion and, to a lesser extent, a change in magnitude of the rotation. Subtracting off the passive Vr-Vl rotation through the flexion range reduced the sensitivity of the Vr-Vl envelope calculation to variation in the coordinate systems, reducing the 5% and 95% confidence interval to ±0.46° (Fig. 3.4b).

The variation between observers was smaller than the variation associated with the coordinate systems; the resulting envelopes from each observer are shown in Fig. 3.6. The primary difference between researchers was the overall magnitude of the applied torques. Despite this variation, the predicted envelopes were very similar between researchers. The maximum I-E standard deviation of 0.94° was observed in internal rotation at full extension (Table 3.1). For Vr-Vl, the maximum standard deviation of 0.36° was observed in valgus rotation at 120° knee flexion.

3.4 Discussion

In this experiment, the effect of total knee replacement on cadaveric knees' Vr-Vl and I-E laxity was assessed using a novel manual manipulation procedure. The experiment was intended to assess knee balance at full extension and 90° flexion, where surgeons typically balance the knee, and also in knee mid-flexion where knee balance is often overlooked. This experiment showed the Vr-Vl laxity of the knee joint was unchanged at full extension and 90° flexion, but showed a significant increase in varus rotation at 30° and 60° knee flexion. No significant changes were documented in the I-E laxity of the knee joint.

While most ligament balancing procedures strive towards balanced flexion and extension gaps, recent research has noted asymmetry in the laxity of the natural

knee joint in mid and deep flexion [53, 58, 67]. The findings of the present study support this observation, noting that varus rotation accounted for 59% and 63% of the overall natural Vr-Vl ROM at 60° and 90° knee flexion, respectively. This ratio was consistent after TKR, with varus rotation accounting for 64% of the overall Vr-Vl ROM at both 60° and 90° knee flexion. While this is not evidence that surgeons should stop striving for a balanced flexion gap, it does reinforce the classical notion of a medial pivoting knee with a less constrained lateral condyle. Most modern tibial inserts have a more conforming lateral plateau than the natural knee, which could change the role of the lateral soft tissue in restraining lateral condyle translation, and therefore the optimum balance after TKR.

The current study noted significant changes in the varus laxity of the knee after total knee replacement at 30° and 60° knee flexion. Similarly, Draganich and Pottenger [60] reported a 2° increase in Vr-Vl ROM at 20° knee flexion for patients with TKR, although this difference was not significant. As shown by the current study, the laxity of the knee joint increased rapidly from full extension to 30° knee flexion after TKR. Perhaps if Draganich and Pottenger had performed the Vr-Vl laxity assessment at 30° knee flexion, the reported increase in Vr-Vl ROM may have been significant. In a cadaveric study of knees before and after TKR, Bull et al. [63] also did not note a significant increase in overall Vr-Vl ROM after TKR; however, their results did demonstrate an increase in varus laxity in conjunction with a decrease in valgus laxity beyond 30° knee flexion.

Van Damme et al. [53] reported contradictory findings in a similar cadaveric study noting a significant decrease in the varus laxity of the knee after TKR at 30° and 90° knee flexion. Likewise, Casino et al. [59] reported no significant change in Vr-Vl knee laxity after TKR at 30° knee flexion measured intra-operatively using a CAS system and manual manipulation of the leg. While each of these studies have reported slightly different levels of Vr-Vl laxity, most agree with the current study that there is little change in the I-E laxity of the knee joint after TKR [59, 60, 63].

Given the variability in surgical technique, implant alignment, ligament balancing, implant design, and loading conditions between the different studies discussed above, there is little surprise that inconsistencies exist in the Vr-Vl ROM results. In general, the standard deviations of the reported Vr-Vl laxity after TKR in the current study were larger than the standard deviations in the natural knee, which is evidence that surgical technique alone can introduce a large amount of variation into the knee's overall response. In addition to surgical technique, femoral implant articular geometry likely played a role in the increased knee laxity. Most current implants simplify the asymmetric geometry of the natural femur [2] into symmetric femoral condyles with equal radii, including the implant in this study, and may not accurately recreate the curvature of the natural femur in mid flexion. Additional experimentation and analyses are needed to determine the potential contribution of each confounding factor to increased varus laxity.

The relatively simple experimental method used to determine knee laxity in this study proved effective in determining the subtle differences in knee laxity before

and after TKR. The inter-observer repeatability for most measured rotations was on the order of 0.1-0.2° for Vr-Vl rotations, and 0.3°-0.4° for I-E rotations. Likewise, the approximation of the experimental error associated with perturbation of knee coordinate systems (0.46° and 2.42° for Vr-Vl and I-E rotations, respectively) would not effect intra-specimen comparisons since the same coordinate system was used for analysis before and after TKR. Since the significant changes in knee laxity observed after TKR (increased varus rotations at 30° and 60° knee flexion) were much larger than the overall repeatability of the procedure, the potential error in the procedure would not likely influence the results.

The current experiment was subjected to a number of limitations. As with any experimentation on cadaveric tissue, tissue degradation throughout the experiment was a major concern. To preserve the soft tissue surrounding the knee joint, the skin was left in place to prevent dehydration, the knees were routinely sprayed with a physiological saline solution, and the envelope assessments were performed directly after the TKR was complete. Another drawback to cadaveric testing is the lack of muscular contraction that may contribute to lateral stability. In particular, because of the experimental configuration, all musculature that spans from the knee to the pelvis were transected, including the hamstrings and iliotibial band. The iliotibial band, in particular, has been shown to stabilize varus rotations of the knee in mid-flexion [68]. Since this loss of musculature constraint applied to both the natural and TKR evaluations, the overall change in laxity after TKR would be unaffected.

The surgeries in this study were performed by four different surgeons, who each employed their own surgical philosophy. While this approach was useful to assess the robustness of knee laxity after TKR to different surgical techniques, it also introduced a confounding variable to the analysis. Although a CAS system was not used in this experiment to standardize knee component placement, CAD models of the implanted components were registered to MRI-generated solid models of the patients' bones. Future analyses will assess the impact of implant alignment relative to the patients' existing articular geometry on the resulting knee laxity. Also, in future testing, an instrumented gap-balancing tensor will be used to categorize inter-operative ligament balance.

Once the mechanisms influencing knee laxity are understood, the fundamental question of what is the optimal knee balance still exists. Some authors have suggested, based on clinical outcomes, that 8° of Vr-Vl rotation at full extension are acceptable [56], while others have suggested that patients who have bi-lateral knee replacements claim the looser knee feels more natural [69]. Each of the knees tested in this experiment underwent dynamic simulations of a deep knee bend and a gait cycle in the Kansas Knee Simulator [70]. Future work will focus on determining the influence of knee laxity on knee kinematics during these dynamic assessments.

3.5 Tables and Figures

Table 3-1: The standard deviations of the rotations observed at 5 N-m of internal-external torque and 10 N-m of varus-valgus torque calculated from five different observers performing the I-E and Vr-Vl envelope assessments on the same natural knee specimen.

Flexion Angle	Standard Deviations			
	Ext.(°)	Int.(°)	Val(°)	Var.(°)
0°	0.31	0.94	0.19	0.09
30°	0.30	0.33	0.12	0.12
60°	0.43	0.37	0.19	0.08
90°	0.37	0.33	0.27	0.10
120°	0.41	0.78	0.36	0.08

Table 3-2: The average (± standard deviation) varus and valgus rotations and overall Vr-Vl ROM observed at 10 N-m of Vr-Vl torque during the Vr-Vl envelope assessments before and after TKR for eight specimens. Bars indicate significant differences ($p < 0.05$).

Flexion Angle	Natural Vr-Vl ROM			TKR Vr-Vl ROM		
	Val.(°)	Var.(°)	ROM(°)	Val.(°)	Var.(°)	ROM(°)
0°	1.4 ± 0.8	1.2 ± 0.7	2.6	2.0 ± 1.4	2.5 ± 1.8	4.5
30°	3.1 ± 1.9	3.6 ± 4.1	6.7	3.9 ± 3.0	6.6 ± 2.2	10.5
60°	2.9 ± 2.0	4.1 ± 1.5	7.0	3.9 ± 2.6	6.8 ± 1.9	10.6
90°	2.7 ± 1.5	4.6 ± 1.7	7.3	3.2 ± 1.1	5.7 ± 2.3	8.9

Table 3-3: The average (± standard deviation) internal and external rotations and overall I-E ROM observed at 5 N-m of I-E torque during the I-E envelope assessments before and after TKR for eight specimens.

Flexion Angle	Natural I-E ROM			TKR I-E ROM		
	Ext.(°)	Int.(°)	ROM(°)	Ext.(°)	Int.(°)	ROM(°)
0°	7.8 ± 3.2	6.2 ± 1.5	14.0	6.8 ± 4.7	5.8 ± 4.1	12.6
30°	14.2 ± 4.4	14.9 ± 2.7	29.1	14.5 ± 5.7	17.7 ± 6.8	32.2
60°	13.6 ± 4.1	15.8 ± 4.5	29.5	14.8 ± 6.1	18.3 ± 7.4	33.1
90°	14.8 ± 4.2	15.7 ± 4.2	30.5	14.4 ± 5.0	17.3 ± 6.4	31.7

Table 3-4: The average (± standard deviation) medial and lateral condyle lift off observed at 10 N-m of valgus and varus torque, respectively, during the Vr-Vl envelope assessments after TKR for eight specimens.

Flexion Angle	Medial Liftoff (mm)	Lateral Liftoff (mm)
0°	1.2 ± 1.1	1.8 ± 0.9
30°	2.6 ± 2.1	5.4 ± 1.2
60°	2.8 ± 2.0	5.2 ± 1.6
90°	2.6 ± 1.8	3.7 ± 2.0

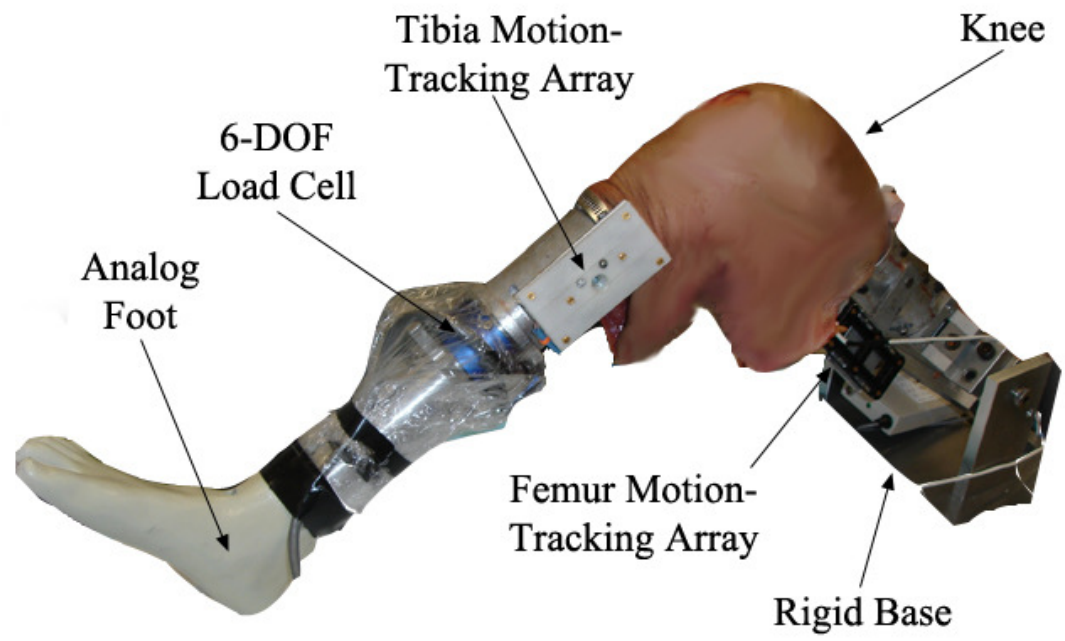

Figure 3-1: The experimental setup whereVr-Vl and I-E envelope assessements were administered to cadaveric knees. Loads to the knee via the prosthetic foot were measured by a 6-DOF load cell mounted between the foot and the tibia. Knee kinematics through the assessment were tracked by arrays of infrared emitting diodes attached to the tibia and femur.

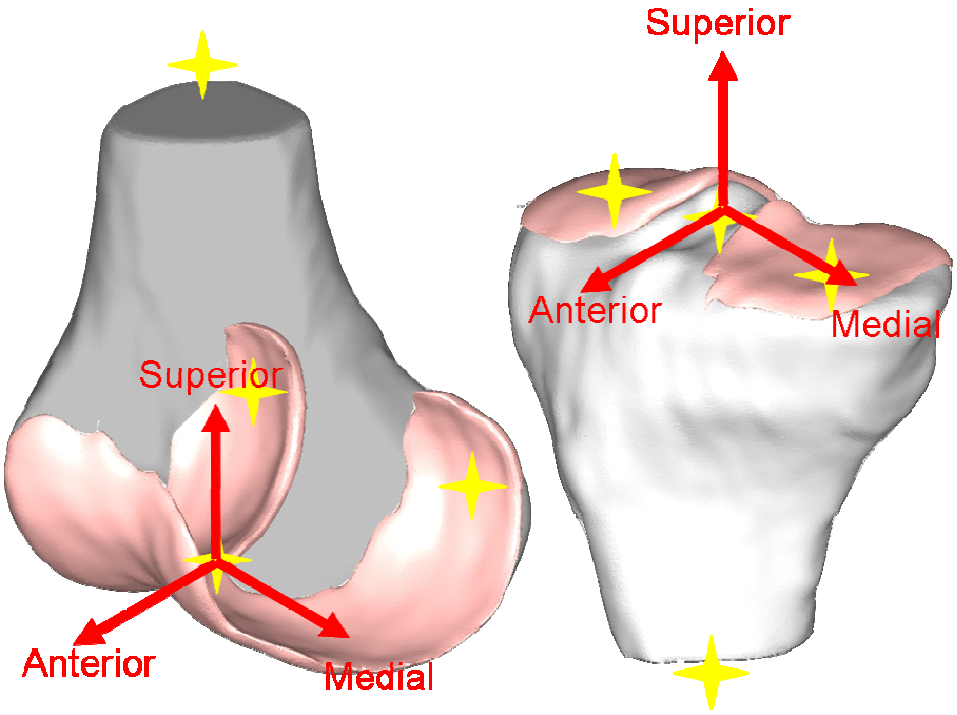

Figure 3-2: Coordinate systems were created on the femur and tibia (red arrows) using anatomical features on the bones (yellow stars), including the most posterior points on the medial and lateral femoral condyles, the center of the superior end of the femoral intermedulary canal, the most anterior point on the intercondylar notch, the centers of the medial and lateral tibial plateaus, the central point between the intercodylar eminences, and the center of the intermedulary canal at the distal end of the tibia.

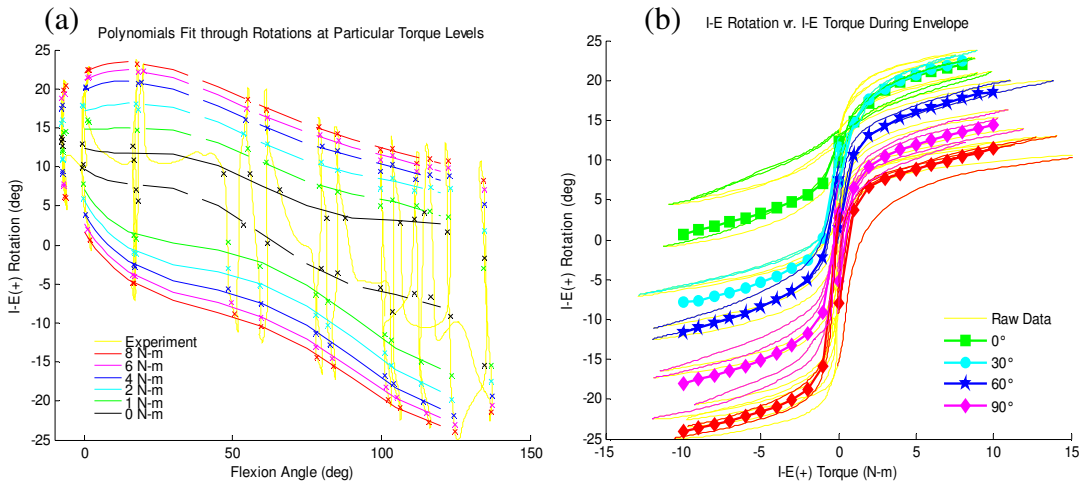

Figure 3-3: (a) Raw experimental I-E rotation (yellow) were recorded during an I-E envelope assessment as a function of flexion angle. I-E rotations at particular torque levels (-8 N-m through 8 N-m) were identified through the flexion range from the load cell feedback (x's), and then fifth-order polynomials were fit to those rotations (solid colored lines (internal rotation) and dashed colored lines (external rotation)). (b) The polynomials were evaluated at 0°, 30°, 60° and 90° knee flexion to determine the I-E rotation for each torque level.

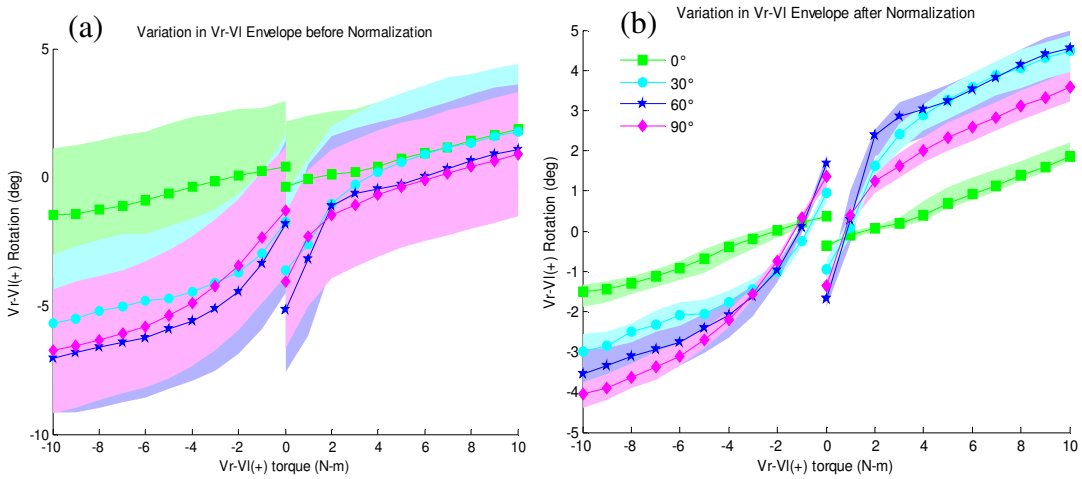

Figure 3-4: (a) Mean and 5%-95% confidence intervals of variation in the Vr-Vl rotations due to potential variation in defining tibial and femoral coordinate systems. These bounds were calculated for a particular subject during a Vr-Vl envelope using a Monte-Carlo simulation of perturbations of the tibial and femoral coordinate systems. (b) The variation in calculated Vr-Vl rotation was dramatically reduced by subtracting the average neutral Vr-Vl rotation with knee flexion from the envelope calculations. This indicates that changes in the tibial and femoral coordinate systems primarily affect the amount of Vr-Vl rotation observed with flexion and, to a lesser extent, the overall magnitude of Vr-Vl rotation from the neutral position at a given flexion angle.

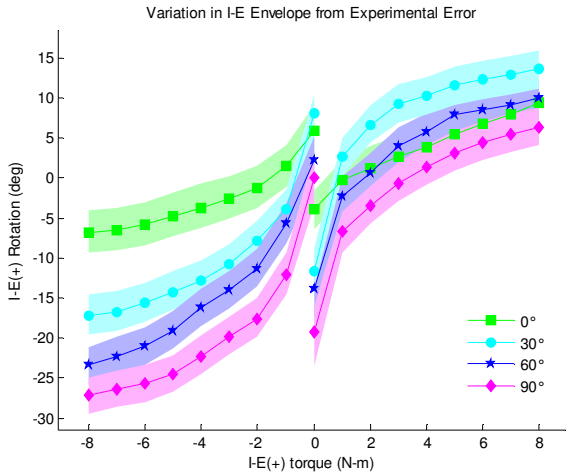

Figure 3-5: Mean and 5%-95% confidence intervals of variation in the I-E rotations due to potential variation in defining tibial and femoral coordinate systems. These bounds were calculated for a particular subject during an I-E envelope using a Monte-Carlo simulation of perturbations to the tibial and femoral coordinate systems.

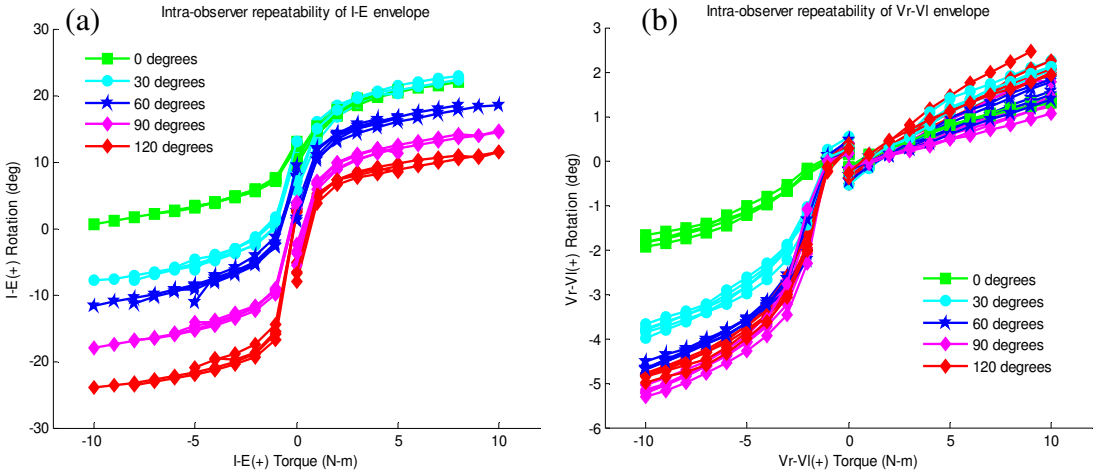

Figure 3-6: (a) I-E envelope calculations from 5 different observers performing I-E envelope assessments on the same natural specimen. While all observers followed the same protocol, they applied the I-E torque at different magnitudes, although this did not significantly affect the calculated I-E rotation values. (b) The Vr-Vl envelope calculations from the same 5 observers.

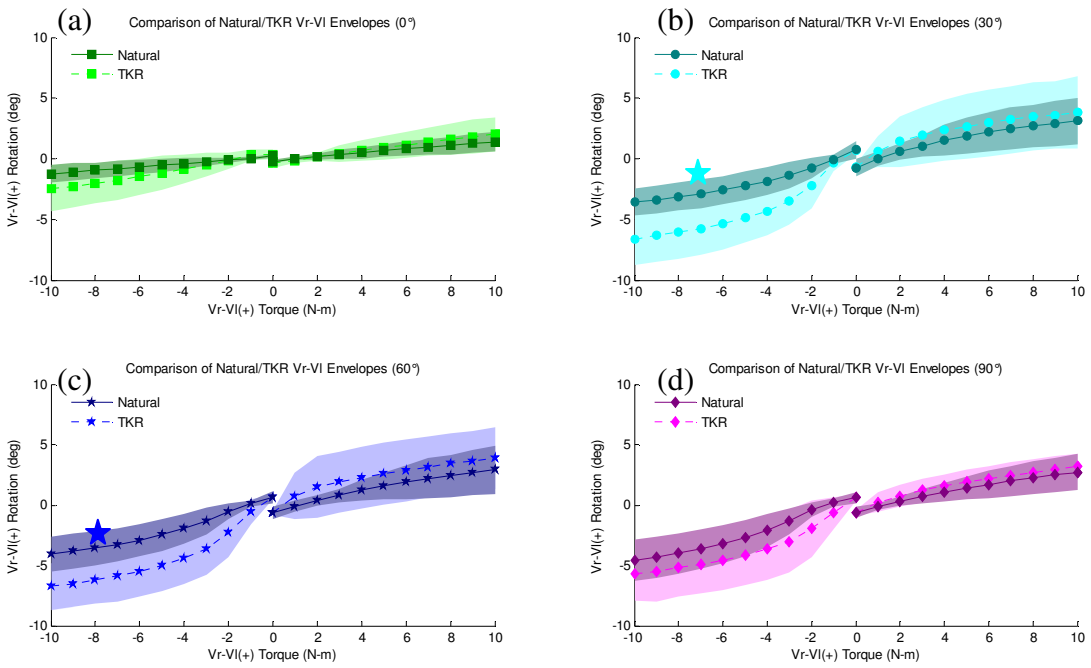

Figure 3-7: Mean and ± one standard deviation (shaded region) of Vr-Vl rotations before and after TKR at (a) full extension, (b) 30°, (c) 60°, and (d) 90° knee flexion. Significant ($p<0.05$) increases in Varus rotation were observed at 30° and 60° knee flexion after TKR (indicated by stars).

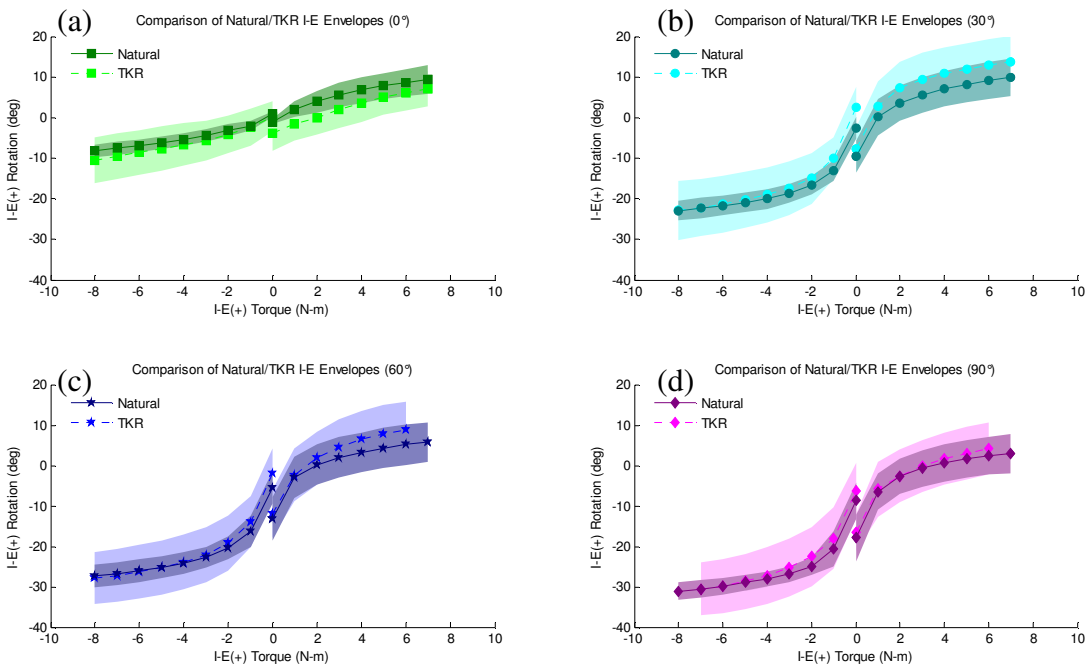

Figure 3-8: Mean and ± one standard deviation (shaded region) of I-E rotations before and after TKR at (a) full extension, (b) 30°, (c) 60°, and (d) 90° knee flexion. No significant differences in I-E rotation were observed at any flexion angle after TKR.

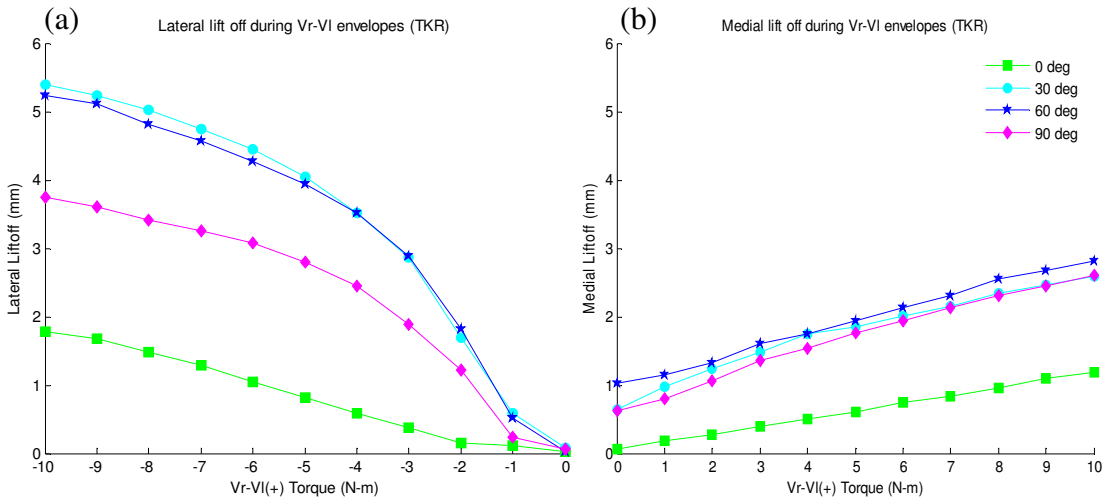

Figure 3-9: Average lift off of the (a) lateral condyle during varus torque and of the (b) medial condyle during valgus torque applied to the knees after TKR. Lift off increased dramatically from full extension to 30° flexion for both the medial and lateral condyle. At each flexion angle, the lateral condyle experienced more lift off, on average, than the medial codyle.

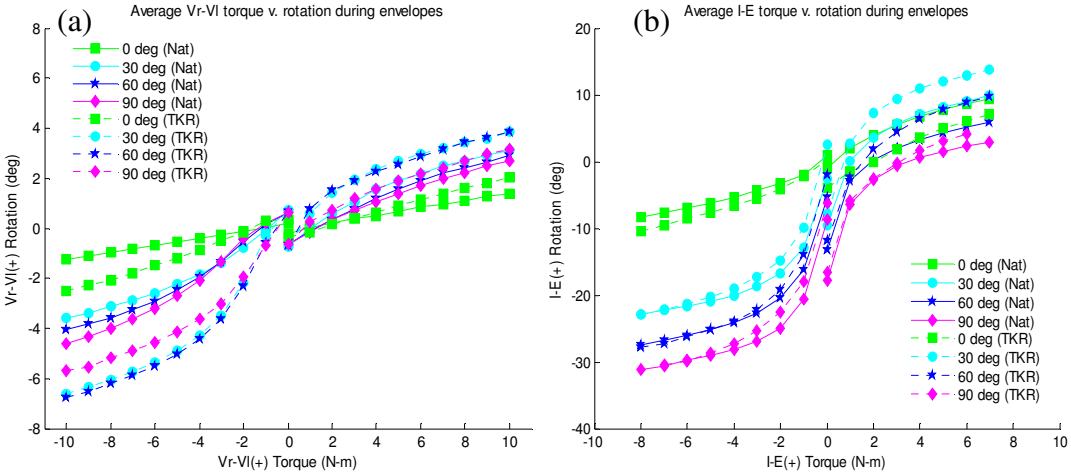

Figure 3-10: Alternate to Figs. 3.7 and 3.8. A comparison of knee rotations during the (a) Vr-Vl and (b) I-E envelope before (solid lines) and after (dashed lines) TKR.

Chapter 4: Assessment of a Computational Knee Model's Ability to Predict Patient-Specific Knee Laxity

4.1 Introduction

Computational models of the knee after total knee replacement have provided valuable insight into knee kinematics [71-74], contact mechanics [75, 76], wear properties [77, 78], and the effect of variation in surgical technique [79, 80]. These models range in sophistication from 2-dimensional sagittal-plane models [74] to full 3-dimensional representations of the articular geometry and soft tissue constraint [81]. As computational knee models grow more sophisticated, an opportunity exists to incorporate these models, coupled with computer-aided surgery, into the operating room as a tool for surgeons. Efficient generation of patient-specific knee models remains a significant barrier to this process [36].

Perhaps the most difficult challenge in building patient-specific knee models is accurate representation of the constraint provided by soft tissue structures surrounding the knee. Several different approaches have been used to model soft tissue in a computational environment, ranging from computationally efficient non-linear springs [26, 33, 62, 75, 79, 82-84] to computationally expensive continuum models of the ligament geometry [23, 25, 37, 38, 81]. For all of these representations, a fundamental question persists: how sophisticated do ligament models need to be to accurately capture the ligament constraint provided at the knee *in vivo*?

Several authors have used anatomic configurations of non-linear springs that mimic the ligament geometry of the knee to predict knee laxity. In a series of studies,

Mommersteeg and Blankevoort [30, 33, 35] constructed a patient-specific model of the natural knee using multiple non-linear springs to represent the MCL, LCL, ACL, and PCL based on cadaveric experiments. The model-predicted laxity showed good agreement with experimentally-observed Vr-Vl and A-P laxity, lending credence to the concept that multi-bundle non-linear springs could recreate the appropriate ligament constraint in the natural knee. However, in a similar study, Blankevoort et al. also demonstrated that using non-optimized values for ligament stiffness and reference strain led to a poor prediction of joint laxity [85]. Abdel-Rahman et al. later proposed a model incorporating additional structures, including posterior-capsular elements, although this model was not derived from a particular subject so no comparison could be made with the laxity of the actual knee [26].

Despite their extensive use in literature, no study has ever expressly evaluated the ability of anatomic configurations of non-linear springs to provide the appropriate level of constraint for patient-specific knee models after total knee replacement. Furthermore, it is unclear how uncertainty in the ligament parameters used in the models, including attachment site, reference strain, and stiffness, would impact laxity predictions.

Based on the success of Blankevoort and colleagues to predict patient-specific natural knee I-E laxity using non-linear springs, the objective of the current study is to evaluate the ability of an anatomic configuration of non-linear springs, incorporating uncertainty associated with ligament parameters, to recreate I-E and Vr-

Vl knee laxity through the flexion range after total knee replacement. Additionally, the sensitivity of these ligament parameters affecting knee laxity will be determined.

4.2 Methods

4.2.1 Experimental Assessment of Stability Envelope

Two fresh frozen whole cadaveric legs (Both Male, Ages = 80 and 68 years, BMI = 28.1 and 30.2) were acquired for this experiment. The knees were prepared for experimental testing as previously described [Chapter 3], including acquisition of MR images of the knees. A total knee replacement was performed on both knees, using either a posterior-stabilized (Knee 1) or cruciate-retaining (Knee 2) Sigma fixed-bearing total knee replacement (DePuy Orthopedics, Warsaw, IN). The surgeries were performed through a medial sub-vastus approach using standard instrumentation. Implant alignment and soft tissue balancing were performed at the discretion of the surgeons until "well-balanced knees" were attained.

Following the surgeries, manual "envelope of motion" assessments of Vr-Vl and I-E knee stability were performed, as previously described [Chapter 3]. The knees were then dis-articulated and point clouds of the TKR components, the existing bones, and the origin and insertion sites of the major remaining knee ligaments (MCL, LCL, PFL, and PCL (for the CR knee)) were recorded relative to their respective experimental tibial or femoral reference frames using a digitizing probe (Fig. 4.1). CAD geometry supplied by the manufacturer of the tibia and femur

components were manually placed into their respective experimental reference frames, in line with their probed location during the experiment.

Using the implanted component geometry as reference, local coordinate systems on the femur and tibia were established. The femoral S-I axis was perpendicular to the distal-cut surface of the implant, the femoral M-L axis was along a line between the geometric centers of radii used to define the distal femoral articular geometry (sometimes referred to as the "femoral facets"), and the A-P axis was the cross product of the S-I and M-L axes. The origin of the femoral coordinate system was on the M-L axis and centered in the frontal plane at the midpoint between the femoral facets.

The tibial S-I axis was perpendicular to the distal plane of the tibial implant, the M-L axis was parallel to the posterior edge of the implant, and the A-P axis was the cross product of the S-I and M-L axes. The origin of the tibial coordinate system in the sagittal plane was placed at the lowest point of sagittal plane curvature of the tibial articular geometry and in the frontal plane at the midpoint between medial and lateral plateaus. Using these coordinate systems and the instrumented load cell in the leg, knee torque versus rotation through the flexion range was calculated from the manual envelope assessments [Chapter 3]. In addition, the lowest point on the femoral mesh in the S-I direction was tracked during the I-E envelopes, such that condylar A-P translation could be represented as a function of I-E torque and flexion angle.

4.2.2 Computational Knee Model

Computational models of both experimental knees were created using MSC/Adams (MSC Software, Santa Ana, CA), a software that has been used previously to evaluate total knee replacement behavior [86]. The models included the implant articular geometries, non-linear springs to represent ligament constraint (Fig. 4.2), and a set of linkages to apply loads between the tibia and femur (Fig. 4.3).

Parasolid models of the total knee replacement articular geometry, obtained from DePuy, Inc. (Warsaw, IN), were used to represent the articulating surfaces of the implants. The tibia and femur geometries were positioned in an initial configuration of the knee at full extension in neutral alignment. Rigid contact was assumed between the tibia and femur using a Hertzian contact model based on the ratio of the radii for the femoral condyles to the sagittal plane curvature of the tibial tray. The parameters for the contact definition were an impact stiffness of 30,000 N/mm, a damping of 250 N*s/mm, an exponent of 1.5, and a maximum penetration depth of 0.1 mm [87]. The static and dynamic coefficients of friction between titanium (femur) and polyethylene (tibia) were assumed to be 0.02 [87].

A set of non-linear springs acting between nodes on the tibia and femur, adapted from formulations by Abdel-Rahman et al. [26] and Mommersteeg et al. [33] were used to constrain motion between the tibia and femur (Fig.4.2). Three springs were used to represent the superficial layer of the MCL (anterior, central, and posterior bundles), which originated on the medial epicondyle and inserted obliquely along the anterior ridge of the tibial shaft. An additional spring, spanning from the

medial epicondyle to the posterior-medial rim of the tibia, was included to represent the posterior-medial capsule (PMC).

On the lateral side, the LCL was composed of three springs (anterior, central, and posterior bundles) spanning from the lateral epicondyle to the head of the fibula. A spring, spanning from distal and anterior of the lateral epicondyle to the posterior-superior face of the fibula, was included to represent the popliteal-fibular ligament (PFL). An anterior-lateral capsule structure (ALC), which spanned from the lateral epicondyle to the anterior-lateral border of the tibia, was included to represent constraint provided by the anterior-lateral capsular fibers [28].

A semi-anatomic spring configuration was used to represent the constraint provided by the posterior capsule: two vertical spring elements for the posterior capsule, which spanned superior to inferior over the medial and lateral posterior condyles, and two oblique springs, analogous to the oblique popliteal ligament (OPL) and the popliteus capsular extension (PCE) [14], which formed an "x" crossing the posterior aspect of the knee. In the CR model (Knee 2), a PCL was included, composed of two springs, an antero-lateral (a-PCL) and a postero-medial (p-PCL) bundle. Origin and insertion sites of the each ligament element, in both the PS and CR models, were positioned coincident with the centroid of the ligament attachment footprint probed during the experimental testing. For ligaments composed of multiple springs (MCL and LCL), the central spring was positioned at the center of the ligament attachment footprint. The anterior and posterior bundles were set an equal

length anterior or posterior to the central spring insertion based on the A-P size of the ligament footprint.

Each spring had a linear stiffness with a parabolic toe-in region based on the mathematical-model used by Abdel-Rahman et al [26]. The behavior of each element was parameterized so that the force vs. displacement behavior was defined by four variables: the ligament length (L), the ligament free length (L_0), the transition strain from toe-in to linear region (ε_t), and the linear stiffness (K^2). For the j^{th} ligament element, the force produced (F_j) was determined by Eqns. 4.1 and 4.2.

$$F_j = \begin{cases} 0, & \varepsilon_j \le 0 \\ K_j^1 (L_j - L_{0j})^2, & 0 \le \varepsilon_j \le 2\varepsilon_t \\ K_j^2 [L_j - (1+\varepsilon_t) L_{0j}], & \varepsilon_j \ge 2\varepsilon_t \end{cases} \qquad \text{(Equation 4.1)}$$

Where:

$$K_j^1 = \frac{K_j^2}{4 L_{0j} \varepsilon_t} \qquad \text{(Equation 4.2)}$$

The reference strain (ε_P) in each ligament was defined as the amount of strain in each element in the initial configuration of the model at full extension and used to determine the ligament free length using the equation:

$$L_{0j} = \frac{1}{\varepsilon_{Pj}} \sqrt{[\left(x_{0j}^o - x_{0j}^i\right)^2 + \left(y_{0j}^o - y_{0j}^i\right)^2 + \left(z_{0j}^o - z_{0j}^i\right)^2]} \qquad \text{(Equation 4.3)}$$

Where, x, y, and z are the locations of the origin and insertion sites in the initial configuration of the model at full extension. A ligament reference strain of 1.0 would indicate the length of the ligament at full extension was the free length, while reference strains of 0.99 or 1.01 would indicate that the ligament was loose or tense, respectively, in the initial position Values for ligament stiffness (K^2) were derived from tensile tests published in the literature [9, 11, 13] and a transition strain (ε_t) of 0.03 was used

External loads and motions were applied to the femur and tibia components via a virtual linkage system based on a three-cylindric knee kinematic description [65]. The linkage system (Fig. 4.3) that connected the tibia to the femur was composed of three rigid mass-less links and three mass-less, frictionless linear bearings The medial-lateral linkage was affixed to the femur, the superior-inferior linkage was affixed to the tibia, and the varus-valgus linkage was a floating axis mutually perpendicular to the first two linkages. In this configuration, the tibia was rigidly affixed to the ground, and all motions occurred at the femur.

During the computational envelope assessments, isolated sequential varus, valgus, internal, and external torques were applied about the Vr-Vl and I-E linkages at 0°, 30°, 60° and 90° knee flexion. The application of each torque ramped from 0 N-m to the full amplitude (10 N-m for Vr-Vl torques, and 5 N-m for I-E torques) and back to 0 N-m following a cosine curve. A small compressive load was applied and released to the knee joint before each torque application to ensure the knee was in the neutral position. Total model run time to initialize the model and evaluate all loading

cycles at all flexion angles was approximately 6 minutes on a computer with dual quad-core 2.66 GHz processors and 3 GB of RAM. Up to seven simulations could be run in parallel with little effect on overall run time.

Three-cylindrical open-chain knee kinematics were extracted from the model using the same coordinate system used in the experiment. In addition, the spatial locations of reference nodes on the femoral mesh were exported at each time step. In post-processing of the model, a surface mesh of the femur implant was registered to the reference nodes and the medial and lateral lowest points on the femoral mesh in the tibial S-I direction were determined using a custom Matlab script.

4.2.3 Monte-Carlo Simulation

To investigate the effect of variation in ligament properties on the knee laxity predicted by the model, a Monte-Carlo simulation was performed. Each model (PS and CR) was evaluated 1000 times with unique sets of randomly generated ligament parameters, including ligament attachment sites, linear spring stiffness (K^2), and spring reference strain (ε_p). To reduce the number of variables, some relationships between ligament variables were assumed. In particular, on the medial side of the knee, the origin of the three bundles of the MCL and the origin PMC were moved together as a group, although the A-P width of the MCL origin was variable. Likewise, the insertion sites of the three bundles of the MCL were also moved as a group, but independent of the insertion site of the PMC. A single stiffness was chosen for the entire MCL, which was equally divided between the three bundles; however, each MCL bundle was assigned a unique reference strain.

On the lateral side of the knee, the locations of the origin of the three bundles of the LCL were moved with the origin of the ALC, although the overall A-P width of the LCL origin site was variable. The origin site of the PFL was variably placed distal and anterior relative to the origin of the LCL. The insertions of the LCL were moved independently of the ALC and the PFL. Like the MCL, a single overall stiffness was assigned for the LCL, which was equally divided between the three bundles. Each LCL bundle was assigned a unique reference strain value.

On the posterior aspect of the knee, the origin site of the posterior-medial bundle of the PCL was placed a variable distance posterior and superior from the origin chosen for the anterior-lateral bundle. Likewise, the insertion of the posterior-medial bundle of the PCL was placed variably posterior and medial to the insertion of the anterior-lateral bundle. Stiffness and reference strain values for the two bundles of the PCL were chosen independently. The attachment sites of the springs in the posterior capsule were held constant, although the stiffness and reference strain of each spring in the configuration were variable.

Values for each variable representing attachment sites, stiffness, and free length were randomly chosen from normal distributions. In general, mean locations for the medial and lateral ligament attachment sites were based on their experimentally recorded locations. Suitable standard deviations for perturbation of the insertion sites were determined by comparing the potential for error in identifying the ligament attachment sites and the sensitivity of the model to error in ligament placement. In general, 5-mm was chosen for as the standard deviation for most

attachment sites. Using the probed attachment sites, an initial sensitivity study was performed by varying the reference strains in each ligament. From this analysis, ranges of appropriate reference strains were identified where each ligament provided reasonable forces through the flexion range (i.e. greater than zero, but less than the yield strength of the ligament).

Mean and standard deviations for ligament stiffnesses were adopted from uniaxial ligament tensile tests where available [9, 11, 13]. For ligament stiffnesses without literature estimates (PC, PMC, and ALC stiffness), an arbitrary stiffness of 40±10 N/mm was assigned. The mean and standard deviations for all these distributions are specified in Table 4.1.

From the output kinematics of the models, 5%-95% confidence intervals for knee kinematics in response to applied Vr-Vl and I-E torques were calculated. The experimental data for both individual knees included some hysteresis at low load levels between the loading and unloading curves. For purposes of comparison, the loading portion of the knee laxity curves from both the experiment and the computational models were compared. Additionally, the peak rotations for each loading condition at each flexion angle were extracted from the model results. Correlation coefficients were calculated between each variable in the model and the peak rotations observed. These correlation coefficients represent the sensitivity of the magnitude of the peak rotation to particular input variables. For example, if variation in a particular parameter caused a consistent change in peak varus rotation at 30° flexion, this pair would have a high correlation coefficient.

Two separate steps were taken to ensure that 1000 model evaluations were sufficient to accurately establish the potential laxity response of the knee model. First, a theoretical approach was employed developed by Haldar and Mahadevan [88] using the assumption that the model response followed a normal distribution. Under this formulation, the percent error of the confidence interval prediction is a function of the number of model evaluations in the form:

$$E\% = \sqrt{\frac{1 - p_f}{N \times p_f}} \times 200\% \qquad \text{(Equation 4.3)}$$

Where E% is the percent error of the confidence interval prediction, p_f is the confidence level of the interval, and N is the number of Monte-Carlo trials. Evaluation of this equation for the 5% confidence interval (p_f=0.05) yielded a prediction error of 27.6%. In terms of the confidence intervals, 27.6% error of the 5% and 95% confidence interval equates to 5% ± 1.4% and 95% ± 1.4%. To illustrate the corresponding range in laxity response, the range of confidence levels were compared against the cumulative distribution functions for a particular set of laxity responses in the PS model (I-E and Vr-Vl rotation under maximum torque at 60° knee flexion) (Fig. 4.4). The same calculation was performed through the full loading range at each flexion angle for the PS model, as illustrated at 60° knee flexion in Fig. 4.5.

As a more practical form of verification, the population of 1000 model evaluations was divided in half to form two subsets of 500 model evaluations each. The 5% and 95% confidence intervals were calculated from these two independent populations, and are illustrated for the laxity responses of the PS model at 60° knee

flexion. The resulting confidence intervals from both the theoretical and practical approaches described above indicated that although some uncertainty existed in the exact locations of the 5% and 95% confidence intervals, 1000 model evaluations were sufficient to reasonably predict those confidence intervals and that additional model evaluation was not necessary.

4.3 Results

With a few exceptions, the laxity observed during the experimental assessments of Knee 1 (PS) and Knee 2 (CR) fell near of within the 5%-95% confidence intervals predicted by the Monte-Carlo performed on the respective computational knee models. In particular, there was good agreement between the Vr-Vl laxity observed in Knee 1 (PS design) and the model predicted kinematics at all flexion angles (Fig 4.7). The experimental and predicted I-E laxity also matched well, although the experimentally observed I-E laxity was along the confidence bound predicted by the model at full extension, indicating that the model may have been slightly under-constrained at this flexion angle (Fig 4.8). The hysteresis observed in the experimental evaluation was not present in the idealized computational model, which caused disagreement between the experimentally observed laxity and the computational laxity predicted at low torque levels. A closer inspection of the condylar A-P translations under I-E torque for Knee 1 indicated that while the overall experimental I-E rotation may have been smaller in magnitude, the predicted condylar translations between the experiment and the model were in agreement (Fig. 4.9).

In Knee 1 (PS) the tibial post contributed to I-E stability by contacting the internal box structure of the femur. In Knee 2, the CR geometry did not have the same stabilizing feature, and relied on the spring structures to restrain the motion between the tibia and femur. Like Knee 1, Knee 2 showed good agreement between the experimental and model-predicted Vr-Vl rotation (Fig. 4.10). In I-E rotation, however, the computational model predicted more internal rotation at full extension and 30° knee flexion, compared to the experimental observations (Fig. 4.11). The increased internal laxity predicted by the model was a result of increased anterior translation of medial condyle of the femur relative to the tibia, while the lateral condyle tracked within the predicted bounds (Fig. 4.12). With the current ligament configuration, and without the passive laxity from the extensor mechanism soft tissue structures, no structures were oriented such that they would resist anterior translation of the medial condyle relative to the tibia in knee extension.

Correlation coefficients (also called sensitivity factors) represent the strength of the relationship between variables in the model and the predicted laxity. In the PS model (Knee 1), pre-tensions in the LCL and other lateral structures were the dominant factor controlling varus laxity at full extension in the model (Fig. 4.13). At 30° flexion and beyond, the A-P location of the LCL origin became a strong factor in varus rotation, while in deeper flexion, the S-I position of the LCL origin also had a large influence. The corollary for valgus rotation was that reference strain in the MCL and other medial structures controlled valgus rotation in full extension, while A-P and S-I position of the MCL origin were more important in deeper flexion.

The variables most influential in Vr-Vl rotation were clear, but the relative contributions to I-E rotations were more ambiguous. No single structure played a dominant role in controlling I-E rotation at any flexion angle (Fig. 4.14). In full extension, the lateral oblique posterior capsule and the posterior medial capsule influenced internal rotation, while the medial oblique posterior capsule and medial collateral ligament influenced external rotation. From 30° through 90°, the A-P location of the anterior-lateral capsule insertion was the most significant influence on internal rotation. Reference strain in the MCL had the largest effect on external rotation at 30°, while the S-I position of the lateral collateral ligament and popliteal-fibular ligament origins were the most influential factors at 60° and 90° flexion.

Sensitivity factors were similar for the CR model (Knee 2), with the most dominant factors being the same in the CR and PS models for varus, valgus, and external laxity (Figs. 4.15, 4.16). There was notable difference in factors influencing internal rotation, with the A-P location of the anterior lateral capsule insertion as the most influential factor in full extension and the S-I location of the PCL origin as the most significant factor at 60° and 90° flexion. In both knees, neither MCL or LCL tibial insertions sites, nor any ligament stiffness demonstrated a clear correlation with the resulting knee laxity.

4.4 Discussion

In this study, two independent computational models were constructed based on two cadaveric knees after surgical implantation of either a posterior stabilized (Knee 1) or cruciate retaining (Knee 2) total knee replacement. A probabilistic

approach was used to assess how variation in ligament attachment sites and mechanical properties influenced the predicted laxity of the joint. The laxities predicted by the patient-specific models were compared with experimental assessments of knee laxity performed on the cadaveric knees.

Many computational models of the knee, including the models in this study, utilize non-linear springs to represent the constraint provided by knee ligaments. While non-linear springs are simple to formulate and computationally efficient to evaluate, they are unable to simulate wrapping of the ligament around bones and simplify the complex ligament recruitment patterns seen in real ligaments [89]. Blankevoort et al. [90] illustrated that wrapping of the MCL improved the mechanical efficiency of the MCL, although the same constraint was provided by the MCL without wrapping through increased reference strain in the ligament. Many authors have attempted to recreate anatomic recruitment patterns by discretization of ligaments into multiple non-linear springs [30, 82]. In the current study, the MCL and LCL were divided into three bundles (anterior, center, and medial); each displayed different recruitment patterns throughout the flexion range. While including additional springs may more accurately recreate ligament recruitment patterns, it would also introduce additional variables (attachment coordinates, stiffness, and reference strain values) that must be addressed.

Despite their extensive use in the literature, few attempts have been made to assess the ability of non-linear springs to reproduce subject-specific knee laxity under both Vr-Vl and I-E torques through the flexion range after TKR. With some notable

exceptions, the experimental observations of Vr-Vl and I-E laxity in this study fell within the bounds predicted by the computational models; however, both the PS and CR versions of the model were slightly under-constrained in internal rotation at full extension, and additionally at 30° for the CR model. The CR version of the model over-predicted the amount of anterior translation of the medial condyle. Only the posterior-medial capsule had the appropriate line of action to resist anterior medial condyle translation, and since PMC quickly slackened with knee flexion, there were no structures active at 30° knee flexion to resist this motion. This deficiency was not evident in the PS model because contact between the edge of the post and the wall of the femur box resisted excessive anterior translation of the medial condyle. A similar inability to properly restrain internal rotation was observed in natural knee models by Blankevoort et al. utilizing an equivalent ligament configuration [1]. Robinson et al. noted in cadaveric laxity assessments that the deep bundle of the MCL restricted anterior translation of the medial condyle [8], a structure not included in the current model. Perhaps inclusion of such a structure would improve the prediction of internal rotation in the computational models.

There exists a large amount of patient-to-patient variation in the mechanical properties of knee ligaments [9, 11]. In the current study, a probabilistic approach was used to address uncertainty in these mechanical properties in the computational model. Because the model was sensitive to small changes in ligament parameters, use of average values for ligament parameters would not accurately predict a particular subject's knee laxity. A probabilistic approach to bound knee function or

use of optimization techniques to refine ligament function would be necessary if this type of model were used to predict patient-specific knee behavior. Fortunately, the computational efficiency of the current model lends itself well to large-scale optimization techniques.

The sensitivity analysis suggested that only a handful of the variables included in the Monte-Carlo simulation actually had a significant influence on the predicted laxity. In general, ligament free-lengths for the MCL, LCL, and posterior capsular structures were the most sensitive factors affecting the model. Unfortunately, ligament free-length is difficult to determine experimentally and is highly dependent on native anatomy and the ligament balancing procedure employed by the surgeon during TKA. Surprisingly, the overall ligament stiffness had a minor influence on predicted laxity compared to the other factors.

The origins of the LCL and MCL on the femur in the sagittal plane also had a significant influence on knee laxity. While it is possible to experimentally measure the footprints of the major ligaments, there is a large amount of room within the footprint to place the springs that represent the ligament. Even though only a small amount of variation was allowed (± 5-mm standard deviation from the geometric center of the ligament footprint) in the probabilistic analyses, movement of the origins accounted for the majority of the variation in laxity at 60° and 90° flexion. The location of the LCL or MCL origin relative to the flexion axis of the knee influenced the amount of elongation that occurred in the ligament with knee flexion. If the origin was posterior or superior to the flexion axis, the spring went slack with

flexion allowing increased laxity. If the origin were anterior or inferior to the flexion axis, it was stretched with knee flexion. Arms et al. [89] reported similar trends, noting elongation of the anterior MCL and shortening of the posterior MCL with knee flexion.

There were a few limitations associated with the current study. Previous work has shown that alignment of femoral and tibial coordinate systems influence the observed kinematics [66]. Identical coordinate systems were used to compare the experimental and computation kinematics in this study, although there may have been small errors associated with registration of the computational and experimental coordinate systems. In the computational model, a pressure over-closure relationship was used to define contact pressure between the rigid femur and tibia. Allowing deformation of the tibial insert may more accurately resolve the complex contact between the insert post and femoral box in the PS design, although improved contact predictions would increase the computational cost. Finally, the current model was only used to predict knee laxity; it is unclear how effective the current ligament representation would be at predicting behavior during dynamic activities.

The configuration of non-linear springs used in this study, applied with a probabilistic approach for ligament parameter uncertainty, demonstrated that non-linear springs can be used, with some reservations, to predict knee behavior after total knee replacement. In particular, the Vr-Vl laxity predicted by the model showed excellent agreement with the experimental observations; however, caution should be used when modeling large internally-directed torques applied to the tibia, particularly

near extension. In future work, multi-variable optimization routines will be used to tune individual ligament parameters to the experimentally observed laxity. Additionally, more sophisticated ligament representations, which include ligament wrapping, will be incorporated into the computational model. Finally, the ability of these optimized ligaments to constrain knee motion during dynamic, weight-bearing activities will be assessed.

4.5 Tables and Figures

Table 4-1: Variables included in the Monte-Carlo Simulation of ligament variation. Mean position of the origin and insertion sites for the major ligaments were placed corresponding to the probed locations during experimental testing. Stiffness values for ligaments were adopted from uniaxial tensile tests reported in the literature, while reasonable reference strain values were assumed based on the maximum elongation observed during the experiment.

Structure	Variable	Relative to:	Mean	Std. Dev.	Source
MCL	Origin A-P	Probed Femoral Origin	From Experiment	5	
	Origin S-I	Probed Femoral Origin	From Experiment	5	
	Origin M-L	Probed Femoral Origin	From Experiment	2	
	Origin A-P Width	Absolute	15	5	Diameter of probed origin site
	Insertion A-P	Probed Tibial Insertion	From Experiment	5	
	Insertion S-I	Probed Tibial Insertion	From Experiment	5	
	Insertion M-L	Probed Tibial Insertion	From Experiment	5	
	Overall Stiffness	Absolute	80	10	Robinson et al.
	Anterior Prestrain	Length in IP	1	0.03	
	Central Prestrain	Length in IP	1	0.03	
	Posterior Prestrain	Length in IP	1	0.03	
PMC	Stiffness	Absolute	40	10	Robinson et al.
	Prestrain	Absolute	1	0.03	
LCL	Origin A-P	Probed Femoral Origin	From Experiment	5	
	Origin S-I	Probed Femoral Origin	From Experiment	5	
	Origin M-L	Probed Femoral Origin	From Experiment	2	
	Origin A-P Width	Absolute	8	6	Diameter of probed origin site
	Insertion A-P	Probed Tibial Insertion	From Experiment	5	
	Insertion S-I	Probed Tibial Insertion	From Experiment	5	
	Insertion M-L	Probed Tibial Insertion	From Experiment	5	
	Insertion A-P Width	Absolute	8	4	Diameter of probed origin site
	Overall Stiffness	Absolute	58	23	Sugita et al.
	Anterior Prestrain	Length in IP	1	0.03	
	Central Prestrain	Length in IP	1	0.03	
	Posterior Prestrain	Length in IP	1	0.03	
ALS	Insertion A-P	Probed Tibial Insertion	From Experiment	10	
	Insertion S-I	Probed Tibial Insertion	From Experiment	3	
	Insertion M-L	Probed Tibial Insertion	From Experiment	3	
	Stiffness	Absolute	40	10	
	Prestrain	Length in IP	1	0.03	
PFL	Origin Anterior Offset	LCL origin	6	5	
	Origin Distal Offset	LCL origin	11	5	
	Insertion Posterior Offset	LCL insertion	5	5	
	Insertion Superior Offset	LCL insertion	10	5	
	Insertion Medial Offset	LCL insertion	10	5	
	Stiffness	Absolute	44	15	Sugita et al.
	Prestrain	Length in IP	0.6	0.1	
Anterior-Lateral PCL	Origin A-P	Probed Femoral Origin	From Experiment	5	
	Origin S-I	Probed Femoral Origin	From Experiment	5	
	Origin M-L	Probed Femoral Origin	From Experiment	2	
	Insertion A-P	Probed Tibial Insertion	From Experiment	5	
	Insertion S-I	Probed Tibial Insertion	From Experiment	5	
	Insertion M-L	Probed Tibial Insertion	From Experiment	5	
	Stiffness	Absolute	125	25	Race et al.
	Prestrain	Length in IP	0.64	0.05	
Posterior-Medial PCL	Origin Posterior Offset	PCL origin	From Experiment	3	
	Origin Distal Offset	PCL origin	From Experiment	3	
	Stiffness	Absolute	60	15	Race et al.
	Prestrain	Length in IP	0.71	0.05	
Posterior Capsule	Medial Stiffness	Absolute	40	10	
	Medial Prestrain	Length in IP	1	0.03	
	Lateral Stiffness	Absolute	40	10	
	Lateral Prestrain	Length in IP	1	0.03	
	Medial Oblique Stiffness	Absolute	40	10	
	Medial Oblique Prestrain	Length in IP	1	0.03	
	Lateral Oblique Stiffness	Absolute	40	10	
	Lateral Oblique Prestrain	Length in IP	1	0.03	

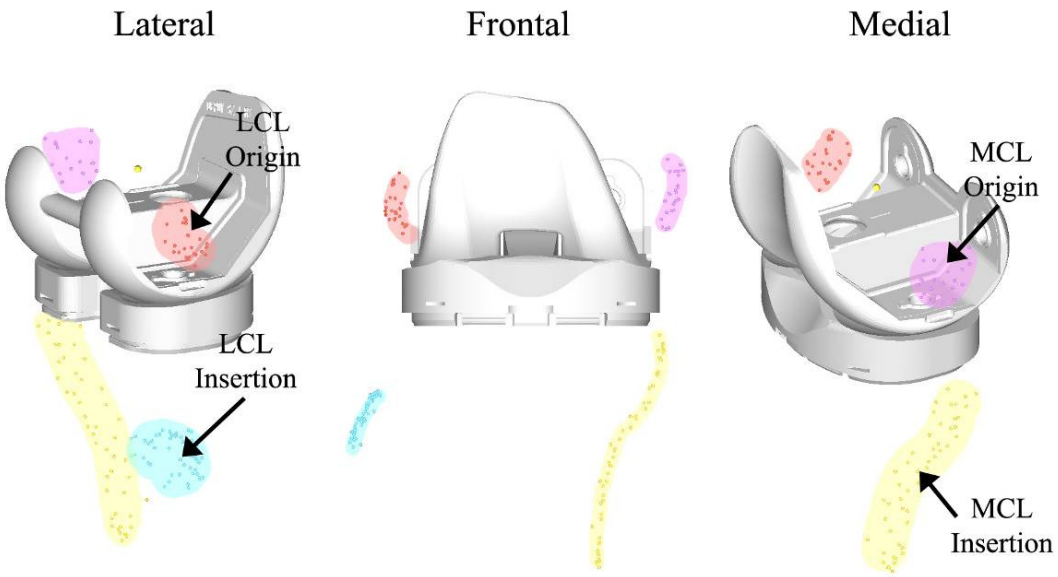

Figure 4-1: Location of points probed during the experimental evaluation identifying the attachment sites of the major ligaments for Knee 1. Multiple non-linear springs were placed about the geometric center of the highlighted areas to represent the ligaments. During the probabilistic analysis, attachment sites were perturbed within highlighted areas. Note: for the MCL insertion, the springs were placed at the most distal end of the highlighted region (yellow).

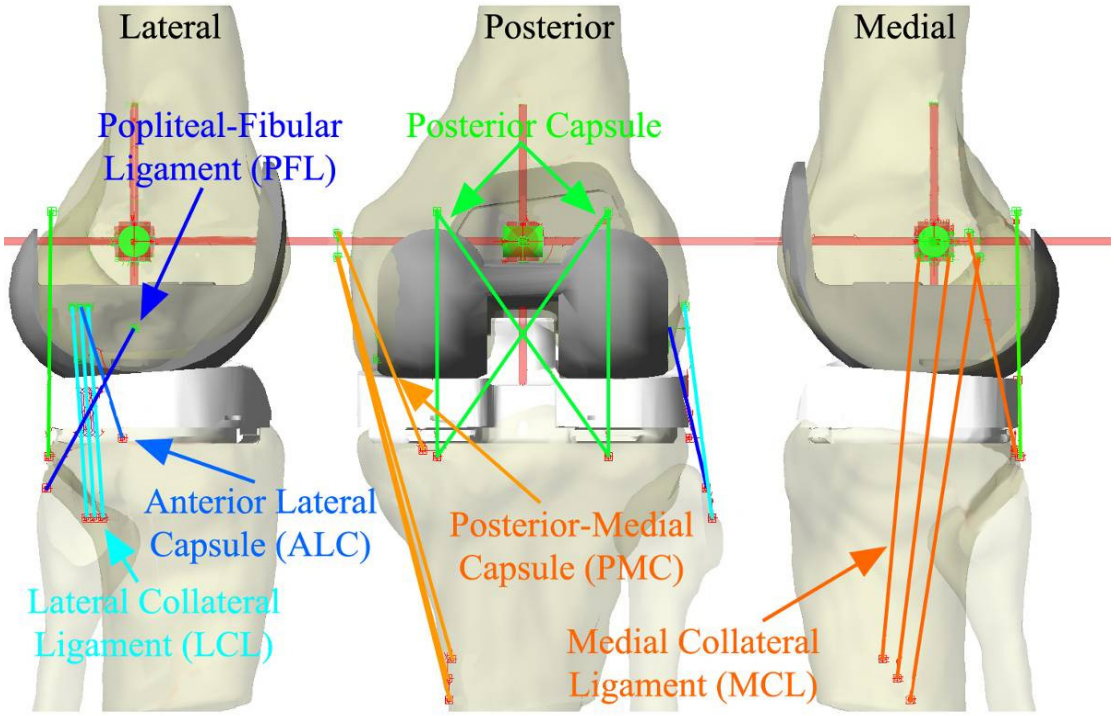

Figure 4-2: The computational model developed, based on Knee 1, to predict the laxity observed in the cadaveric experiment. Highlighted are the 13 non-linear springs used to represent the soft tissue structures surrounding the knee. Two additional springs were included in the CR version of the model to represent the PCL.

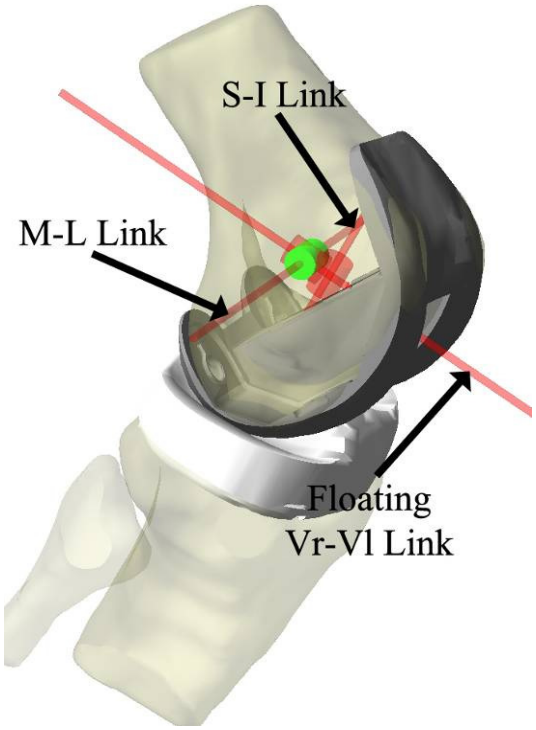

Figure 4-3: The computational knee model at 30° of flexion highlighting placement of the mechanical linkage system relative to the knee implant. Isolated Vr-Vl and I-E torques were applied to the femur via the linkage system, which was also used to prescribe knee flexion.

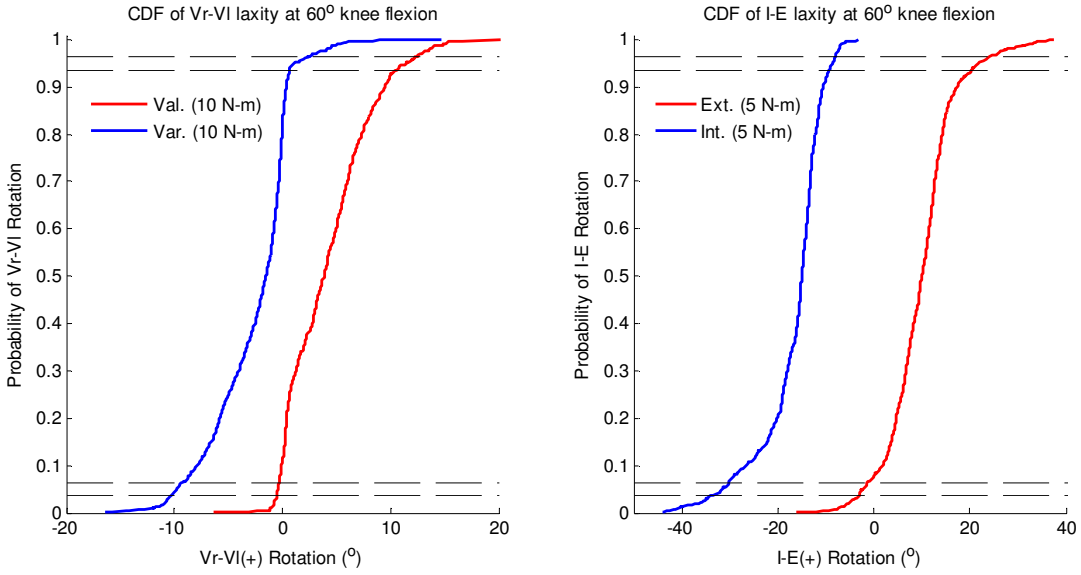

Figure 4-4: The CDF for Vr-Vl and I-E rotations of the PS model under maximum torque at 60° knee flexion. The dashed lines identify the error bounds around the 5% and 95% confidence intervals for predicted knee laxity.

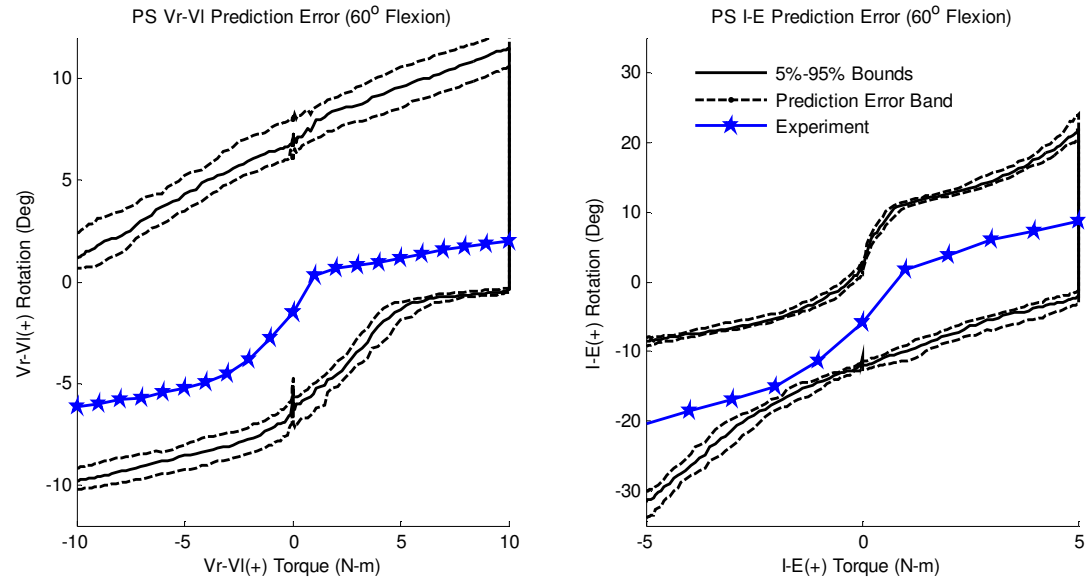

Figure 4-5: The 5% and 95% confidence intervals (solid black lines) for Vr-Vl and I-E rotations of the PS model at 60° knee flexion, along with the error bounds for these confidence intervals (dashed black lines).

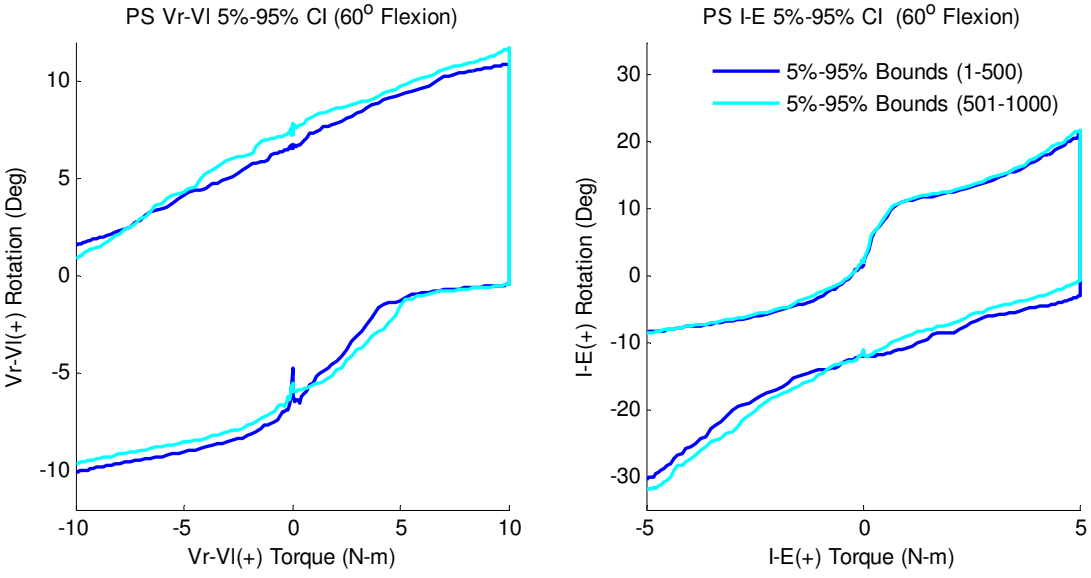

Figure 4-6: Two approximations of the 5% and 95% confidence intervals for Vr-Vl and I-E rotations of the PS model at 60° knee flexion calculated from two independent sets of 500 Monte-Carlo evaluations of the model.

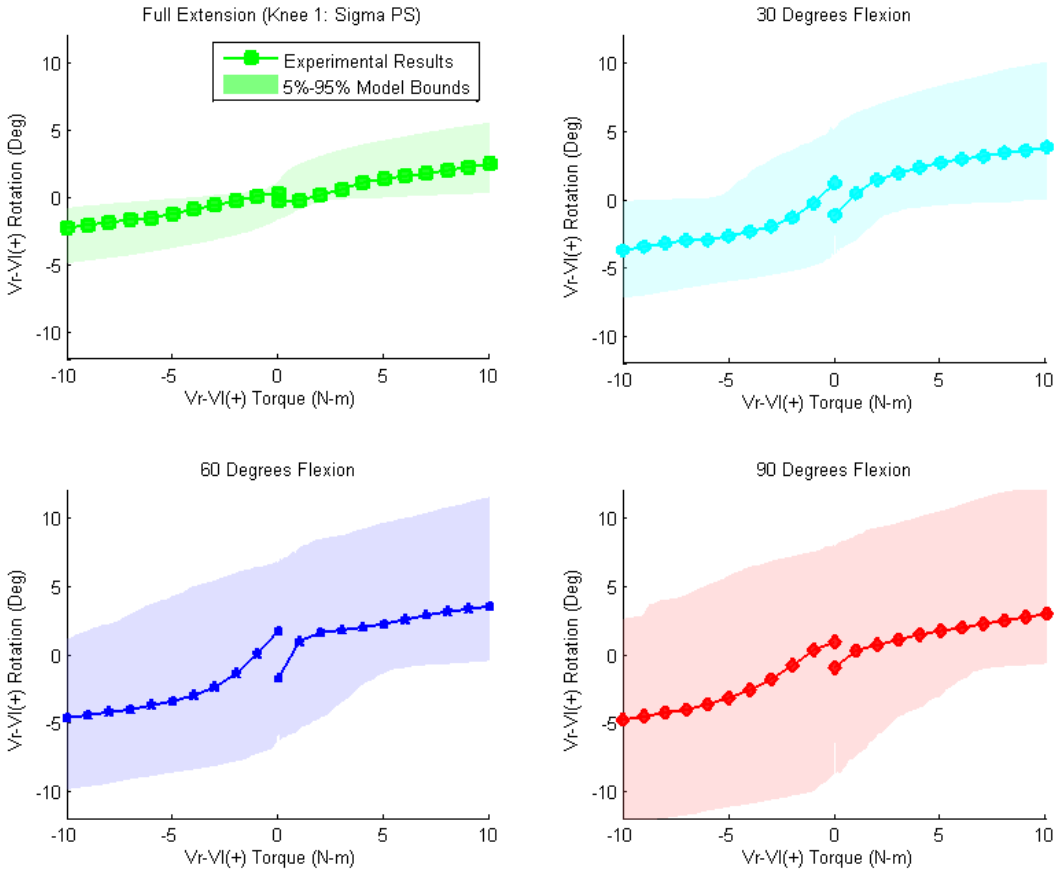

Figure 4-7: Comparison of Vr-Vl laxity through the flexion range between the experimental assessment and the corresponding model for Knee 1. The solid lines represent the experimentally observed laxity, while the shaded regions represent the 5% and 95% confidence intervals calculated by the corresponding model. Experimentally observed Vr-Vl laxity fell within the computationally predicted bounds at all flexion angles.

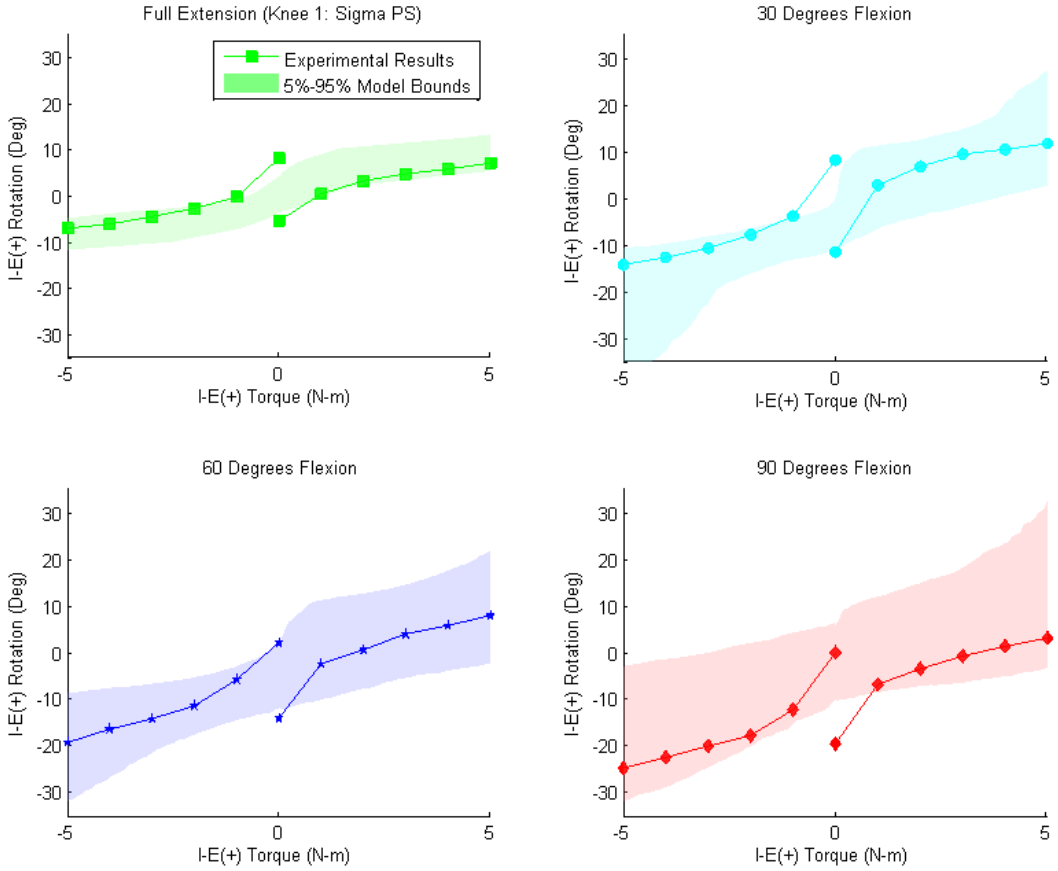

Figure 4-8: Comparison of I-E laxity through the flexion range between the experimental assessment and the corresponding model for Knee 1. The solid lines represent the experimentally observed laxity, while the shaded regions represent the 5% and 95% confidence intervals calculated from the corresponding model. Experimentally observed I-E laxity fell within the computationally predicted bounds at all flexion angles except at zero load due to effect of hysteresis. At 0° and 30° flexion, the experimental internal rotation was along the boundary predicted by the model, indicating the model may be slightly under-constrained.

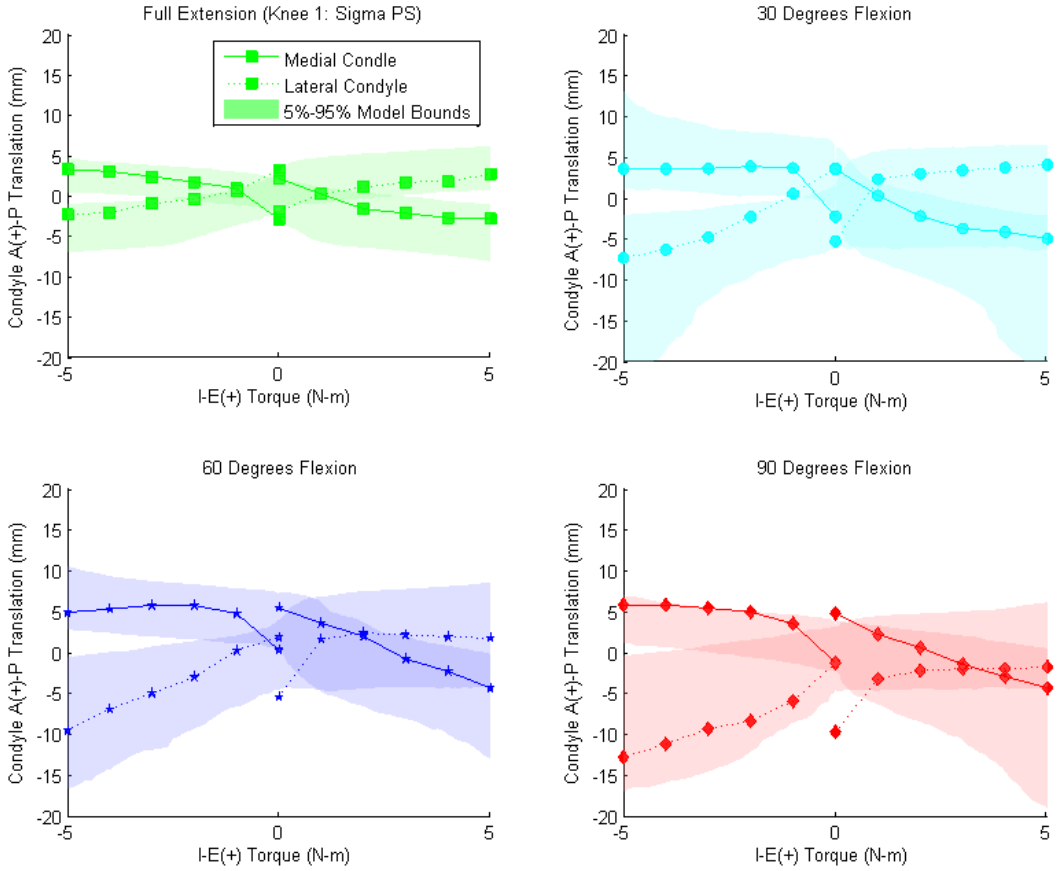

Figure 4-9: Medial (solid lines) and lateral (dashed lines) condylar A-P translation relative to the tibia in response to I-E torques compared with 5%-95% bounds calculated by the corresponding knee model (shaded regions) for Knee 1. Although the internal rotation in the model was slightly under-constrained, the condylar translations were with the predicted bounds at all loaded levels.

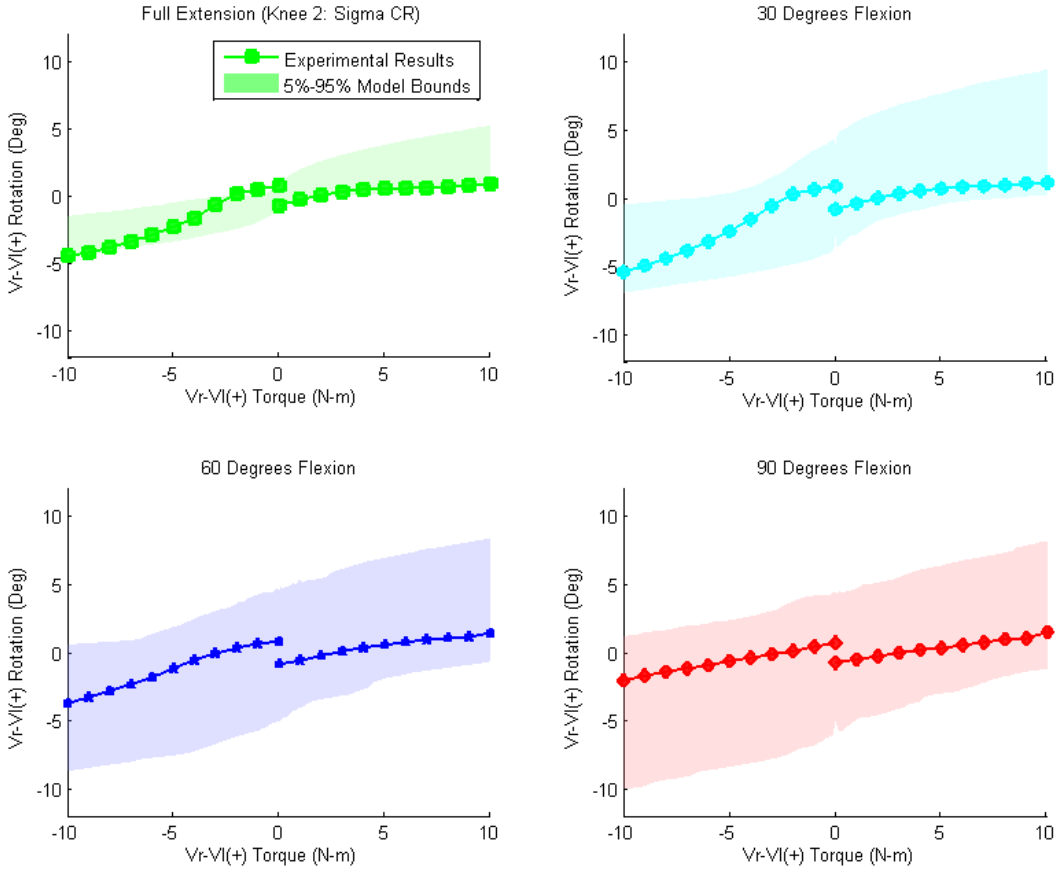

Figure 4-10: Comparison of Vr-Vl laxity through the flexion range between the experimental assessment and the corresponding model for Knee 2. The solid lines represent the experimentally observed laxity, while the shaded regions represent the 5% and 95% confidence intervals calculated by the corresponding model. Experimentally observed Vr-Vl laxity fell within the computationally predicted bounds, except in valgus rotation at full extension.

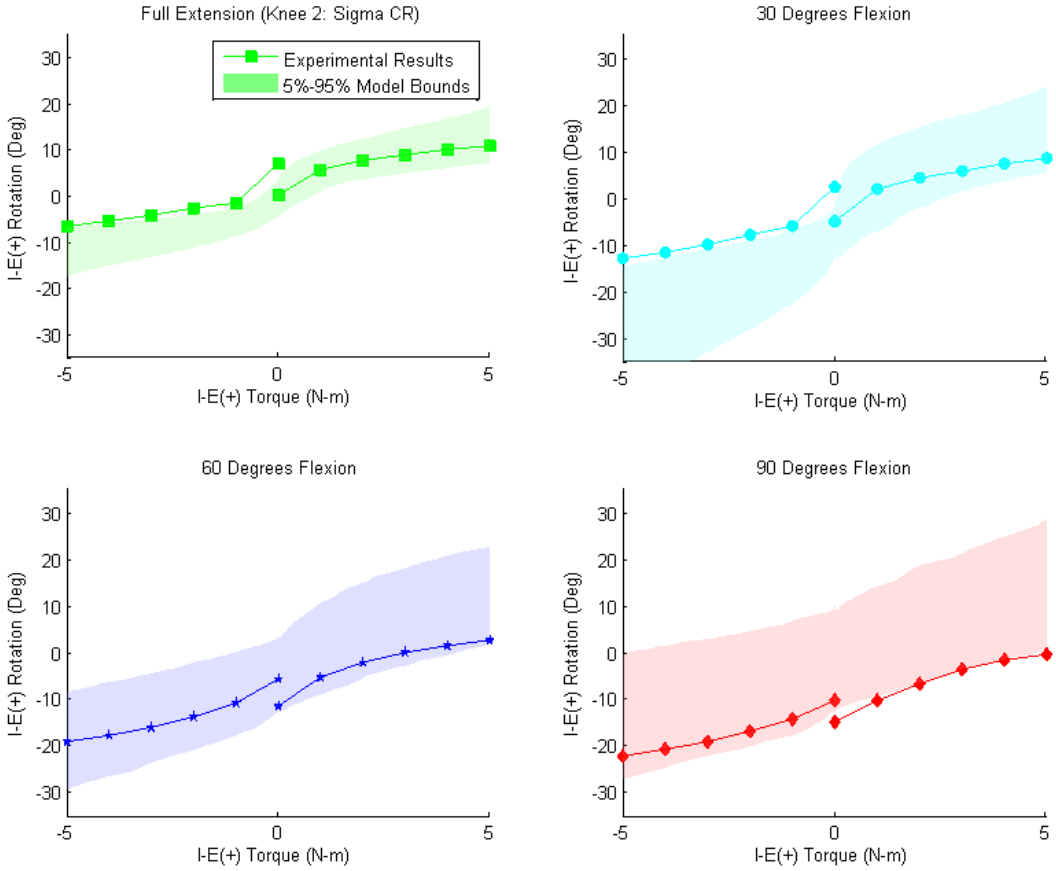

Figure 4-11: Comparison of I-E laxity through the flexion range between the experimental assessment and the corresponding model for Knee 2. The solid lines represent the experimentally observed laxity, while the shaded regions represent the 5% and 95% confidence intervals calculated by the corresponding model. The experimentally observed I-E laxity fell within the computationally predicted bounds at 60° and 90° flexion. At 0° and 30° flexion, the experimental internal rotation was slightly beyond the boundary predicted by the model, indicating the model was under-constrained in early flexion.

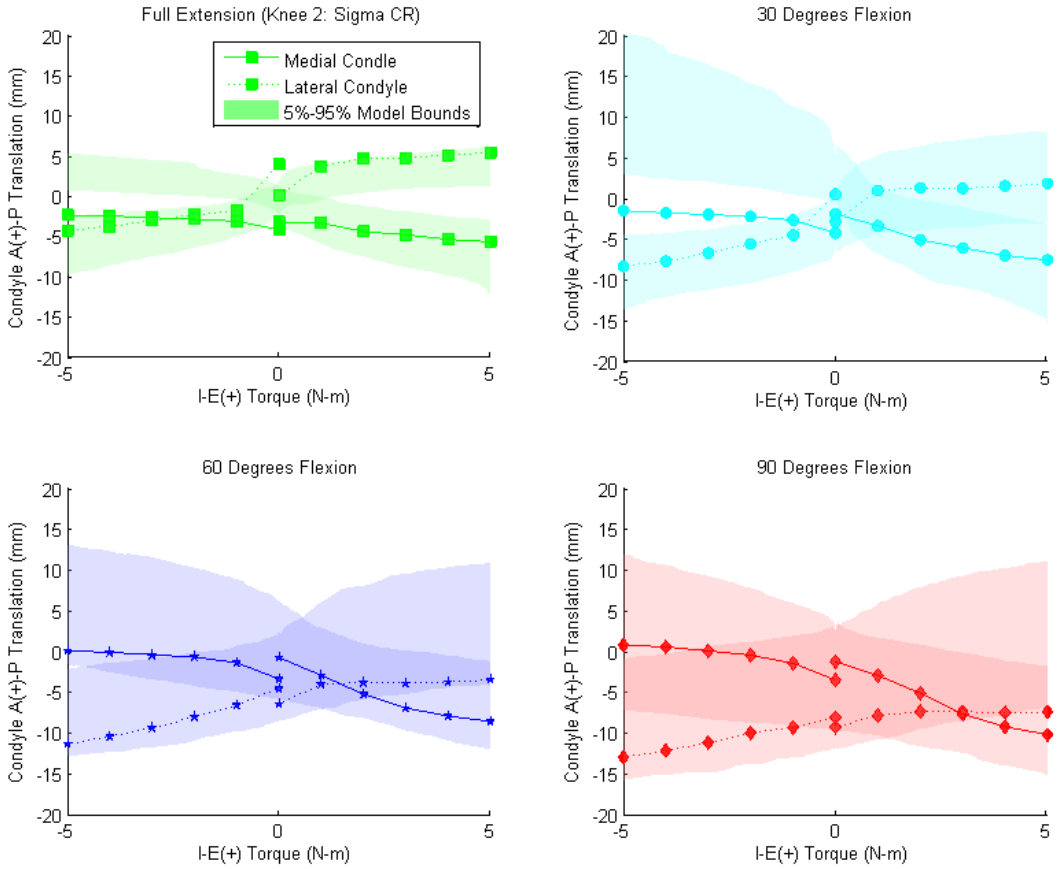

Figure 4-12: Medial (solid lines) and lateral (dashed lines) condylar A-P translation relative to the tibia in response to I-E torques compared with 5%-95% bounds calculated by the corresponding knee model (shaded regions) for Knee 2. Most condylar translations fell within the predicted bounds, except for the medial condyle's anterior translation under internal torque and 0° and 30° knee flexion. Over-predicted anterior translation of the medial condyle led to an over-predicted amount of internal rotation for the CR knee model.

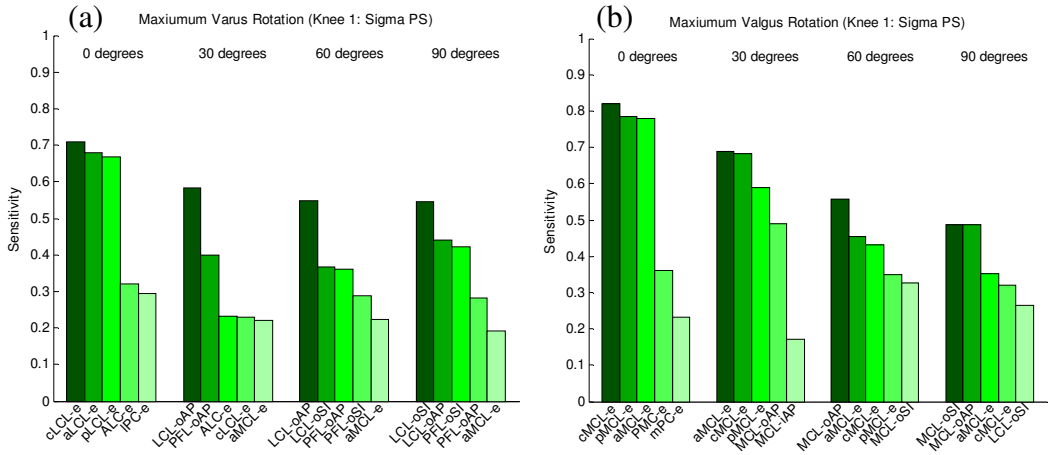

Figure 4-13: Factors influencing (a) varus and (b) valgus knee rotation through the flexion range for Knee 1. LCL reference strain was the most influential factor on varus rotation at full extension. As the knee flexed, the origin location of the LCL replaced the reference strain as the most influential factor in varus rotation. Similarly, reference strain of the MCL was the most influential factor for valgus rotation at full extension and 30° flexion. As the knee flexed to 60° and 90°, the origin location of the MCL became the dominant factor in valgus rotation.

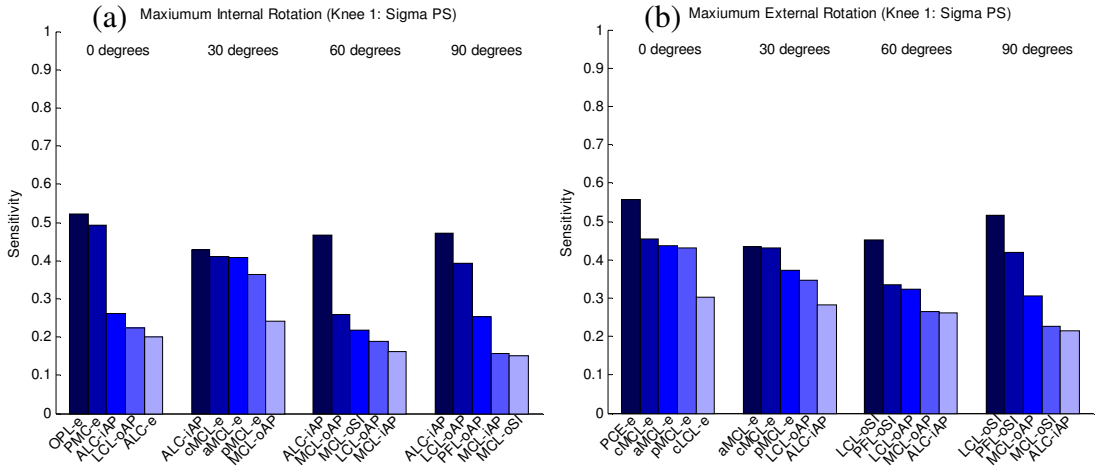

Figure 4-14: Factors influencing (a) internal and (b) external knee rotation through the flexion range for Knee 1. The oblique popliteal ligament (OPL) and posterior medial capsule (PMC) had the highest influence on internal rotation at full extension. The anterior location of the insertion site of the anterior lateral capsule (ACL) had the most influence on internal rotation throughout the rest of the flexion range. Similarly, the posterior capsular extension (PCE), along with the reference strain (e) of the MCL, had the most influence on external rotation at full extension. In deeper flexion, the location of the LCL and PFL were the most influential factors on external rotation.

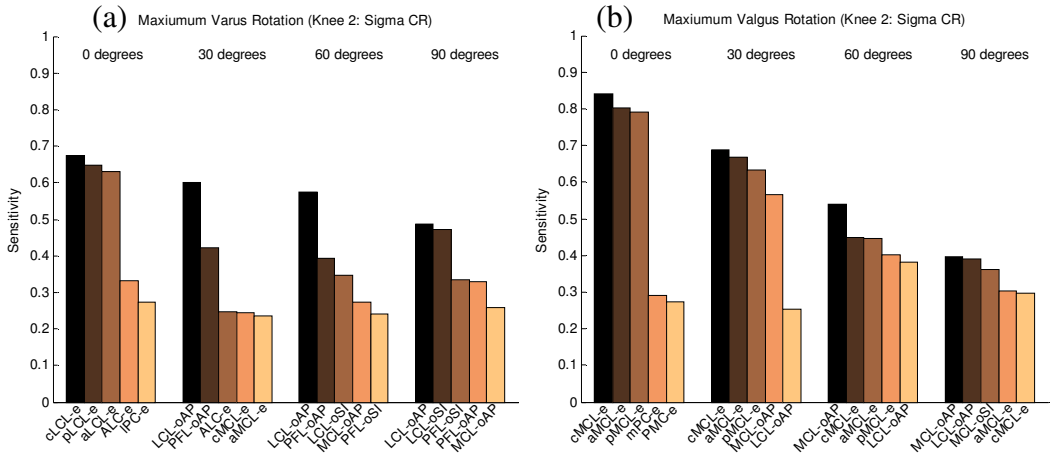

Figure 4-15: Factors influencing (a) varus and (b) valgus knee rotation through the flexion range for Knee 2. LCL reference strain was the most influential factor on varus rotation at full extension. As the knee flexed, the origin location of the LCL replaced the reference strain as the most influential factor in varus rotation. Similarly, reference strain of the MCL was the most influential factor for valgus rotation at full extension and 30° flexion. As the knee flexed to 60° and 90°, the origin location of the MCL became the dominant factor in valgus rotation.

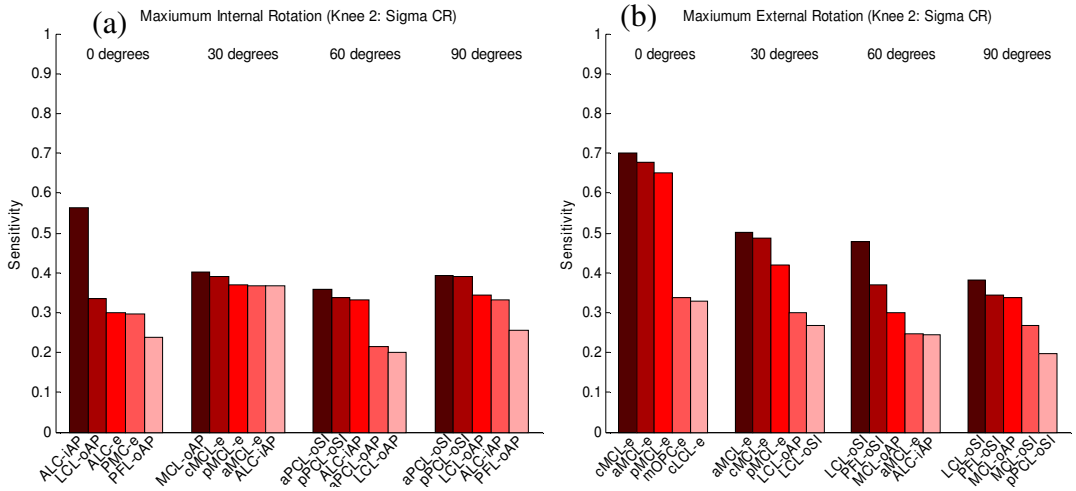

Figure 4-16: Factors influencing (a) internal and (b) external knee rotation through the flexion range for Knee 2. The anterior-lateral capsule had the highest influence on internal rotation at full extension. The origin location of the PCL had the most influence on internal rotation in deeper flexion. The reference strain of the MCL, had the most influence on external rotation at full extension. In deeper flexion, the location of the LCL and PFL were the most influential factors on external rotation.

Chapter 5: Optimization of a Computational Knee Model Using Patient-Specific Knee Laxity

5.1 Introduction

Computational models of total knee replacements are often constructed for a representative knee, thereby limiting the clinical opportunity to utilize these models for prediction of subject-specific total knee replacement function. While these models have provided valuable insight into knee kinematics [71-74], contact mechanics [75, 76], wear properties [77, 78], and the effect of variation in surgical technique [79, 80], additional steps are required to apply their predictions to a particular subject. While modern imaging modalities can quantify the bony geometry at the knee, and computer-aided surgery can accurately monitor implant alignment, there are limited existing methods to generate accurate models of ligamentous constraint around the knee. A combined experimental-computational approach that yielded a subject-specific computational knee ligament constraint model would be a critical step forward for building subject-specific knee models.

Several authors have used anatomic configurations of non-linear springs to predict knee laxity [26-28, 72, 74, 75, 79, 83, 84, 91-94]. The common use of this representation warrants investigation into whether multi-bundle non-linear springs could recreate the appropriate ligament constraint in the knee after total knee replacement. While many of these previous models of ligament constraint have used literature reported mean values to define ligament properties (i.e. attachment location, ligament stiffness, and ligament reference strain), these values vary significantly

between subjects. Therefore, when attempting to reproduce the laxity of a particular subject, literature defined values often yield poor predictions [1]. Some authors have quantified how ligament parameter uncertainty affects knee laxity using probabilistic methods [95]; however, until recently, optimization of the knee's ligament constraint has been computationally prohibitive due to the large number of variables to be optimized and the computational time required to evaluate knee computational models. Recent advances in efficient rigid body modeling solvers, increased processor speed, parallel computing, and large-scale optimization techniques have made ligament constraint optimization possible within a reasonable time-frame.

Previous attempts in the literature to optimize computational ligament constraint for a particular subject are scarce. Blankevoort et al. optimized the reference strains in computational ligament models for four knees to recreate experimentally observed internal-external laxities through the flexion range [1]. The authors determined optimum solutions that closely recreated the appropriate I-E laxity of each knee, but found that these solutions did not accurately predict the A-P translation during the same laxity assessments. Incorporating A-P translation into the optimization cost function improved the A-P kinematic prediction with only a marginal decrease in the accuracy of the I-E prediction. This suggested that the true optimum solution for any isolated laxity motion may not be the best solution for the overall laxity of the knee, but including additional laxities in the optimization may improve the fidelity of the optimized solution.

While Blankevoort and colleagues were able to predict internal-external laxity of the natural knee, there still exists a variety of questions regarding optimization of ligament constraint. These questions include whether unique optimum ligament configurations exist to represent the overall knee laxity of a particular subject, how sophisticated ligament representations must be to recreate the appropriate knee constraint, and which axes of knee laxity should be used in the optimization. The purpose of the current study was to investigate these questions by applying a robust large-scale optimization method to optimize a generic model of knee ligament constraint using experimentally collected patient-specific knee laxity, then use the optimized model to predict knee kinematics.

5.2 Methods

5.2.1 Experimental Assessment of Post-TKR Knee Laxity

Four fresh frozen whole cadaveric legs (All Male, Age = 67.3±18.4 years, BMI = 27.4±2.7) were acquired for this experiment. The legs were prepared for experimental testing as previously described [Chapter 3]. Total knee replacements were performed on the knees using posterior-stabilized fixed-bearing total knee replacements (DePuy, Inc., Warsaw, IN). Surgeries were performed through a medial sub-vastus approach using standard instrumentation. Implant alignment and soft tissue balancing were performed at the discretion of the surgeons until "well-balanced knees" were attained. Following the surgeries, manual "envelope of motion" assessments of Vr-Vl and I-E knee stability were performed, as previously described

[Chapter 3]. I-E and Vr-Vl knee laxities were extracted from these envelope assessments [Chapter 3].

5.2.2 Computational Models of the Knees

Custom knee models were created for each knee in the study adapted from a previously described computational model of the knee [Chapter 4], which was composed of the implanted replacement components and a set of non-linear springs configured to represent the ligamentous constraint. The model included three springs each to represent the MCL and LCL, four springs for the posterior capsule, and three additional oblique structures (anterior-lateral capsule, popliteal-fibular ligament, and posterior-medial capsule). Appropriate sized implants were included in the model of each knee, and ligament attachment sites were set based on the experimentally recorded locations.

5.2.3 Optimization of Soft Tissue Constraint

Results from a previously published sensitivity analysis [Chapter 4] that assessed the influence of ligament parameters on model-predicted knee laxity, were used to formulate an optimization algorithm for the knee's soft tissue. Ligament parameters with the highest sensitivity coefficients were identified and subsequently optimized in the current study. These parameters were discussed in detail in the previous chapter, and are listed in Table 5.1. Notably, tibial attachment locations for the MCL and LCL had the lowest sensitivity scores and were therefore excluded from the optimization.

To ensure an accurate representation of ligament constraint through the flexion range, optimization was performed at full extension, 30°, 60°, and 90° knee flexion. Experimental assessments of knee constraint have shown that ligaments in the posterior capsule and posterior medial capsule only contribute to knee stability near full extension [96]. This behavior was also observed in the present computational model of the knee, where ligaments in the posterior capsule slackened after only a few degrees of knee flexion. Since virtually all the ligaments in the model contribute to knee stability at full extension, several combinations of ligament parameters could potentially generate the appropriate laxity; conversely, at 30° flexion and beyond, knee stability is solely influenced by the medial and lateral structures. Based on this observation, a two-phase optimization was proposed. In the primary phase, parameters defining the MCL, LCL, PFL, and ALC were optimized at 30°, 60° and 90° flexion. In the secondary phase, the optimized parameters from the primary phase were held constant, and optimization of the ligaments in the posterior and posterior-medial capsule was performed at full extension to supplement the existing medial and lateral constraint.

Optimization was performed by minimization of an objective function based on the root-mean-square (RMS) error between the experimentally-observed and computationally-predicted knee rotations. RMS errors between the experiment and model rotations were calculated for each loading direction (internal, external, varus, and valgus) at each flexion angle (0°, 30°, 60°, and 90°) over specified load ranges, using the generalized form below for a specified flexion angle and load direction:

$$RMS_{\substack{Flexion\\Direction}} = \sqrt{\frac{\sum_{i=Loads} (\theta_i^{Exp} - \theta_i^{Model})^2}{N_{Loads}}} \qquad \text{(Equation 5.1)}$$

Where θ was the Vr-Vl or I-E knee rotation under the specified load, in the specified direction, and at the specified flexion angle and N was the number of loads across which the RMS error was calculated. For varus and valgus laxity, the RMS error was calculated at increments of 1 N-m from 2 through 10 N-m of applied torque. For internal and external laxity, the RMS error was calculated at increments of 1 N-m from 1 through 5 N-m of applied torque.

To compose the objective function for the primary phase of the optimization, RMS errors were summed for each loading direction at flexion angles of 30°, 60° and 90° knee flexion. Weight factors were applied to the summed I-E and Vr-Vl RMS errors to determine the total average RMS error, in the form:

$$RMS^{Total} = \alpha * \sum_{j=30°,60°,90°} (RMS_{Int}^{j} + RMS_{Ext}^{j}) + \beta * \sum_{j=30°,60°,90°} (RMS_{Var}^{j} + RMS_{Val}^{j}) \quad \text{(Equation 5.2)}$$

Where α and β were weight factors ranging from zero to one for I-E and Vr-Vl rotations, respectively. In this form, if α=1 and β=0, the optimization was driven solely by I-E laxity. Conversely, if α=0 and β=1, the optimization was driven solely by the Vr-Vl laxity. Three optimization runs were performed for each of the four knees in the study: 1) optimization of I-E rotation (α=1, β=0), 2) optimization of Vr-

Vl rotation (α=0, β=1), and 3) simultaneous optimization of I-E and Vr-Vl rotations (α=0.5, β=0.5). In the secondary phase of the optimization, an equivalent objective function was evaluated at 0° flexion.

Due to the large number of variables and a solution space with multiple local minima, typical gradient-based optimization algorithms were not effective at minimizing the objective function. Multiple researchers have employed a "simulated annealing" algorithm for global optimization of problems with large numbers of variables and complex objective functions with multiple local minima [45, 46]. More recently, simulated annealing (SA) optimization has been effectively applied to biomechanical applications like muscle-activation prediction in dynamic models of human movement [42, 43].

Simulated annealing overcomes the limitations of gradient-based optimization methods by incorporating a stochiastic heuristic that allows the optimization to escape local minima. The optimization is governed by the "temperature" (T) of the algorithm, analogous to the temperature of cooling metals during the annealing process, which governs the probability of accepting "uphill" moves of the optimization. Throughout the optimization, the temperature is reduced according to a cooling schedule until "uphill" moves are no longer accepted and the optimization performs like a gradient based method.

Suppose x is a vector in R^n containing ligament parameters (x_1, x_2, … , x_n). The function to be minimized, f(x), is the objective function calculated from the difference between model laxity predictions and the experimental laxity described

earlier (Equation 5.2), given a set of ligament parameters x. SA performs a random search of the solution space by serially perturbing each input variable in x to form a new vector x^i and evaluating the objective function $f(x^i)$. If the perturbation reduces the objective function, the current state of the ligament parameters in x´ is set to the new vector x^i. If the objective function is not improved, the metropolis criterion is invoked to determine if the perturbation is accepted, in the form:

$$p(accept) = e^{\left(\frac{f(x^i)-f(x')}{T}\right)} \quad \text{if} \quad f(x^i)-f(x') \geq 0 \quad \text{(Equation 5.3)}$$

Where *p(accept)* is the probability that the "uphill" move will be accepted and *T* is the current "temperature" of the model. Early in the optimization, these "uphill" moves have a higher probability of acceptance; later in the optimization, only "downhill" moves are accepted. To ensure reasonable ligament loading in the optimum solution, ligament forces were monitored for each model evaluation, and combinations of model parameters that generated ligament forces higher than the ligament failure forces reported in literature [9, 11] were not accepted. If at anytime, $f(x^i)$ was less than the best solution encountered in the algorithm thus far (x^*), then x^i became x^*. For more details of the algorithm, refer to Corana et al. [45] and Goffe et al. [46].

The simulated annealing algorithm, diagramed in Fig. 5.1, was employed for optimization of the current ligament parameters. The algorithm was composed of three loops: a variable perturbation loop, a step-size adjustment loop, and a

temperature reduction loop. The variable perturbation loop serially perturbed each of the input variables in x, evaluated the objective function f(x), and then accepted or rejected the perturbation based on improvement of the objective function and the metropolis criteria discussed previously, before moving onto the next variable. This loop was performed N_s times while tracking the acceptance rate for each variable. Following the N_s^{th} evaluation, the step-size for each variable was adjusted such that the acceptance rate would be approximately 60% and the variable perturbation loop was repeated N_s times. The process of variable perturbation and step-size adjustment was performed N_t times before a temperature reduction was performed, reducing the probability of accepting solutions that do not improve the objective function, and the process repeated.

Because the optimization was comprised of a relatively limited number of variables and the long computational time required to evaluate the computational model, an aggressive SA optimization routine was performed that produced manageable convergence times. The parameters governing the SA optimization were: an input temperature of 10, a cooling schedule of 0.5, an N_t of 5, and an N_s of 5. With these parameters and the 18 variables in phase-one of the ligament optimization, 450 evaluations of the computational model were performed before each temperature reduction.

Optimizations were performed on a desktop computer with eight processors, facilitating parallelization of the algorithm. Parallelization was performed through decision tree decomposition [97], simultaneously evaluating perturbations to three

input variables (seven variable combinations) over seven processors, while the eighth processor executed a Matlab script coordinating the optimization.

RMS errors between the computational laxity predictions and experimentally observed laxity were calculated for the different optimized solutions. To assess the convergence of the optimization routine, the same optimization was performed three times on a single knee. The optimizations were performed simultaneously for both I-E and Vr-Vl rotations (α=0.5, β=0.5). Afterwards, the similarity of the optimized solutions were compared.

To characterize ligament recruitment patterns, the maximal force predicted by each ligament in the model in response to the applied Vr-Vl and I-E torques were extracted at each flexion angle. The peak ligament forces for knees 1, 2, and 3 were averaged to determine a general pattern of ligament recruitment. Knee 4 was excluded from the averaged results because it exhibited a very different recruitment pattern from the other three knees, with the LCL becoming overly recruited in deep flexion. Although this recruitment pattern was noted during the experimental assessment of this particular knee, and is demonstrated in the laxity envelope of the knee, the remaining three knees demonstrated relaxation of the LCL with flexion.

5.2.4 Predictions of Knee Kinematics

For each knee, the optimized ligament parameters derived from the combined I-E and Vr-Vl optimizations were used to predict knee kinematics during laxity flexion evaluations in the Quasi-Static Knee Rig (QKR). The QKR was chosen for comparison because it represents a different loading condition from those used to

optimize the models, but does not incorporate significant inertial loads present during dynamic, muscle driven activities that would require more sophisticated modeling techniques. Using the loading rig, isolated I-E and Vr-Vl laxity assessments were performed on each knee by applying either a 3 N-m I-E torque, or 12 N-m Vr-Vl torque to the tibia in full extension with minimal compressive load across the joint, then slowly flexing and extending the knee from full extension to 90° flexion.

Equivalent I-E and Vr-Vl loading conditions to the QKR were recreated via the linkage system in the current model, while femoral flexion was prescribed in displacement control. For comparison purposes, a set of literature based ligament parameters were developed for each knee, with ligament attachment sites positioned in the center of the probed locations during the experiment, stiffness values from uniaxial tensile tests reported in the literature [9, 11], and reference strains in the medial and lateral ligaments reported by Blankevoort et al. [85]. The RMS difference between experimental kinematics and model-predicted kinematics through the flexion range were calculated for all four specimens using both the literature-based and optimized ligament parameters.

5.3 Results

5.3.1 Repeatability of Solution

The convergence of the optimization routine was similar for all four knees, with a majority of the improvement in combined RMS error occurring within the first 500 model evaluations (Fig. 5.2a). This corresponded to just over one full temperature reduction cycle in the simulated annealing algorithm. Although the

optimizations were carried out through at least three temperature reductions, the improvements in total RMS error were only marginal after the second temperature reduction (Fig. 5.2b).

Repeating the optimization routine three times on the same knee yielded similar RMS errors for each trial by the second temperature reduction (Fig. 5.2a, Tables 5.2 and 5.3); however, the optimization found three distinct ligament parameter combinations that yielded roughly the same level of fitness. In particular, the three sets of optimized parameters had different MCL, LCL, and PFL origin locations, LCL stiffness, and LCL reference strain. Conversely, all three solutions had similar MCL stiffness, MCL, PFL, and posterior capsule reference strains, and anterior lateral capsule (ALC) properties (Table 5.1).

5.3.2 Quality of Laxity Predictions

The experimentally observed I-E and Vr-Vl laxity for all four knees fell near or within the probabilistically predicted 5%-95% kinematic bounds from the computational model reported in the previous chapter (Fig. 5.3 and 5.4). Optimization of the ligament parameters improved the accuracy of laxity predictions from the subject specific ligament models to near, or within, the reported experimental 5% and 95% confidence intervals (± 2.5° for I-E rotation and ± 0.5° for Vr-Vl rotation) determined in Chapter 3 (Fig. 5.5 and 5.6). As expected, optimization of the ligament constraint to a particular axis of motion (i.e. Vr-Vl rotation) led to decreased error about that axis compared with the combined Vr-Vl and I-E optimized solution (Tables 5.2 and 5.3). However, the decrease in RMS error about the axis of

interest was always accompanied by a dramatic increase in error about the non-optimized axis. In knee 4, optimization of the ligament constraint to Vr-Vl laxity resulted in a dislocation of the knee at 60° and 90° knee flexion under external torque. Conversely, simultaneous optimization of the ligament constraint to both I-E and Vr-Vl laxity yielded solutions with only marginally increased error about each axis of laxity when compared to isolated optimization of that laxity (Table 5.2 and 5.3).

5.3.3 Ligament Recruitment

The models of knees 1, 2, and 3, optimized to both I-E and Vr-Vl rotations exhibited similar ligament recruitment patterns through the flexion range. On the medial side of the knee, the central and posterior bundle of the MCL were stressed in early flexion by valgus, internal, and external moments, then tension shifted to the central and anterior bundles of the MCL in deeper flexion (Fig. 5.6). The PMC provided constraint to valgus and internal torques primarily at 0° and 30° knee flexion. On the lateral side of the knee, the LCL was stressed under varus torque, with the largest force generated at 30° knee flexion (Fig. 5.7). As the knee flexed past 60°, the varus stressed transferred to the PFL. The LCL also resisted external tibial rotation at 0° and 30° flexion, beyond which the PFL resisted the external torque. The ALC was only loaded during internal tibial torque from 30° to 90° knee flexion.

5.3.4 Kinematic Predictions

The use of optimized ligament parameters consistently improved the prediction of knee kinematics during laxity assessments in the QKR compared to literature based ligament parameters. In particular, the RMS differences between experimental and model-predicted kinematics through the flexion range during the equivalent QKR assessments across all four knees were reduced by 50% for internal rotation, 61% for external rotation, 63% for varus rotation, and 56% for valgus rotations (Table 5.4, Figs. 5.8-5.11).

5.4 Discussion

In this study, simulated annealing optimization of ligament constraint was performed on four different knees after total knee replacement. In general, optimization of the ligament constraint to an isolated axis of knee laxity (e.g. I-E laxity) led to excellent agreement between the model and experimental laxity for that particular motion, but resulted in poor predictions for other laxities (e.g. Vr-Vl laxity). On the contrary, including both I-E and Vr-Vl laxities into the optimization function led to good predictions for laxity about both axes of knee rotation, which were only marginally less accurate than when optimized to that laxity in isolation.

5.4.1 Uniqueness of Optimized Ligament Parameters

While repeatedly performing the optimization on the same knee using the same loads and optimization parameters led to similar fitness scores, these optimized ligament parameters were not identical. Despite their different ligament parameters,

the RMS difference between the optimized model predictions and the experimentally measured laxity were within the 5%-95% confidence intervals of uncertainty associated with the laxity measurements reported experimentally. Therefore, the utility of increasing the initial temperature or decreasing the cooling schedule of the optimization to improve the convergence of the optimization is unclear, especially when compared with the dramatically increased optimization run time associated with those options.

The results of the convergence test showed that there were multiple ligament configurations that produce an acceptable level of constraint. Blankevoort et al. had similar findings when they demonstrated that including A-P translations (in addition to I-E rotation) into an I-E laxity optimization yielded a more accurate prediction of A-P translation without significantly reducing the accuracy of the I-E rotation prediction [1]. This is also supported by the current finding that simultaneously optimizing to both I-E and Vr-Vl rotations yielded improved predictions for both laxities, without significantly reducing the accuracy of either laxity prediction compared to optimization of that laxity in isolation. Perhaps a more unique solution could be generated by including additional laxity measurements, such as A-P laxity, or combined laxity like simultaneous valgus and internal torques.

5.4.2 Optimized Ligament Function

The ligament configurations used in this study were not able to predict the motion for all knees equally. Some particular laxity patterns, like the one exhibited by Knee 3, with increased varus rotation but less internal rotation in mid-flexion,

were difficult for the optimization to reproduce. Most ligament configurations that allowed increased varus laxity resulted in dislocation of the lateral condyle under internal tibial torque, which was not observed experimentally. Increasing the number of oblique structures in the model would have improved the ability of the ligament configuration to restrict that type of laxity.

While the spring structures used to represent ligaments in the current model do an acceptable job of providing knee constraint for most loading conditions, a comparison with literature is necessary to ensure they provide this constraint in the same manner as the actual knee ligaments. The average medial ligament forces generated in the computational models were compared to ligament forces measured *in vitro* in the natural knee under similar loading conditions [98]. In general, the medial ligament forces in the computational model followed a similar pattern to those observed *in vitro,* but were of much larger magnitude. In particular, Griffeth et al. measured force in the MCL and the PMC under valgus, internal, and external moments through the flexion range [98]. In their study, the distal portion of the MCL generated approximately 70 N of force under 10 N-m of valgus torque at full extension, approximately 100 N at 30° and 60° flexion, and 85 N at 90° flexion. In the current model, the MCL generated on average 91 N of force in full extension, peaked with 180 N at 60° flexion, then dropped slightly to 169 N at 90° flexion. It is unknown how much valgus restraint was provided in the *in vitro* experiment by the deep MCL, the medial meniscal attachments, and other capsular structures that are removed with total knee replacement. The increased forces generated in the model's

MCL may have been inflated by neglecting bone-ligament wrapping and representing the continuum of ligament structures around the knee, including the knee capsule, by a small number of springs. The model also generated much larger loads in the MCL under internal torque than were observed experimentally, which indicates that additional structures were recruited in the natural knee, like the cruciate ligament complex and menisci, to resist internal tibial rotation that are not present in the knee after TKR or in the current model.

Unlike the medial ligaments, the loads predicted in the LCL were closer to those measured *in vitro* in the natural knee [99]. LaPrade et al. reported LCL forces under 10 N-m of varus torque at 30° flexion of approximately 110 N, compared to 119 N in the current model [99]. LaPrade et al. did not observe the PFL resisting varus loads in deeper flexion as observed in the model. Therefore, the LCL forces generated in the model were significantly less than those observed experimentally at 60° and 90° flexion. Although not the primary stabilizer against varus torque, the PFL has been shown to resist varus rotation in previous cadaveric experiments [100]. Representing the complex architecture of the popliteal fibular ligament and popliteal tendon as a single spring likely led to increased recruitment of the structure. However, the PFL was primarily responsible for restricting external tibial rotation in the model and therefore a necessary structure to recreate the appropriate knee laxity.

While the ACL and PCL resist internal tibial torque in the natural knee at 90° flexion [101], it is unclear from the literature which structures resist internal tibial torque after total knee replacement. In the current model, neither the LCL nor PFL

had the appropriate line of action to resist posterior translation of the lateral condyle under internal tibial torque. To restrict this motion, an anterior-lateral capsular spring was included in the model that spanned from the lateral epicondyle to the anterior-lateral border of the tibia, as observed during the experimental assessments (Fig. 5.12). The ALC was the primary constraint on the lateral side against internal tibial rotation by resisting posterior translation of the lateral femoral condyle relative to the tibia.

5.4.3 Improvement in Kinematic Predictions

As expected, the ligament optimization yielded a set of ligament parameters capable of more accurately predicting knee kinematics through the flexion range under relatively simple loading conditions compared to literature-based parameters. Despite the improved predictions, differences still existed between experimental and computationally predicted kinematics that introduces the question of how accurate ligament representations should be to yield reasonable model predictions. This question is inherently application specific; for laxity predictions in the QKR, ligament constraint and articular geometry are the largest factor affecting the experimental kinematics. Even in this simple model, experimental uncertainty in the applied loads may have a larger effect on the observed knee kinematics than the current error observed using optimized ligament parameters. In more sophisticated dynamic muscle-driven models, uncertainty in muscle lines of actions, or inertial properties may be much larger than errors introduced by the ligament configuration.

Previous studies have used non-linear springs to predict knee mechanics during dynamic, weight-bearing activities; however, it is unclear if ligaments tuned to knee laxity provide the appropriate dynamic constraint during weight-bearing activities. Each of the knees included in the current study were also subjected to dynamic evaluations in the Kansas Knee Simulator (KKS), a dynamic knee testing device. In future analysis, the ability of ligament configurations optimized using the current experimental-computational method to improve dynamic knee kinematic predications will be evaluated in a computational model of the KKS. Such an analysis would indicate the utility of the current ligament optimization process for computational models that predict mechanics during more sophisticated dynamic activities like gait.

5.4.4 Model Limitations and Future Work

The non-linear springs used in this study provided a computationally efficient representation of the knee's constraint particularly well suited for large-scale optimization problems. While more sophisticated ligament representations, including continuum models, provide more accurate representation of ligament function, their evaluation time is prohibitive for use in optimization routines. The optimized ligament configurations determined in the current study could be used to configure the reference strain distribution, stiffness, and femoral attachment locations for more sophisticated ligament representations. Coupling the computationally efficient representation with a more sophisticated ligament representation would overcome the

limitations associated with the spring representation while preserving the benefit of efficient ligament parameter optimization.

As discussed previously, the computational ligament configuration used in this study was not always able to exactly replicate the observed experimental laxity, primarily when optimized to both Vr-Vl and I-E rotations. The potential causes for these discrepancies are likely systematic in the experimental assessment, the computational ligament representation, and the performance of the optimization routine. First, there is some experimental error associated with the target laxity curves, which may lead to a laxity behavior that no ligament model would be able to replicate. This error is due to uncertainty in registration of the implant geometries to their respective experimental reference frames, the resulting variation in kinematic descriptions, potential calibration error in the load cell measurements and load cell orientation, and inertial and gravitational effects which may alter the true loading state of the knee. Some of this error would be reduced by incorporating dimple points on the implant geometry which could be more easily identified during the experiment, although some error will remain due to the accuracy of the motion tracking system. An attempt was made in Chapter 3 to quantify some of this error; however, several potential error sources were not included in that analysis.

Several assumptions were made to simplify the complex ligament architecture of the human knee into the discrete number of spring elements used in the computational ligament representation. While the primary structures were represented in the model along their predominant lines of action, the oblique connective tissue

around the knee, particularly in the knee capsular structures were not included, along with the knee extensor mechanism. Additionally, the existing spring structures were not allowed to wrap around the knee geometry, altering their lines of action. Incorporation of additional structures and wrapping effects would likely improve the ability to optimize the model to both Vr-Vl and I-E motions.

The optimization procedure was very successful in replicating an isolated axis of knee laxity; however, little analysis was performed to understand the influence of the weighting parameters α and β on the accuracy of the laxity predictions. There were likely optimum values for these weight factors that would minimize the overall error between the experiment and the model. These optimum values may also be application specific and should be tuned for the particular purpose of the model into which these ligaments are incorporated and the primary loading that model undergoes.

Additional experimental testing is required to understand the applicability of the current ligament representation to evaluate potential modifications to the knee joint, like the effect of implant alignment and ligament balancing activities. It is unclear from the current analysis if the optimized ligament configuration remains valid when the articular constraint at the knee changes. Future evaluation will focus on the ability of the optimized ligament configuration to predict controlled changes to the knee joint, such as partial ligament resection, increased implant thickness, or altered implant alignment. Such validation is necessary for the current ligament configurations to be used as a predictive tool to evaluate potential intra-operative

decisions. Ideally, the ligament optimization used in this study could be applied to the natural knee before joint replacement surgery. Doing so would allow the optimized model of the natural knee to be used in surgical planning.

In summary, anatomically based spring representations of knee ligamentous constraint were capable of reproducing subject-specific knee laxity. The computationally-efficient nature of the spring elements, combined with an efficient rigid body solver, allowed optimization of the ligament parameters within a reasonable time-frame. The combined experimental-computational method employed in this study could be modified for use in a clinical setting to generate subject-specific ligament models for use in computational models of the knee joint after total knee arthroplasty. However, additional experimentation and computational analysis are needed to determine the ability of the optimized ligament configurations to predict changes in knee mechanics after ligament balancing or implant re-alignment.

5.5 Tables and Figures

Table 5-1: List of ligament parameters included into the optimization for each ligament in the knee. Included are the optimized ligament parameters for Knee 1 after three independent optimization runs.

Structure	Parameter	Run 1	Run 2	Run 3	St. Dev.
LCL	Origin A(+)-P Offset (mm)	-4.91	-3.78	-4.16	0.58
	Origin S(+)-I Offset (mm)	0.31	3.13	4.29	2.04
	Total Stiffness (N/mm)	88.42	66.44	80.79	11.16
	Ref. Strain (Ant.)	1.02	1.02	1.00	0.01
	Ref. Strain (Mid.)	0.99	0.98	1.01	0.01
	Ref. Strain (Post.)	0.98	0.99	1.03	0.03
MCL	Origin A(+)-P Offset (mm)	-3.39	0.69	2.86	3.17
	Origin S(+)-I Offset (mm)	-4.23	1.95	-0.18	3.14
	Total Stiffness (N/mm)	94.04	87.51	94.42	3.89
	Ref. Strain (Ant.)	0.98	0.99	0.95	0.02
	Ref. Strain (Mid.)	1.04	1.02	1.00	0.02
	Ref. Strain (Post.)	1.05	1.04	1.05	0.00
ALC	Insertion A(+)-P Offset (mm)	-4.57	-4.87	-3.67	0.63
	Stiffness (N/mm)	25.75	23.31	26.29	1.59
	Ref. Strain	0.97	0.97	0.96	0.00
PFL	Origin A(+)-P Offset (mm)	0.48	-4.49	1.63	3.25
	Origin S(+)-I Offset (mm)	-3.00	-4.58	0.15	2.41
	Ref. Strain	0.82	0.82	0.86	0.03
Posterior Capsule	MPC Ref. Strain	0.98	1.02	1.01	0.02
	LPC Ref. Strain	1.05	1.04	1.03	0.01
	OPC-m Ref. Strain	0.97	1.01	1.01	0.02
	OPC-l Ref. Strain	1.03	1.03	1.03	0.00
	PMC Ref. Strain	0.98	0.98	1.01	0.01

Table 5-2: The root mean square difference between the experimental internal and external laxity assessments and the laxity predictions of the optimized ligament models for all four knees. The ligament configurations were optimized to isolated Vr-Vl laxity, isolated I-E laxity, and to both Vr-Vl and I-E laxities simultaneously. *The ligament configuration of Knee 4 optimized to isolated Vr-Vl rotation allowed dislocation of the knee under I-E torques at 60° and 90° knee flexion.

		Internal RMS Difference (°)					External RMS Difference (°)				
Knee	Optomized to:	0°	30°	60°	90°	**Average**	0°	30°	60°	90°	**Average**
1	Vr-Vl	1.1	2.2	4.2	5.6	**3.3**	0.3	0.5	1.6	3.3	**1.4**
	I-E	0.4	1.3	1.0	1.7	**1.1**	0.3	0.2	0.9	1.6	**0.7**
	Combo (1)	0.4	1.3	0.7	2.4	**1.2**	0.6	0.4	1.0	1.4	**0.8**
	Combo (2)	0.4	1.5	1.4	2.5	**1.4**	0.2	0.3	1.4	1.8	**0.9**
	Combo (3)	0.4	1.7	1.3	2.9	**1.6**	0.3	0.6	1.0	2.3	**1.0**
2	Vr-Vl	1.3	3.4	2.6	2.0	**2.3**	0.6	3.5	1.5	6.6	**3.1**
	I-E	0.2	2.1	0.9	1.0	**1.1**	0.4	1.1	0.8	1.2	**0.9**
	Combo	0.4	2.8	2.0	1.7	**1.7**	0.7	0.8	1.2	1.6	**1.1**
3	Vr-Vl	0.8	1.3	3.0	9.8	**3.7**	6.2	6.6	2.8	2.1	**4.4**
	I-E	0.2	1.9	2.0	1.8	**1.5**	2.0	1.3	1.0	2.0	**1.6**
	Combo	0.3	1.9	2.8	0.4	**1.4**	3.8	4.9	1.8	1.7	**3.1**
4	Vr-Vl	8.1	10.8	NA*	NA*	**NA***	2.6	5.3	NA*	NA*	**NA***
	I-E	4.6	2.9	1.1	1.4	**2.5**	1.5	1.0	1.4	2.3	**1.5**
	Combo	2.2	2.6	0.7	5.2	**2.7**	2.1	2.0	1.1	1.3	**1.6**

Table 5-3: The root mean square difference between the experimental varus and valgus laxity assessments and the laxity predictions of the optimized ligament models for all four knees. The ligament configurations were optimized to isolated Vr-Vl laxity, isolated I-E laxity, and to both Vr-Vl and I-E laxities simultaneously.

		Varus RMS Difference (°)					Valgus RMS Difference (°)				
Knee	Optomized to:	0°	30°	60°	90°	**Average**	0°	30°	60°	90°	**Average**
1	Vr-Vl	0.3	0.2	0.2	0.3	**0.2**	0.1	0.3	0.5	0.6	**0.4**
	I-E	0.9	2.3	2.8	2.4	**2.1**	0.7	3.6	4.1	5.2	**3.4**
	Combo (1)	0.2	0.1	0.3	0.2	**0.2**	0.4	0.5	0.4	0.3	**0.4**
	Combo (2)	0.3	0.3	0.7	0.2	**0.4**	0.1	0.2	0.5	1.1	**0.5**
	Combo (3)	0.2	0.1	0.2	0.3	**0.2**	0.1	0.3	0.4	0.6	**0.4**
2	Vr-Vl	0.4	0.5	0.4	0.5	**0.5**	0.1	0.3	0.6	0.5	**0.4**
	I-E	0.7	2.1	1.9	2.0	**1.7**	0.1	1.2	0.5	0.9	**0.6**
	Combo	0.3	0.8	0.7	0.7	**0.6**	0.1	0.3	0.8	1.5	**0.7**
3	Vr-Vl	0.3	1.2	1.2	0.2	**0.7**	0.4	0.3	0.4	0.6	**0.4**
	I-E	2.1	5.4	5.0	2.8	**3.8**	0.6	1.6	2.3	3.3	**1.9**
	Combo	0.3	1.3	1.2	0.7	**0.9**	0.4	0.8	0.9	0.5	**0.7**
4	Vr-Vl	0.2	0.2	0.5	0.4	**0.3**	0.6	0.3	0.8	1.0	**0.7**
	I-E	0.5	0.6	1.4	1.9	**1.1**	1.0	2.3	3.0	3.2	**2.4**
	Combo	0.7	1.2	1.7	0.9	**1.1**	0.9	1.0	1.1	0.2	**0.8**

Table 5-4: RMS difference (°) between the knee I-E or Vr-Vl kinematics observed during the experimental QKR I-E and Vr-Vl laxity assessments and the equivalent model predicted kinematics using literature-based (Lit) and optimized (Opto) ligament parameters.

Knee	Ligaments	RMS Difference (°)			
		Int.	Ext.	Var.	Val.
1	Opto	2.1	1.7	0.3	1.2
	Lit	3.3	3.9	2.8	1.3
2	Opto	1.3	2.3	0.7	0.8
	Lit	4.7	7.4	0.9	1.8
3	Opto	2.0	1.0	0.9	1.1
	Lit	6.1	2.3	3.6	2.0
4	Opto	5.5	3.0	3.2	0.6
	Lit	7.8	7.2	6.6	3.1

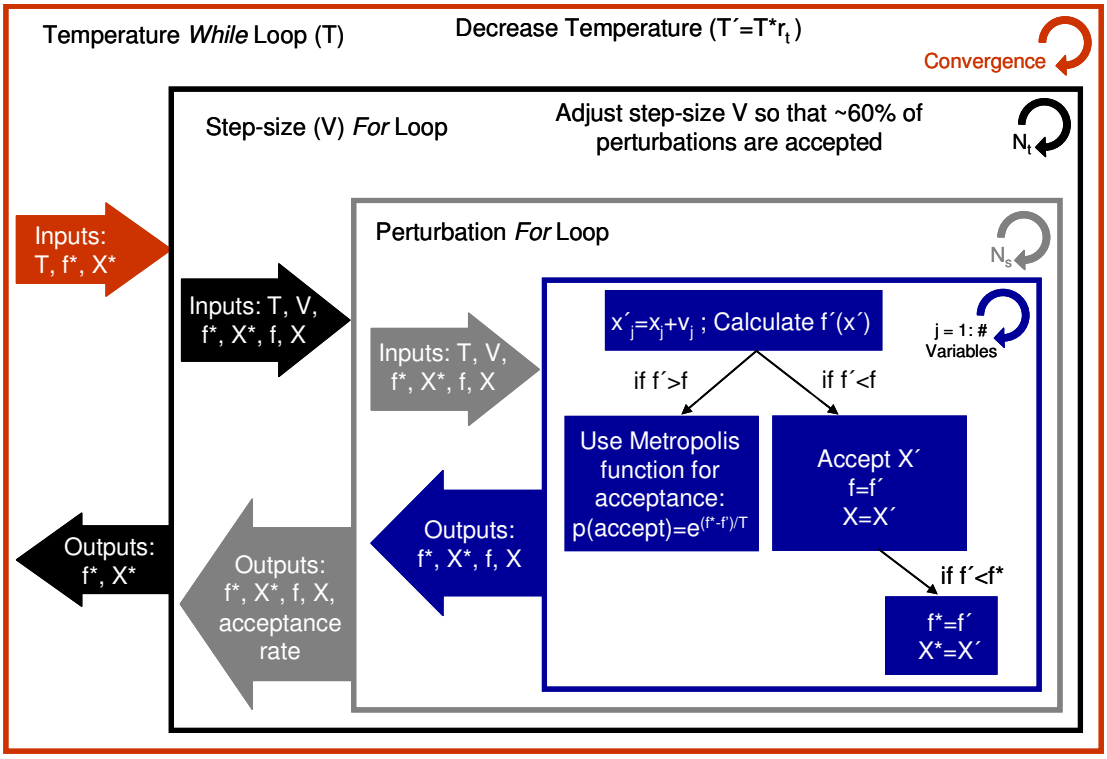

Figure 5-1: Schematic of the simulated annealing optimization algorithm used to optimize the ligament parameters for each specimen.

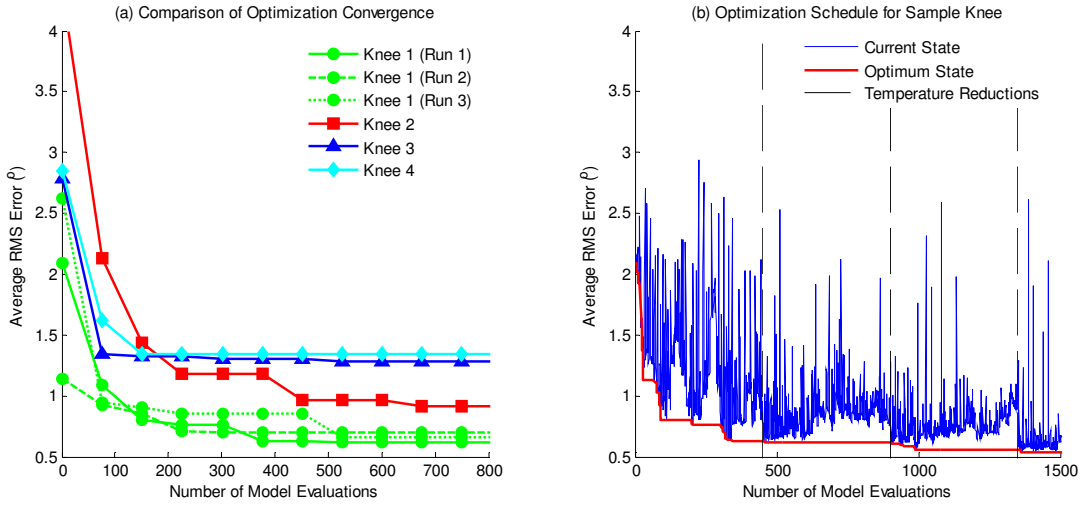

Figure 5-2: Performance of the simulated annealing optimization algorithm for minimization of the RMS error between observed experimental laxity and laxity predicted by the computational model. (a) Comparison of the convergence times for all four specimens (including three optimizations of Knee 1). (b) Sample convergence for Knee 1, carried out to 1500 model runs, with only marginal improvement after the first 500 runs.

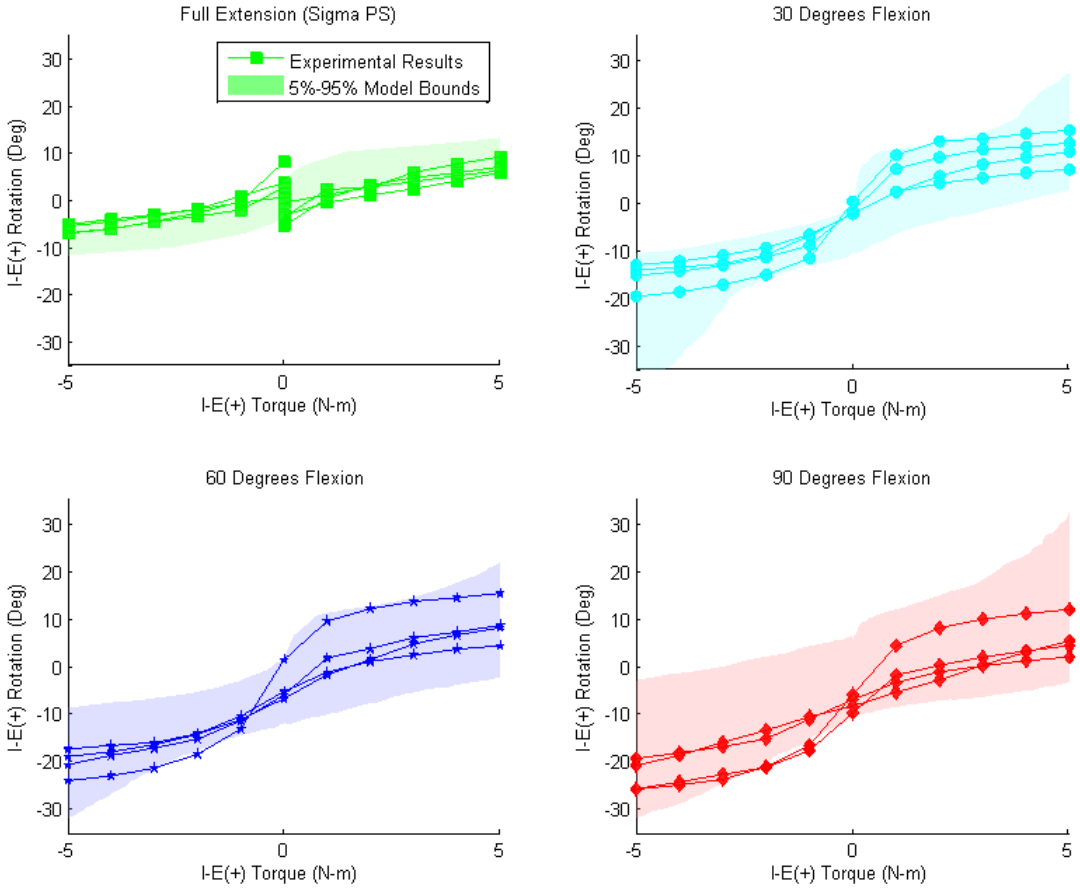

Figure 5-3: Comparison of I-E laxity through the flexion range between the experimentally observed laxity for all four knees and the corresponding probabilistic predictions from the knee ligament model. The solid lines represent the experimentally observed laxity, while the shaded regions represent the 5% and 95% confidence intervals calculated by the model. Experimentally observed I-E laxity fell along or within the computationally predicted bounds.

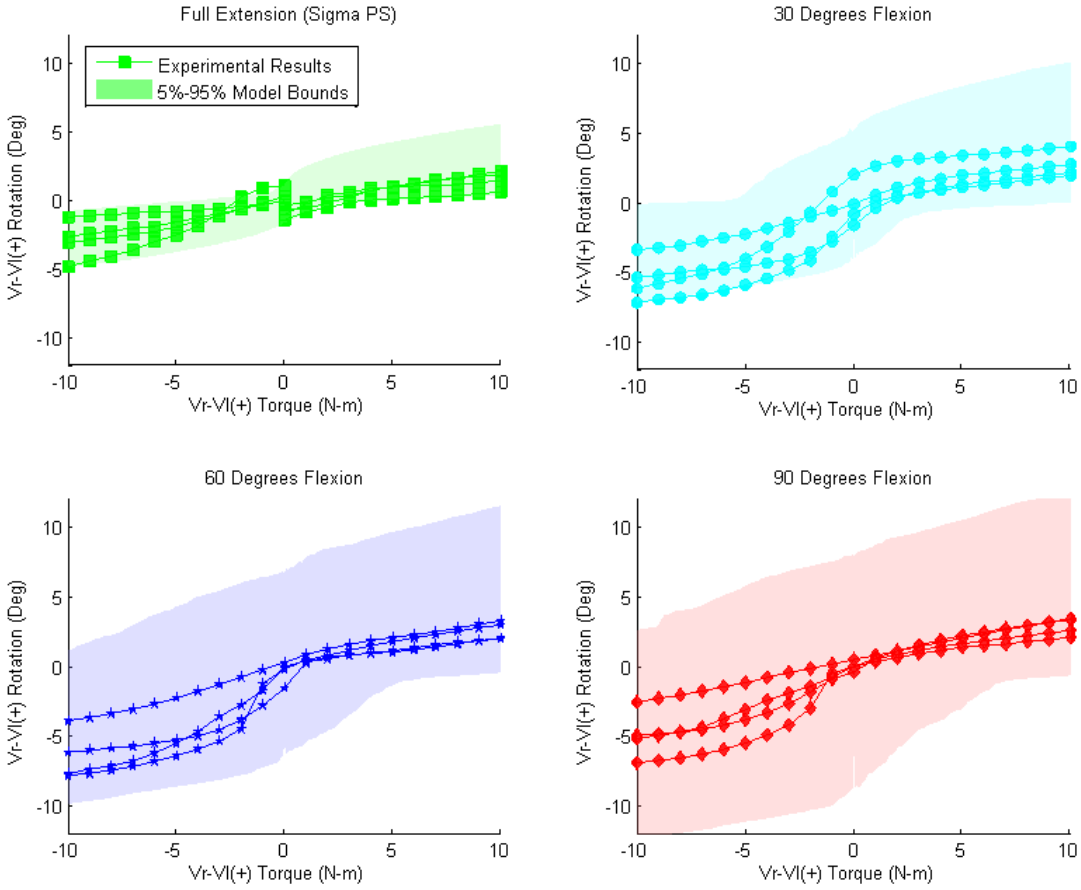

Figure 5-4: Comparison of Vr-Vl laxity through the flexion range between the experimentally observed laxity for all four knees and the corresponding probabilistic predictions from the knee ligament model. The solid lines represent the experimentally observed laxity, while the shaded regions represent the 5% and 95% confidence intervals calculated by the model. Experimentally observed Vr-Vl laxity fell along or within the computationally predicted bounds.

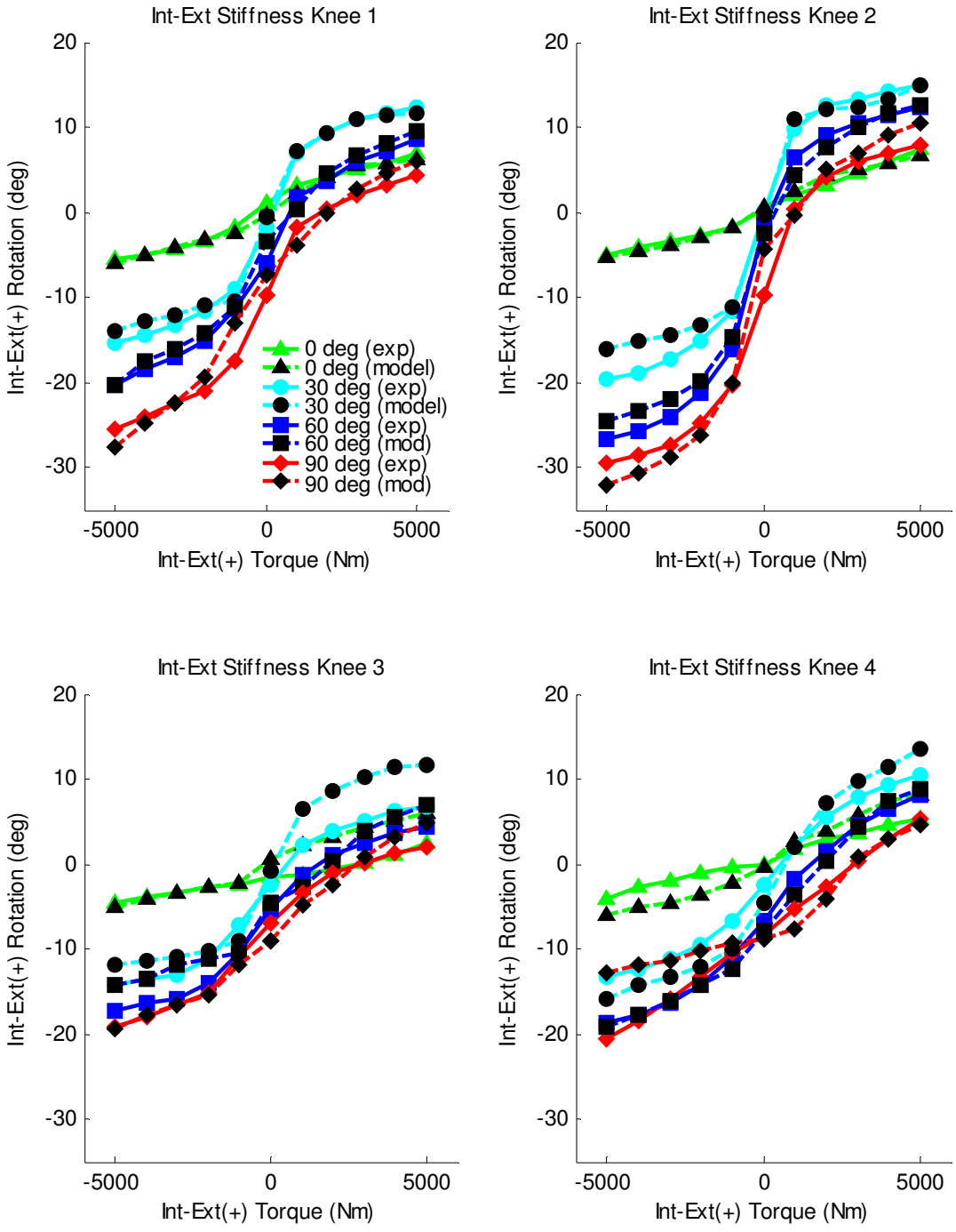

Figure 5-5: Comparison of experimentally observed I-E laxity (solid lines) and predicted laxity from the computational models optimized to both I-E and Vr-Vl laxity (dashed lines) for all four specimens at 0°, 30°, 60°, and 90° knee flexion

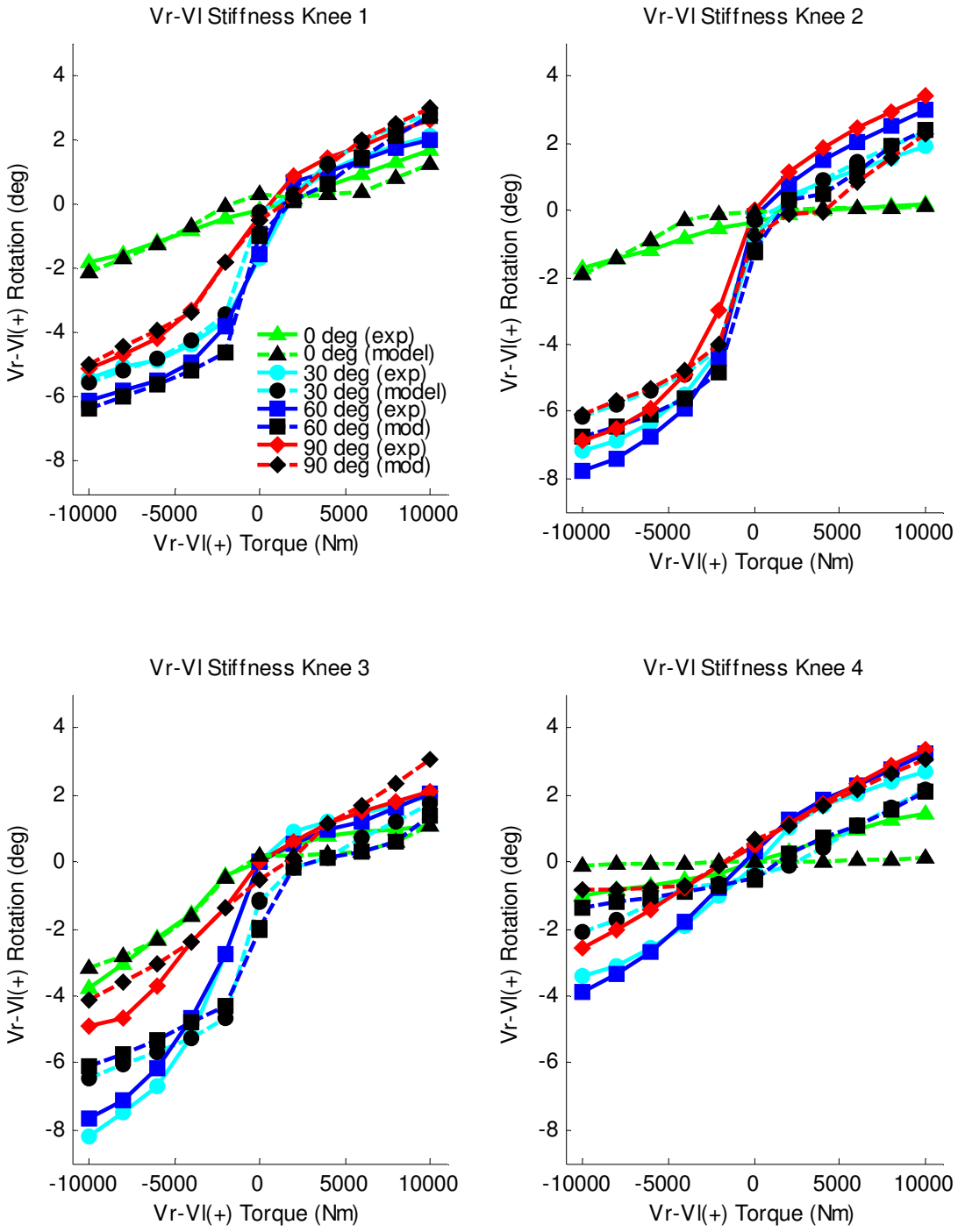

Figure 5-6: Comparison of experimentally observed Vr-Vl laxity (solid lines) and predicted laxity from the computational models optimized to both I-E and Vr-Vl laxity (dashed lines) for all four specimens at 0°, 30°, 60°, and 90° knee flexion.

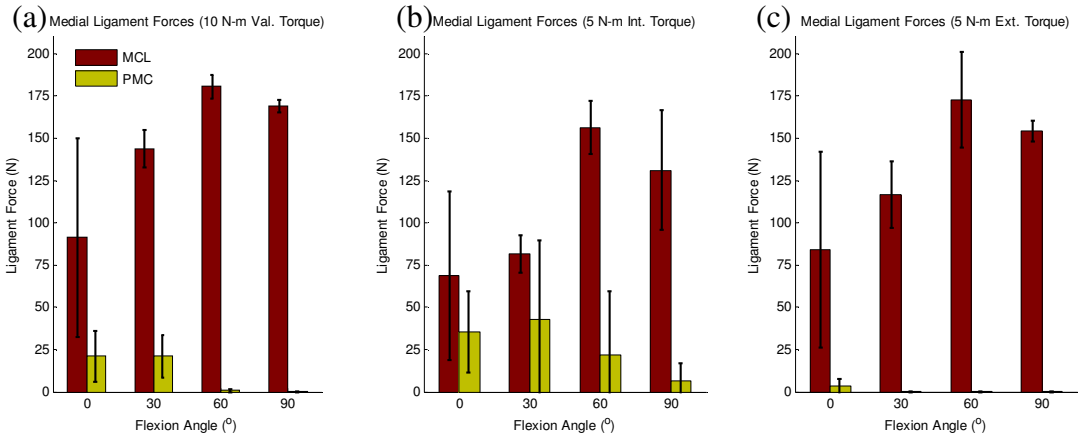

Figure 5-7: Average MCL and PMC forces generated by the optimized ligaments in knees 1, 2, and 3 in response to (a) valgus, (b) internal, and (c) external tibial torques. Knee 4 was excluded from the analysis because it exhibited a very different LCL recruitment pattern to the first three knees in deep flexion.

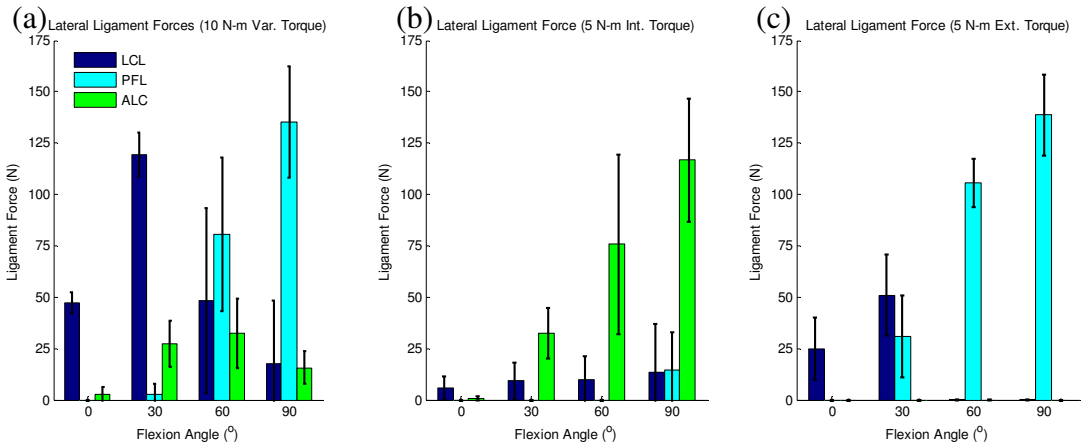

Figure 5-8: Average LCL, PFL, and ALC force generated by the optimized ligaments in knees 1, 2, and 3 in response to (a) varus, (b) internal, and (c) external tibial torques.

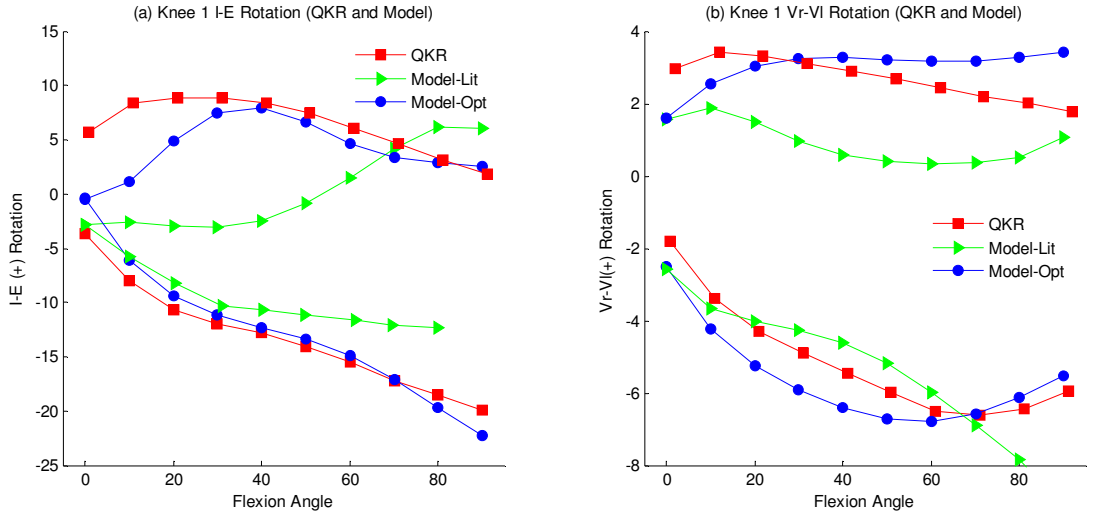

Figure 5-9: Comparison of Knee 1 kinematics during the (a) I-E and (b) Vr-Vl laxity evaluations in the QKR and the model predicted kinematics under equivalent loading conditions using literature-based and optimized ligament parameters.

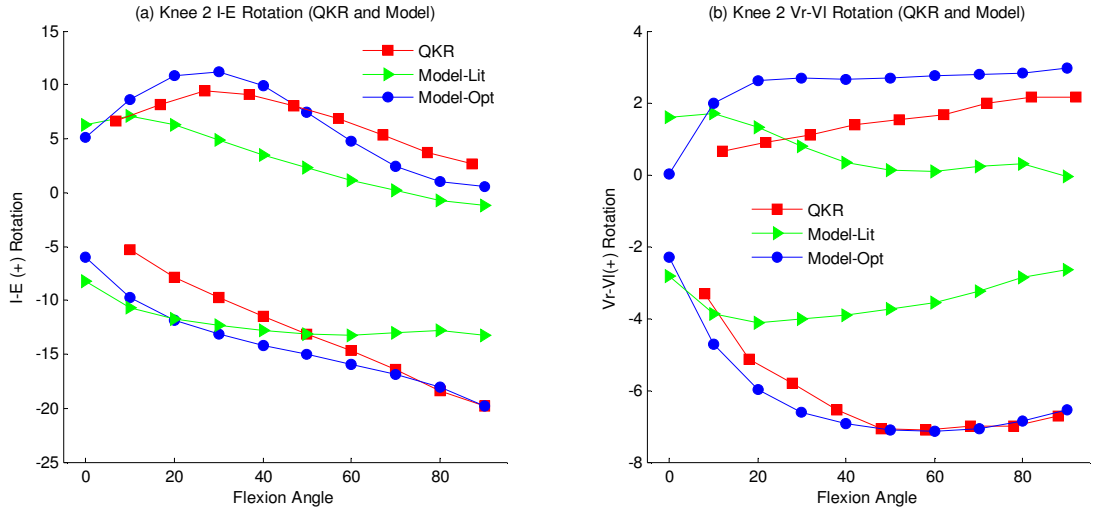

Figure 5-10: Comparison of Knee 2 kinematics during the (a) I-E and (b) Vr-Vl laxity evaluations in the QKR and the model predicted kinematics under equivalent loading conditions using literature-based and optimized ligament parameters.

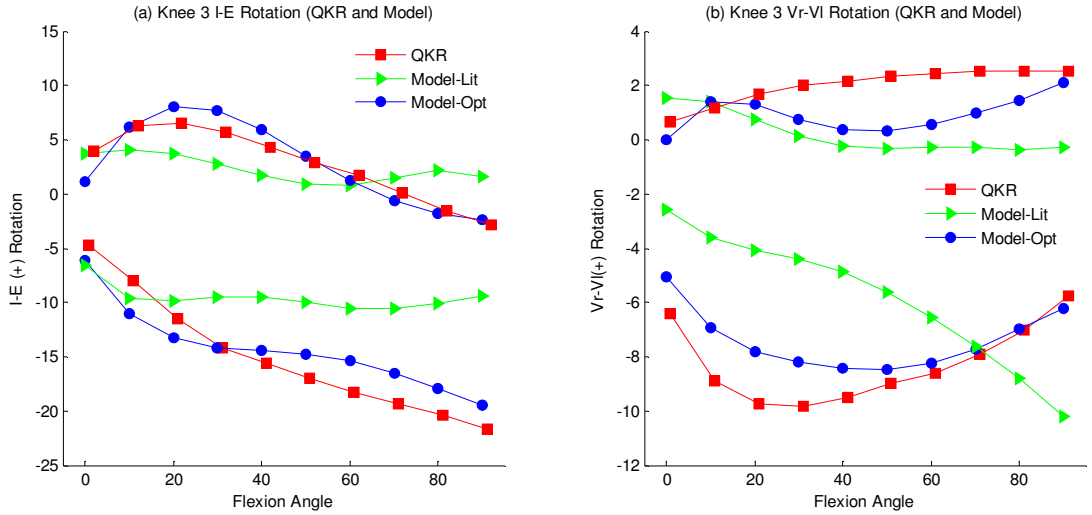

Figure 5-11: Comparison of Knee 3 kinematics during the (a) I-E and (b) Vr-Vl laxity evaluations in the QKR and the model predicted kinematics under equivalent loading conditions using literature-based and optimized ligament parameters.

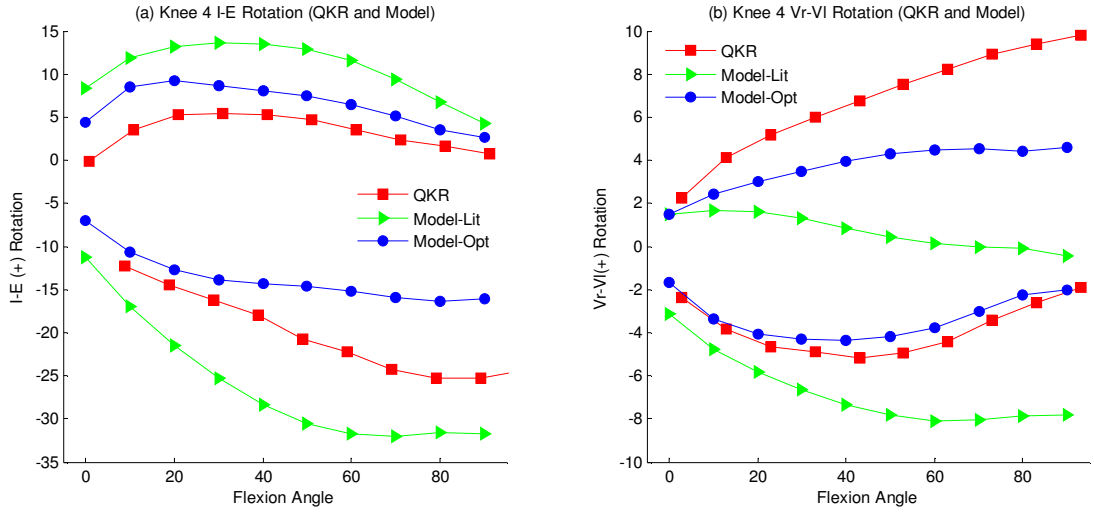

Figure 5-12: Comparison of Knee 4 kinematics during the (a) I-E and (b) Vr-Vl laxity evaluations in the QKR and the model predicted kinematics under equivalent loading conditions using literature-based and optimized ligament parameters.

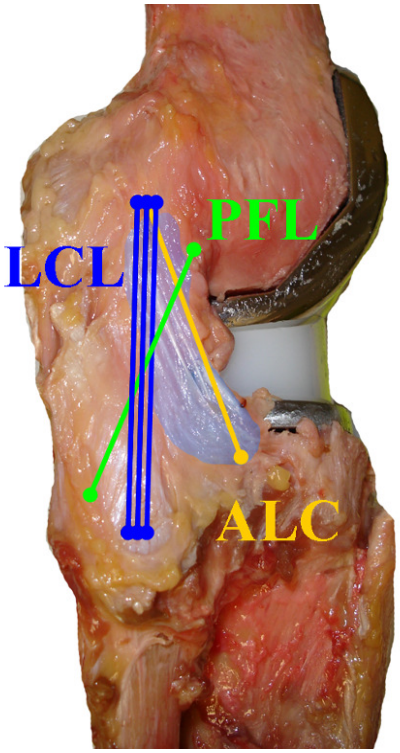

Figure 5-13: Lateral view of a sample knee after dissection illustrating the spring structures used to approximate the posterior-lateral soft tissue structures, including the LCL, PFL, and ALC.

Chapter 6: Conclusions and Future Work

As stated in the introduction, the overarching goal of the current research was to combine experimental methods for evaluation of knee laxity with an accurate and efficient computational model of knee ligament constraint to efficiently generate subject specific ligament models. These ligament representations could then be used in conjunction with existing models of knee mechanics to aid surgeons in intra-operative decision-making. The studies described in the previous chapters represent a significant step towards this goal (Fig. 6.1).

The experimental methods in Chapter 3 described a manual approach to reliably assess knee laxity, despite the inherent variation with loading the joint by hand. The manual approach was chosen because surgeons currently use this method to assess knee stability, and would likely be more comfortable utilizing this form of manipulation in the operating room. The primary challenge with adapting the reported methods performed on cadavers to patients in the operating room would be measurement of the loads applied by the surgeon to the knee. However, recent work by Musahl et al., who described an instrumented boot placed on the foot that allows measurement of applied loads [102], and by Swank et al., who described an inter-joint tensioning device [103], both represent means of collecting applied joint loads *in vivo*. Combined with knee kinematics collected by a CAS system, the algorithm developed in Chapter 3 could be used to quickly generate knee laxity profiles.

Using the current experimental method, a number of future studies should be conducted and some are currently under way. As discussed in Chapter 5, additional motions included in the optimization function improved the fidelity of the optimized ligament parameters. In future testing, combined laxities should be collected, i.e. combined valgus and internal torque, to provide additional laxity profiles for the optimization. In addition, the laxity envelopes should be performed with an instrumented tibial insert to measure joint compressive load. Joint loading during the envelope would be valuable in demonstrating that the optimized ligament representations indeed recreated the appropriate constraint at the knee. To improve the fidelity of the solution, the compressive force on each condyle could be included in the cost function of the optimization.

While the envelope assessment was able to differentiate changes between the natural and post-TKR knee, it is still unclear if the method is sensitive enough to detect small changes in joint constraint, like changing insert thickness, insert geometrical constraint, or slight adjustments to ligament balance. While anecdotal data was collected during the experiments regarding small changes to the knee constraint, a systematic approach should be employed where changes to the joint constraint are methodically performed on a knee, envelope examinations are used to assess the magnitude of these changes, and the ability of the optimized ligament models to predict these changes are tested. Doing so would demonstrate the sensitivity of the envelope model to clinically relevant changes to knee constraint,

and also provide additional validation data for the predictive ability of the ligament constraint model.

Finally, most surgeons perform a manual assessment of knee stability intra-operatively to assess ligament balance across the knee. During this manipulation, a surgeon applies a Vr-Vl load to the foot and estimates the amount of condylar lift off that occurs. The methods described here could be used to correlate the surgeon's perception of knee stability into an accurate measurement of knee laxity. For example, the amount of condylar lift off and Vr-Vl angulations could be compared between knees perceived as "stable" versus "unstable". A correlation between surgeon perceptions of stability and a true kinetic description of stability would be a valuable set of data for engineers designing instrumentation for implantation of total knee replacements.

Chapters 4 and 5 demonstrated the ability of the current computational model, coupled with an optimization routine, to represent the constraint of the knee after total knee replacement. Perhaps the largest potential limitation to the current approach was the use of a simplified ligament spring configuration. While these structures are commonly used in the literature and, as demonstrated by the results of this research, can recreate reasonable knee constraint, they may not do so in the same manner as the real knee. My current research focuses on application of the experimental-computational methods described here to more sophisticated continuum ligament representations. Continuum representation of ligaments allow for more accurate representation of ligament bone wrapping (as in the MCL) and more accurate

representation of the true ligament geometry. In addition, if tuned properly, these structures can provide estimates of localized ligament stress and strain distributions.

Unfortunately, continuum ligament models are much more computationally expensive, which makes large scale optimization of all the ligament parameters infeasible. For comparison, the ligament configuration model described above was implemented in an explicit finite element solver, resulting in a 2x increase in solution time compared to the rigid body solver described in Chapter 4. Through collaboration with researchers at the University of Denver, continuum ligaments representations were incorporated into the model, increasing the solution time from approximately fifteen minutes for simple springs to eight hours for continuum ligaments. Instead of performing the large-scale optimization on the continuum structures, a hybrid approach was implemented. The optimized ligament spring configurations were used as a starting point for a smaller optimization of the continuum structures. Results using continuum ligament representations optimized using this process improved dynamic predictions of knee kinematics during deep knee bend and gait simulations in the KKS (Manuscript prepared for submission).

Even with the computational efficiency of the current model, optimization of the ligament parameters still took several days. Without dramatic improvement in computational speeds and parallel computing, a different approach would be required to use these methods in the operating room. The first option would be to utilize a probabilistic approach to determine a host of potential ligament configurations before the surgery was performed. For example, a model, including bony geometry and

ligament attachments, could be constructed from preoperative MR-images of the knee. Preoperative surgical planning for implant alignment, coupled with custom alignment jigs to ensure accurate placement of the components, would ensure identical placement of the replacement components in both the model and in the actual knee. With the model constructed, a number of ligament configurations could be generated using a probabilistic representation of ligament properties before the surgery starts, as demonstrated in Chapter 4. After the TKR is implanted in the operating room, the envelope could be collected, and the best ligament representation would be selected for additional analysis.

A more useful option would be to use the techniques described in this document to generate subject specific models of the natural knee. This task would be considerably more complex considering the increased number of structures in the natural knee, including the cruciate ligaments and the meniscus. A model of the natural knee tuned to subject specific laxity could be used as a preoperative planning tool to help surgeons determine the optimal implant alignment considering any ligament deformity due to OA. There exists sufficient experimental data in the data set described in Chapter 3 to perform such an optimization; however, improvements in dynamic computational models of the natural knee, including the meniscus, would be the first critical step in such an exercise.

Independent of ligament representation, the ability of these optimized ligament models to predict changes in knee constraint are unproven. Some simple exercises could be performed using the existing experimental data set that would

illustrate the predictive ability of these models. For example, several experimental knees were evaluated with multiple different styles of implants, i.e. fixed bearing versus rotating platform designs. Ligament parameters could be optimized using one set of knee implants and the optimized model used to predict the change in knee laxity with the different knee implant. Additional experiments should focus on establishing the connection between changes to the subject's knee ligamentous constraint (i.e. ligament balancing releases) and the necessary adjustments in the ligament model to represent these changes. In such an experiment, for example, experimental envelopes could be collected before and after a release of the anterior third of the MCL. Model predictions of the change in knee laxity could be generated by removing the anterior bundle of the MCL and compared with the experimental assessments. Experiments should be performed in a similar fashion to validate the function of all the ligament structures in the model.

The primary contribution of this work to the biomechanics society was development of the combined computational and experimental framework necessary to solve this particular problem. All too often, computational models are developed without the benefit of corroborating experimental data, or experimental data is collected without the due diligence required to build computational models from the experiment. Building subject-specific ligament models described in this study required a synergy between biomedical imaging, assessment of knee laxity, and computational models of the knee not often found in the literature. In addition, several unique techniques were developed in support of the overall goal. A simple

and reliable methodology was developed for collecting knee laxity that could be adopted for use in the exam room. This work also demonstrated the ability of simple spring configurations to reasonably represent the complex soft tissue architecture of the implanted knee with the appropriate ligament parameters, but also demonstrated that researchers who employ this representation without properly tuning the soft tissue parameters should be wary of their results. In the past, ligament parameters were assigned from values reported in the literature. In this work, a significant step forward was taken to improve knee kinematic predictions by applying optimization methods to knee ligament models. Overall, the data and methods reported in this document provide a solid foundation for future research in the development of subject specific knee models.

6.1 Figures

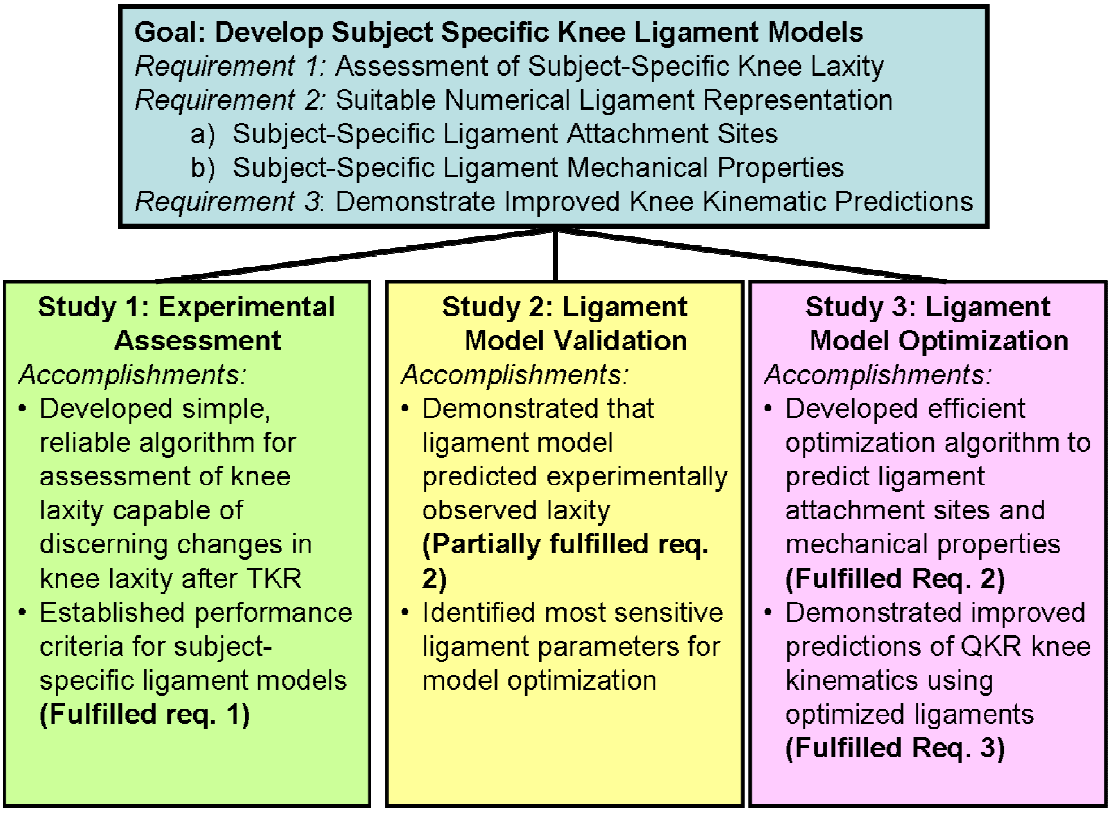

Figure 6-1: Overview of each individual study's contribution to the overarching goal of development of subject-specific knee ligament models.

References

1. Blankevoort, L. and R. Huiskes, *Validation of a three-dimensional model of the knee.* J Biomech, 1996. **29**(7): p. 955-61.
2. Martelli, S. and V. Pinskerova, *The shapes of the tibial and femoral articular surfaces in relation to tibiofemoral movement.* J Bone Joint Surg Br, 2002. **84**(4): p. 607-13.
3. Iwaki, H., V. Pinskerova, and M.A. Freeman, *Tibiofemoral movement 1: the shapes and relative movements of the femur and tibia in the unloaded cadaver knee.* J Bone Joint Surg Br, 2000. **82**(8): p. 1189-95.
4. Kessler, O., L. Durselen, S. Banks, H. Mannel, and F. Marin, *Sagittal curvature of total knee replacements predicts in vivo kinematics.* Clin Biomech (Bristol, Avon), 2007. **22**(1): p. 52-8.
5. Yu, C.H., P.S. Walker, and M.E. Dewar, *The effect of design variables of condylar total knees on the joint forces in step climbing based on a computer model.* J Biomech, 2001. **34**(8): p. 1011-21.
6. Robinson, J.R., J. Sanchez-Ballester, A.M. Bull, W. Thomas Rde, and A.A. Amis, *The posteromedial corner revisited. An anatomical description of the passive restraining structures of the medial aspect of the human knee.* J Bone Joint Surg Br, 2004. **86**(5): p. 674-81.
7. Wymenga, A.B., J.J. Kats, J. Kooloos, and B. Hillen, *Surgical anatomy of the medial collateral ligament and the posteromedial capsule of the knee.* Knee Surg Sports Traumatol Arthrosc, 2006. **14**(3): p. 229-34.
8. Robinson, J.R., A.M. Bull, R.R. Thomas, and A.A. Amis, *The role of the medial collateral ligament and posteromedial capsule in controlling knee laxity.* Am J Sports Med, 2006. **34**(11): p. 1815-23.
9. Robinson, J.R., A.M. Bull, and A.A. Amis, *Structural properties of the medial collateral ligament complex of the human knee.* J Biomech, 2005. **38**(5): p. 1067-74.
10. Meister, B.R., S.P. Michael, R.A. Moyer, J.D. Kelly, and C.D. Schneck, *Anatomy and kinematics of the lateral collateral ligament of the knee.* Am J Sports Med, 2000. **28**(6): p. 869-78.
11. Sugita, T. and A.A. Amis, *Anatomic and biomechanical study of the lateral collateral and popliteofibular ligaments.* Am J Sports Med, 2001. **29**(4): p. 466-72.
12. Takahashi, M., T. Matsubara, M. Doi, D. Suzuki, and A. Nagano, *Anatomical study of the femoral and tibial insertions of the anterolateral and posteromedial bundles of human posterior cruciate ligament.* Knee Surg Sports Traumatol Arthrosc, 2006. **14**(11): p. 1055-9.
13. Race, A. and A.A. Amis, *The mechanical properties of the two bundles of the human posterior cruciate ligament.* J Biomech, 1994. **27**(1): p. 13-24.

14. LaPrade, R.F., P.M. Morgan, F.A. Wentorf, S. Johansen, and L. Engebretsen, *The anatomy of the posterior aspect of the knee. An anatomic study.* J Bone Joint Surg Am, 2007. **89**(4): p. 758-64.
15. Sharma, L., C. Lou, D.T. Felson, D.D. Dunlop, G. Kirwan-Mellis, K.W. Hayes, D. Weinrach, and T.S. Buchanan, *Laxity in healthy and osteoarthritic knees.* Arthritis Rheum, 1999. **42**(5): p. 861-70.
16. van der Esch, M., M. Steultjens, J. Harlaar, N. Wolterbeek, D. Knol, and J. Dekker, *Varus-Valgus motion and functional ability in patients with osteoarthritis of the knee.* Ann Rheum Dis, 2007.
17. van der Esch, M., M. Steultjens, D.L. Knol, H. Dinant, and J. Dekker, *Joint laxity and the relationship between muscle strength and functional ability in patients with osteoarthritis of the knee.* Arthritis Rheum, 2006. **55**(6): p. 953-9.
18. van der Esch, M., M. Steultjens, H. Wieringa, H. Dinant, and J. Dekker, *Structural joint changes, malalignment, and laxity in osteoarthritis of the knee.* Scand J Rheumatol, 2005. **34**(4): p. 298-301.
19. Hanada, H., L.A. Whiteside, J. Steiger, P. Dyer, and M. Naito, *Bone landmarks are more reliable than tensioned gaps in TKA component alignment.* Clin Orthop Relat Res, 2007. **462**: p. 137-42.
20. D'Lima, D.J., S. Patil, N. Steklov, and C.W. Colwell, Jr., *An ABJS Best Paper: Dynamic intraoperative ligament balancing for total knee arthroplasty.* Clin Orthop Relat Res, 2007. **463**: p. 208-12.
21. Matsumoto, T., H. Muratsu, N. Tsumura, K. Mizuno, R. Kuroda, S. Yoshiya, and M. Kurosaka, *Joint gap kinematics in posterior-stabilized total knee arthroplasty measured by a new tensor with the navigation system.* J Biomech Eng, 2006. **128**(6): p. 867-71.
22. Sharkey, P.F., W.J. Hozack, R.H. Rothman, S. Shastri, and S.M. Jacoby, *Insall Award paper. Why are total knee arthroplasties failing today?* Clin Orthop Relat Res, 2002(404): p. 7-13.
23. Hirokawa, S. and R. Tsuruno, *Three-dimensional deformation and stress distribution in an analytical/computational model of the anterior cruciate ligament.* J Biomech, 2000. **33**(9): p. 1069-77.
24. Limbert, G., J. Middleton, and M. Taylor, *Finite element analysis of the human ACL subjected to passive anterior tibial loads.* Comput Methods Biomech Biomed Engin, 2004. **7**(1): p. 1-8.
25. Song, Y., R.E. Debski, V. Musahl, M. Thomas, and S.L. Woo, *A three-dimensional finite element model of the human anterior cruciate ligament: a computational analysis with experimental validation.* J Biomech, 2004. **37**(3): p. 383-90.
26. Abdel-Rahman, E.M. and M.S. Hefzy, *Three-dimensional dynamic behaviour of the human knee joint under impact loading.* Med Eng Phys, 1998. **20**(4): p. 276-90.

27. Perillo-Marcone, A. and M. Taylor, *Effect of varus/valgus malalignment on bone strains in the proximal tibia after TKR: an explicit finite element study.* J Biomech Eng, 2007. **129**(1): p. 1-11.
28. Shelburne, K.B. and M.G. Pandy, *A musculoskeletal model of the knee for evaluating ligament forces during isometric contractions.* J Biomech, 1997. **30**(2): p. 163-76.
29. Caruntu, D.I. and M.S. Hefzy, *3-D anatomically based dynamic modeling of the human knee to include tibio-femoral and patello-femoral joints.* J Biomech Eng, 2004. **126**(1): p. 44-53.
30. Mommersteeg, T.J., L. Blankevoort, R. Huiskes, J.G. Kooloos, and J.M. Kauer, *Characterization of the mechanical behavior of human knee ligaments: a numerical-experimental approach.* J Biomech, 1996. **29**(2): p. 151-60.
31. Mommersteeg, T.J., L. Blankevoort, J.G. Kooloos, J.C. Hendriks, J.M. Kauer, and R. Huiskes, *Nonuniform distribution of collagen density in human knee ligaments.* J Orthop Res, 1994. **12**(2): p. 238-45.
32. Mommersteeg, T.J., R. Huiskes, L. Blankevoort, J.G. Kooloos, and J.M. Kauer, *An inverse dynamics modeling approach to determine the restraining function of human knee ligament bundles.* J Biomech, 1997. **30**(2): p. 139-46.
33. Mommersteeg, T.J., R. Huiskes, L. Blankevoort, J.G. Kooloos, J.M. Kauer, and P.G. Maathuis, *A global verification study of a quasi-static knee model with multi-bundle ligaments.* J Biomech, 1996. **29**(12): p. 1659-64.
34. Mommersteeg, T.J., J.G. Kooloos, L. Blankevoort, J.M. Kauer, R. Huiskes, and F.Q. Roeling, *The fibre bundle anatomy of human cruciate ligaments.* J Anat, 1995. **187 (Pt 2)**: p. 461-71.
35. Momersteeg, T.J., L. Blankevoort, R. Huiskes, J.G. Kooloos, J.M. Kauer, and J.C. Hendriks, *The effect of variable relative insertion orientation of human knee bone-ligament-bone complexes on the tensile stiffness.* J Biomech, 1995. **28**(6): p. 745-52.
36. Weiss, J.A., J.C. Gardiner, B.J. Ellis, T.J. Lujan, and N.S. Phatak, *Three-dimensional finite element modeling of ligaments: technical aspects.* Med Eng Phys, 2005. **27**(10): p. 845-61.
37. Limbert, G., M. Taylor, and J. Middleton, *Three-dimensional finite element modelling of the human ACL: simulation of passive knee flexion with a stressed and stress-free ACL.* J Biomech, 2004. **37**(11): p. 1723-31.
38. Gardiner, J.C. and J.A. Weiss, *Subject-specific finite element analysis of the human medial collateral ligament during valgus knee loading.* J Orthop Res, 2003. **21**(6): p. 1098-106.
39. Chen, E.C. and R.E. Ellis, *An inverse kinematics model for post-operative knee. Ligament parameters estimation from knee motion.* Med Image Comput Comput Assist Interv Int Conf Med Image Comput Comput Assist Interv, 2006. **9**(Pt 1): p. 313-20.
40. Anderson, F.C. and M.G. Pandy, *Static and dynamic optimization solutions for gait are practically equivalent.* J Biomech, 2001. **34**(2): p. 153-61.

41. Shelburne, K.B., M.R. Torry, and M.G. Pandy, *Contributions of muscles, ligaments, and the ground-reaction force to tibiofemoral joint loading during normal gait.* J Orthop Res, 2006. **24**(10): p. 1983-90.
42. Higginson, J.S., R.R. Neptune, and F.C. Anderson, *Simulated parallel annealing within a neighborhood for optimization of biomechanical systems.* J Biomech, 2005. **38**(9): p. 1938-42.
43. Miller, R.H., J.C. Gillette, T.R. Derrick, and G.E. Caldwell, *Muscle forces during running predicted by gradient-based and random search static optimisation algorithms.* Comput Methods Biomech Biomed Engin, 2009. **12**(2): p. 217-25.
44. Koh, B.I., J.A. Reinbolt, A.D. George, R.T. Haftka, and B.J. Fregly, *Limitations of parallel global optimization for large-scale human movement problems.* Med Eng Phys, 2008.
45. Corana, A., M. Marchesi, C. Martini, and S. Ridella, *Minimizing Multimodal Functions of Continuous-Variables with the Simulated Annealing Algorithm.* Acm Transactions on Mathematical Software, 1987. **13**(3): p. 262-280.
46. Goffe, W.L., G.D. Ferrier, and J. Rogers, *Global Optimization of Statistical Functions with Simulated Annealing.* Journal of Econometrics, 1994. **60**(1-2): p. 65-99.
47. Goldberg, D.E., *Genetic Algorithms in Search, Optimization, and Machine Learning*. 1989: Adison-Wesley Publishing Company, Inc.
48. Fehring, T.K. and A.L. Valadie, *Knee instability after total knee arthroplasty.* Clin Orthop Relat Res, 1994(299): p. 157-62.
49. Pagnano, M.W., A.D. Hanssen, D.G. Lewallen, and M.J. Stuart, *Flexion instability after primary posterior cruciate retaining total knee arthroplasty.* Clin Orthop Relat Res, 1998(356): p. 39-46.
50. Wasielewski, R.C., J.O. Galante, R.M. Leighty, R.N. Natarajan, and A.G. Rosenberg, *Wear patterns on retrieved polyethylene tibial inserts and their relationship to technical considerations during total knee arthroplasty.* Clin Orthop Relat Res, 1994(299): p. 31-43.
51. Laskin, R.S., *Flexion space configuration in total knee arthroplasty.* J Arthroplasty, 1995. **10**(5): p. 657-60.
52. Yercan, H.S., T. Ait Si Selmi, T.S. Sugun, and P. Neyret, *Tibiofemoral instability in primary total knee replacement: a review, Part 1: Basic principles and classification.* Knee, 2005. **12**(4): p. 257-66.
53. Van Damme, G., K. Defoort, Y. Ducoulombier, F. Van Glabbeek, J. Bellemans, and J. Victor, *What should the surgeon aim for when performing computer-assisted total knee arthroplasty?* J Bone Joint Surg Am, 2005. **87 Suppl 2**: p. 52-8.
54. Asano, H., A. Hoshino, and T.J. Wilton, *Soft-tissue tension total knee arthroplasty.* J Arthroplasty, 2004. **19**(5): p. 558-61.
55. Asano, H., T. Muneta, and A. Hoshino, *Stiffness of soft tissue complex in total knee arthroplasty.* Knee Surg Sports Traumatol Arthrosc, 2008. **16**(1): p. 51-5.

56. Ishii, Y., Y. Matsuda, R. Ishii, S. Sakata, and G. Omori, *Coronal laxity in extension in vivo after total knee arthroplasty.* J Orthop Sci, 2003. **8**(4): p. 538-42.
57. Matsuda, Y., Y. Ishii, H. Noguchi, and R. Ishii, *Effect of flexion angle on coronal laxity in patients with mobile-bearing total knee arthroplasty prostheses.* J Orthop Sci, 2005. **10**(1): p. 37-41.
58. Okazaki, K., H. Miura, S. Matsuda, N. Takeuchi, T. Mawatari, M. Hashizume, and Y. Iwamoto, *Asymmetry of mediolateral laxity of the normal knee.* J Orthop Sci, 2006. **11**(3): p. 264-6.
59. Casino, D., S. Martelli, S. Zaffagnini, N. Lopomo, F. Iacono, S. Bignozzi, A. Visani, and M. Marcacci, *Knee stability before and after total and unicondylar knee replacement: in vivo kinematic evaluation utilizing navigation.* J Orthop Res, 2009. **27**(2): p. 202-7.
60. Draganich, L.F. and L.A. Pottenger, *The TRAC PS mobile-bearing prosthesis: design rationale and in vivo 3-dimensional laxity.* J Arthroplasty, 2000. **15**(1): p. 102-12.
61. Tsuneizumi, Y., M. Suzuki, J. Miyagi, H. Tamai, T. Tsukeoka, H. Moriya, and K. Takahashi, *Evaluation of joint laxity against distal traction force upon flexion in cruciate-retaining and posterior-stabilized total knee arthroplasty.* J Orthop Sci, 2008. **13**(6): p. 504-9.
62. Blankevoort, L., R. Huiskes, and A. de Lange, *The envelope of passive knee joint motion.* J Biomech, 1988. **21**(9): p. 705-20.
63. Bull, A.M., O. Kessler, M. Alam, and A.A. Amis, *Changes in knee kinematics reflect the articular geometry after arthroplasty.* Clin Orthop Relat Res, 2008. **466**(10): p. 2491-9.
64. Maletsky, L.P., J. Sun, and N.A. Morton, *Accuracy of an optical active-marker system to track the relative motion of rigid bodies.* J Biomech, 2007. **40**(3): p. 682-5.
65. Grood, E.S. and W.J. Suntay, *A joint coordinate system for the clinical description of three-dimensional motions: application to the knee.* J Biomech Eng, 1983. **105**(2): p. 136-44.
66. Lenz, N.M., A. Mane, L.P. Maletsky, and N.A. Morton, *The effects of femoral fixed body coordinate system definition on knee kinematic description.* J Biomech Eng, 2008. **130**(2): p. 021014.
67. Tokuhara, Y., Y. Kadoya, S. Nakagawa, A. Kobayashi, and K. Takaoka, *The flexion gap in normal knees. An MRI study.* J Bone Joint Surg Br, 2004. **86**(8): p. 1133-6.
68. Fairclough, J., K. Hayashi, H. Toumi, K. Lyons, G. Bydder, N. Phillips, T.M. Best, and M. Benjamin, *The functional anatomy of the iliotibial band during flexion and extension of the knee: implications for understanding iliotibial band syndrome.* J Anat, 2006. **208**(3): p. 309-16.
69. Kuster, M.S., B. Bitschnau, and T. Votruba, *Influence of collateral ligament laxity on patient satisfaction after total knee arthroplasty: a comparative bilateral study.* Arch Orthop Trauma Surg, 2004. **124**(6): p. 415-7.

70. Maletsky, L.P. and B.M. Hillberry, *Simulating dynamic activities using a five-axis knee simulator.* J Biomech Eng, 2005. **127**(1): p. 123-33.
71. Barink, M., A. van Kampen, M. de Waal Malefijt, and N. Verdonschot, *A three-dimensional dynamic finite element model of the prosthetic knee joint: simulation of joint laxity and kinematics.* Proc Inst Mech Eng [H], 2005. **219**(6): p. 415-24.
72. Essinger, J.R., P.F. Leyvraz, J.H. Heegard, and D.D. Robertson, *A mathematical model for the evaluation of the behaviour during flexion of condylar-type knee prostheses.* J Biomech, 1989. **22**(11-12): p. 1229-41.
73. Halloran, J.P., A.J. Petrella, and P.J. Rullkoetter, *Explicit finite element modeling of total knee replacement mechanics.* J Biomech, 2005. **38**(2): p. 323-31.
74. Martelli, S., R.E. Ellis, M. Marcacci, and S. Zaffagnini, *Total knee arthroplasty kinematics. Computer simulation and intraoperative evaluation.* J Arthroplasty, 1998. **13**(2): p. 145-55.
75. Donahue, T.L., M.L. Hull, M.M. Rashid, and C.R. Jacobs, *A finite element model of the human knee joint for the study of tibio-femoral contact.* J Biomech Eng, 2002. **124**(3): p. 273-80.
76. Taylor, M. and D.S. Barrett, *Explicit finite element simulation of eccentric loading in total knee replacement.* Clin Orthop Relat Res, 2003(414): p. 162-71.
77. Knight, L.A., S. Pal, J.C. Coleman, F. Bronson, H. Haider, D.L. Levine, M. Taylor, and P.J. Rullkoetter, *Comparison of long-term numerical and experimental total knee replacement wear during simulated gait loading.* J Biomech, 2007. **40**(7): p. 1550-8.
78. Laz, P.J., S. Pal, J.P. Halloran, A.J. Petrella, and P.J. Rullkoetter, *Probabilistic finite element prediction of knee wear simulator mechanics.* J Biomech, 2006. **39**(12): p. 2303-10.
79. Chen, E., R.E. Ellis, J.T. Bryant, and J.F. Rudan, *A computational model of postoperative knee kinematics.* Med Image Anal, 2001. **5**(4): p. 317-30.
80. Kessler, O., S. Patil, C.W. Colwell, Jr., and D.D. D'Lima, *The effect of femoral component malrotation on patellar biomechanics.* J Biomech, 2008. **41**(16): p. 3332-9.
81. Pena, E., M.A. Martinez, B. Calvo, D. Palanca, and M. Doblare, *A finite element simulation of the effect of graft stiffness and graft tensioning in ACL reconstruction.* Clin Biomech (Bristol, Avon), 2005. **20**(6): p. 636-44.
82. Bertozzi, L., R. Stagni, S. Fantozzi, and A. Cappello, *Knee model sensitivity to cruciate ligaments parameters: a stability simulation study for a living subject.* J Biomech, 2007. **40 Suppl 1**: p. S38-44.
83. Li, G., J. Suggs, and T. Gill, *The effect of anterior cruciate ligament injury on knee joint function under a simulated muscle load: a three-dimensional computational simulation.* Ann Biomed Eng, 2002. **30**(5): p. 713-20.
84. Mesfar, W. and A. Shirazi-Adl, *Biomechanics of changes in ACL and PCL material properties or prestrains in flexion under muscle force-implications in*

ligament reconstruction. Comput Methods Biomech Biomed Engin, 2006. **9**(4): p. 201-9.
85. Blankevoort, L., J.H. Kuiper, R. Huiskes, and H.J. Grootenboer, *Articular contact in a three-dimensional model of the knee.* J Biomech, 1991. **24**(11): p. 1019-31.
86. Morra, E.A., M. Rosca, J.F. Greenwald, and A.S. Greenwald, *The influence of contemporary knee design on high flexion: a kinematic comparison with the normal knee.* J Bone Joint Surg Am, 2008. **90 Suppl 4**: p. 195-201.
87. Strickland, M., M Browne, M Taylor, *The Effect of Ligament Variability on TKR Performance - A probabilistic Study.* Transactions of the Orthopedic Research Society, 2007. **32**.
88. Haldar, A. and S. Mahadevan, *Probability, Reliability and Statistical Methods in Engineering Design*. 2000, New York: John Wiley & Sons, Inc.
89. Arms, S., J. Boyle, R. Johnson, and M. Pope, *Strain measurement in the medial collateral ligament of the human knee: an autopsy study.* J Biomech, 1983. **16**(7): p. 491-6.
90. Blankevoort, L. and R. Huiskes, *Ligament-bone interaction in a three-dimensional model of the knee.* J Biomech Eng, 1991. **113**(3): p. 263-9.
91. Akalan, N.E., M. Ozkan, and Y. Temelli, *Three-dimensional knee model: constrained by isometric ligament bundles and experimentally obtained tibio-femoral contacts.* J Biomech, 2008. **41**(4): p. 890-6.
92. Beillas, P., P.C. Begeman, K.H. Yang, A.I. King, P.J. Arnoux, H.S. Kang, K. Kayvantash, C. Brunet, C. Cavallero, and P. Prasad, *Lower Limb: Advanced FE Model and New Experimental Data.* Stapp Car Crash J, 2001. **45**: p. 469-94.
93. Moglo, K.E. and A. Shirazi-Adl, *Cruciate coupling and screw-home mechanism in passive knee joint during extension--flexion.* J Biomech, 2005. **38**(5): p. 1075-83.
94. Shin, C.S., A.M. Chaudhari, and T.P. Andriacchi, *The influence of deceleration forces on ACL strain during single-leg landing: a simulation study.* J Biomech, 2007. **40**(5): p. 1145-52.
95. Baldwin, M.A., P.J. Laz, J.Q. Stowe, and P.J. Rullkoetter, *Efficient probabilistic representation of tibiofemoral soft tissue constraint.* Comput Methods Biomech Biomed Engin, 2009: p. 1.
96. Amis, A.A., A.M. Bull, C.M. Gupte, I. Hijazi, A. Race, and J.R. Robinson, *Biomechanics of the PCL and related structures: posterolateral, posteromedial and meniscofemoral ligaments.* Knee Surg Sports Traumatol Arthrosc, 2003. **11**(5): p. 271-81.
97. Greening, D.R., *Parallel Simulated Annealing Techniques.* Physica D, 1990. **42**(1-3): p. 293-306.
98. Griffith, C.J., C.A. Wijdicks, R.F. LaPrade, B.M. Armitage, S. Johansen, and L. Engebretsen, *Force measurements on the posterior oblique ligament and superficial medial collateral ligament proximal and distal divisions to applied loads.* Am J Sports Med, 2009. **37**(1): p. 140-8.

99. LaPrade, R.F., A. Tso, and F.A. Wentorf, *Force measurements on the fibular collateral ligament, popliteofibular ligament, and popliteus tendon to applied loads.* Am J Sports Med, 2004. **32**(7): p. 1695-701.
100. Veltri, D.M., X.H. Deng, P.A. Torzilli, M.J. Maynard, and R.F. Warren, *The role of the popliteofibular ligament in stability of the human knee. A biomechanical study.* Am J Sports Med, 1996. **24**(1): p. 19-27.
101. Blankevoort, L., R. Huiskes, and A. de Lange, *Recruitment of knee joint ligaments.* J Biomech Eng, 1991. **113**(1): p. 94-103.
102. Musahl, V., K.M. Bell, A.G. Tsai, R.S. Costic, R. Allaire, T. Zantop, J.J. Irrgang, and F.H. Fu, *Development of a simple device for measurement of rotational knee laxity.* Knee Surg Sports Traumatol Arthrosc, 2007. **15**(8): p. 1009-12.
103. Swank, M., I.R. Romanowski, L.L. Korbee, and S. Bignozzi, *Ligament balancing in computer-assisted total knee arthroplasty: improved clinical results with a spring-loaded tensioning device.* Proc Inst Mech Eng [H], 2007. **221**(7): p. 755-61.